NAVAL POSTGRADUATE SCHOOL
MONTEREY, CALIFORNIA

THESIS

FLUID-INTERACTION AND CAVITATION EFFECTS ON A SURFACE SHIP MODEL DUE TO AN UNDERWATER EXPLOSION

by

Leonard D. Santiago

September 1996

Thesis Advisor: Young S. Shin

Approved for public release; distribution is unlimited.

DISCLAIMER NOTICE

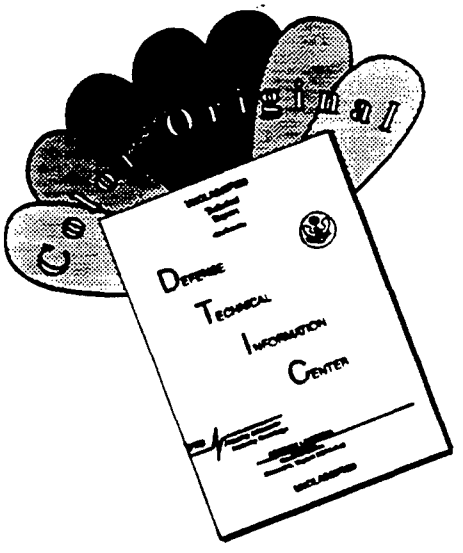

THIS DOCUMENT IS BEST QUALITY AVAILABLE. THE COPY FURNISHED TO DTIC CONTAINED A SIGNIFICANT NUMBER OF COLOR PAGES WHICH DO NOT REPRODUCE LEGIBLY ON BLACK AND WHITE MICROFICHE.

REPORT DOCUMENTATION PAGE

Form Approved OMB No. 0704-0188

1. AGENCY USE ONLY *(Leave blank)*	2. REPORT DATE September 1996.	3. REPORT TYPE AND DATES COVERED Master's Thesis

4. TITLE AND SUBTITLE: FLUID-INTERACTION AND CAVITATION EFFECTS ON A SURFACE SHIP MODEL DUE TO AN UNDERWATER EXPLOSION

5. FUNDING NUMBERS

6. AUTHOR(S) Santiago, Leonard D.

7. PERFORMING ORGANIZATION NAME(S) AND ADDRESS(ES)
Naval Postgraduate School
Monterey CA 93943-5000

8. PERFORMING ORGANIZATION REPORT NUMBER

9. SPONSORING/MONITORING AGENCY NAME(S) AND ADDRESS(ES)

10. SPONSORING/MONITORING AGENCY REPORT NUMBER

11. SUPPLEMENTARY NOTES The views expressed in this thesis are those of the author and do not reflect the official policy or position of the Department of Defense or the U.S. Government.

12a. DISTRIBUTION/AVAILABILITY STATEMENT
Approved for public release; distribution is unlimited.

12b. DISTRIBUTION CODE

13. ABSTRACT *(maximum 200 words)*

A surface ship subjected to an underwater explosion is exposed to shock waves over a short period of time which can vary in magnitude based on charge type, size, and location. The energy of those waves impinging upon the hull is transmitted throughout the ship's structure and vital equipment. The dynamics of the shock waves also influence the fluid surrounding the outer hull of the ship, creating an area of cavitating fluid. The combination of the shock waves, bubble pulsations, and cavitating fluid induce shipwide vibrations on hull supports and mission essential equipment which may become inoperative. In view of congressional requirements for new ship designs and systems to be shock tested, this thesis investigates the modeling of a preliminary design (Flight I) of the Arleigh Burke Destroyer (DDG 51) exposed to an underwater explosion. The effects of cavitation on one and two dimensional models is explored to determine if cavitation effects are substantially important to a three dimensional ship model. Validation of modeling underwater explosion effects upon a ship model can provide potential insight and savings in cost for future live fire testing and evaluation of the Flight IIA (DDG 79) design of the Arleigh Burke Destroyer.

14. SUBJECT TERMS Underwater Shock, Cavitation, Surface Model

15. NUMBER OF PAGES 147

16. PRICE CODE

17. SECURITY CLASSIFICATION OF REPORT	18. SECURITY CLASSIFICATION OF THIS PAGE	19. SECURITY CLASSIFICATION OF ABSTRACT	20. LIMITATION OF ABSTRACT
Unclassified	Unclassified	Unclassified	UL

NSN 7540-01-280-5500

Standard Form 298 (Rev. 2-89)
Prescribed by ANSI Std. 239-18 298-102

Approved for public release; distribution is unlimited.

FLUID-INTERACTION AND CAVITATION EFFECTS ON A SURFACE SHIP MODEL DUE TO AN UNDERWATER EXPLOSION

Leonard D. Santiago
Lieutenant, United States Navy
B.S., University of California, Berkeley, 1988

Submitted in partial fulfillment
of the requirements for the degree of

MASTER OF SCIENCE IN MECHANICAL ENGINEERING

from the

NAVAL POSTGRADUATE SCHOOL
September 1996

Author: 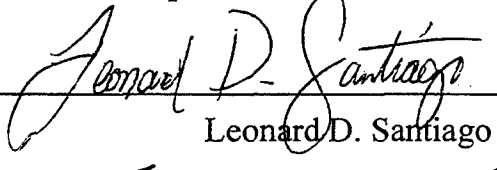
Leonard D. Santiago

Approved by: 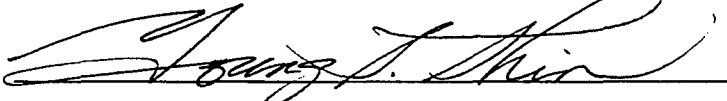
Young S. Shin, Thesis Advisor

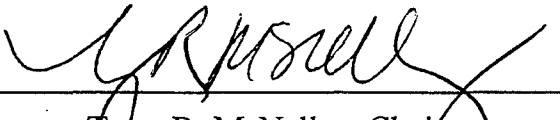
Terry R. McNelley, Chairman
Department of Mechanical Engineering

ABSTRACT

A surface ship subjected to an underwater explosion is exposed to shock waves over a short period of time which can vary in magnitude based on charge type, size, and location. The energy of those waves impinging upon the hull is transmitted throughout the ship's structure and vital equipment. The dynamics of the shock waves also influence the fluid surrounding the outer hull of the ship, creating an area of cavitating fluid. The combination of the shock waves, bubble pulsations, and cavitating fluid induce shipwide vibrations on hull supports and mission essential equipment which may become inoperative. In view of congressional requirements for new ship designs and systems to be shock tested, this thesis investigates the modeling of a preliminary design (Flight I) of the Arleigh Burke Destroyer (DDG 51) exposed to an underwater explosion. The effects of cavitation on one and two dimensional models is explored to determine if cavitation effects are substantially important to a three dimensional ship model. Validation of modeling underwater explosion effects upon a ship model can provide potential insight and savings in cost for future live fire testing and evaluation of the Flight IIA (DDG 79) design of the Arleigh Burke Destroyer.

TABLE OF CONTENTS

ACKNOWLEDGMENTS

I would like to express my deep gratitude and appreciation to Dr. Young S. Shin for his continued guidance and encouragement throughout this research. I would also like to thank Dr. John DeRuntz and LCDR Jim Chisum for their patience, support, and expertise they provided me during my studies in the area of underwater shock research. My gratitude also goes to Mr. Chris Dombkowski and Miss Amy Welbaum at SDRC as well as Mr. Jack Castro at MacNeal-Schwendler Corportation for their quick and efficient support.

Finally, I would like to dedicate this work to my loving wife, Marsha, my beautiful daughter, Danielle Mae, and to my devoted mother-in-law, Gertrude B. Queturas, who have supported and sacrificed for my academic endeavor at the Naval Postgraduate School. Their love and encouragement made it possible.

I. INTRODUCTION

A. BACKGROUND

Today's U.S Navy consisting of technologically advanced ships such as the Ticonderoga class cruiser and the Arleigh Burke class destroyer are being driven to operate in the littoral, close to shore, environment as dilineated in the Department of the Navy's strategic planning document [Ref. 1]. These platforms equipped with the Aegis weapon system were designed for open ocean, "blue water" tactical scenarios but due to the end of the cold war, a shift in emphasis is placed on low intensity conflicts which occur near the sea-land interface. This has increased the potential for "cheap kill" opportunities against U.S. warships such as an underwater mine as ships close the shore and the availability of such weapons is high and the cost low for third world country to purchase.

As recently as 1991 during Operation Desert Storm, the USS Princeton (CG-59), a Ticonderoga class guided missile cruiser, struck a floating mine near the bow. Although the rupture to the hull was localized, the subsequent whipping of the hull caused severe hull girder damage near the stern of the ship and weapon systems to go off line. This type of tactical environment now places a greater responsibility on ship designers and engineers to meet requirements as specified in MIL-S-901D [Ref . 2].

A number of studies have been conducted on submerged cylinder type models exposed to an underwater explosion in order to predict the hull response of structures

such as a submerged submarine. These studies did not include the effects of cavitation on the wet surface of the model or of the cavitation which occurs at the free surface. For surface ship type studies, simplified beam models such as that conducted by Hicks [Ref. 3] have concentrated only on the effects of whipping of surface vessels due to gas bubble dynamics. In this age of improving computer hardware, larger memory and software programs such as the USA (Underwater Shock Analysis) code with the CFA (Cavitation Fluid Analyzer) [Ref. 4] to model underwater shock effects and improving CAD programs with built in FEM (Finite Element Model) generators such as IDEAS [Ref. 5] and MSC/NASTRAN [Ref. 6], the engineer has a greater ability to improve ship modeling and predict the vibrational response of ship hulls and internal equipment.

B. SCOPE OF RESEARCH

This thesis studies the methods of modeling one and two dimensional finite element models with and without an external fluid. Two different computational methods are selected in the USA code for each model arrangement in addition to incorporating the CFA module in the solution process. The goal is to determine the cavitation effects on a surface vessel and develop the most simplest and conservative method in modeling the underwater explosion. A one dimensional model is created from Bleich's paper [Ref. 7] which defines the conditions of a square plate sitting on a fluid surface and a fluid column. In additon, an exponetial decaying plane wave models the underwater explosion. A second finite element model is created to represent the cross-sectional area of a simple

ship hull. This two dimensional model includes the surrounding fluid to the waterline of the hull and introduces the effects of a free surface due to an actual charge placed at a distance from the hull. The results from these first two models provides some simplification for the three dimensional notional hull structure of the Flight I of the Arleigh Burke. Although live fire testing and evaluation has already been conducted on a Flight I design, a Flight IIA design starting with DDG-79 possesses hull differences shown in Fig.1 which may require shock testing. Improvements in the area of modeling a surface ship such as the Flight IIA design from existing CAD programs and fluid behavior during an underwater explosion through the USA code, can create potential savings in future Flight IIA shock trial tests.

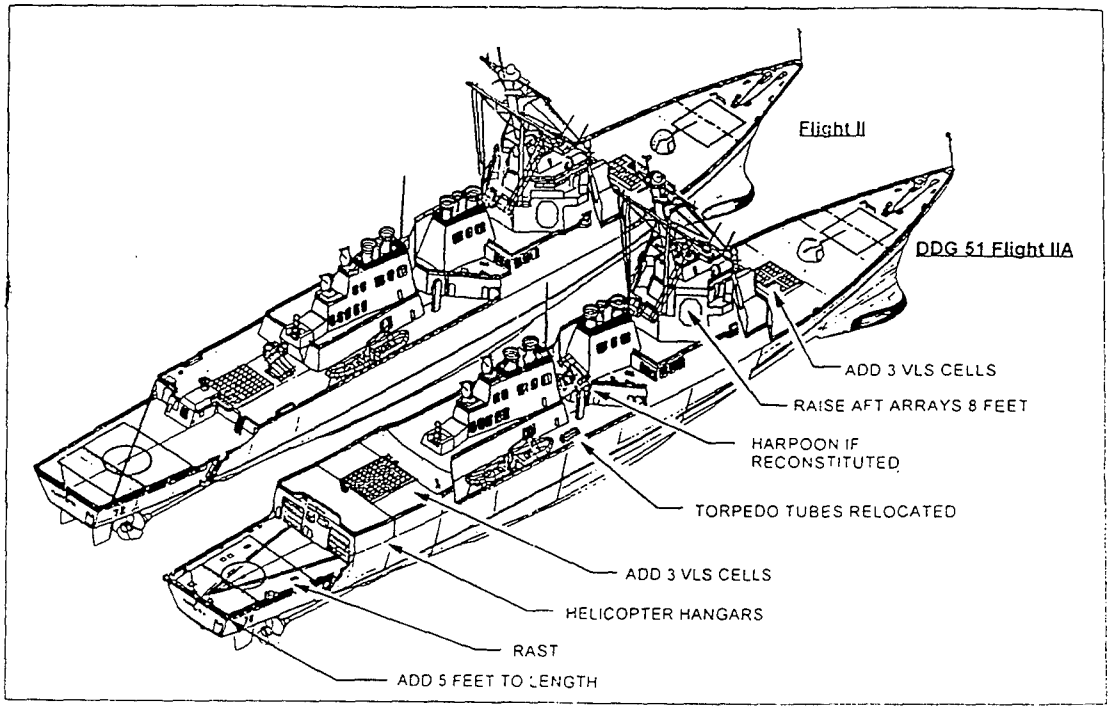

Figure 1. Major Changes (Flight II to Flight IIA) [Ref. 8]

II. UNDERWATER EXPLOSION

A. FLUID BEHAVIOR

When an underwater explosion occurs, the solid explosive material (such as HBX-1, TNT, etc.) suddenly reacts, leaving behind high temperature and pressure of gaseous products. An initial wave of compression is produced due to a sudden discontinuity of pressure which can reach a peak pressure of 2×10^6 psi. This steep fronted wave known as a "shock wave" propagates radially outward at a speed several times the speed of sound in water and roughly decays exponentially. The velocity of the shock wave decreases such that at approximately 10 times the explosive charge radius, the disturbance is essentially traveling at the acoustic velocity in water, 5000 ft/sec. [Ref 9:pp 3-7]

The pressure sensed at a specific point in the fluid or at a structure is essentially a step increase to the peak pressure followed by an exponential decay with time until the pressure has dropped to approximately one third of the peak pressure. After falling to approximately one-third of the peak pressure, the pressure level falls off inversely with distance [Ref 9:pp3-7].

The cavity of gaseous products left behind at high pressure forms a bubble which subsequently expands to relieve the difference in pressure, accelerating the surrounding fluid particles. The bubble continues to expand beyond the point of hydrostatic equilibrium (due to the inertia of the surrounding fluid) until a point of dynamic equilibrium is reached. The bubble then reverses its motion, continuing to contract until

dynamic equilibrium is again reached, where it quickly rebounds and again begins to expand as illustrated in Fig. 2. This oscillating bubble expansion and contraction continues until the energy of the reaction is fully dissipated or the bubble finally reaches the surface, venting the gaseos by products of the explosion. As the bubble rebounds, it greatly accelerates the surrounding water, generating a substantial pressure pulse (known as the bubble pulse). This bubble pulse can impart significant loads on structures in the vicinity.

In addition to the initial shock wave and bubble pulse, based on the location of the expolsive charge with respect to the surface and sea floor, a surface vessel can also experience a combination of the following pressure waves as illustrated in Fig. 3:

1. Free-surface reflection
2. Bottom reflection
3. Bottom refraction (not shown)

The directions of free-surface and bottom reflection waves can be determined through an application of Snell's law at the surface and sea bottom, respectively. At the surface of a fluid, a reflected wave of negative pressure known as the "rarefraction wave" is formed with a value such that the sum of the direct and reflected pressures is zero along the boundary condition between air and water defined by the surface. This rarefraction wave travels through the fluid region shortly after the incident shock wave at any point which causes the incident shock wave pressure profile to be truncated at a point in time called "surface cut-off." Bottom reflected and refracted waves are dependent on the

characteristics of the sea bottom and can contribute significant pressure waves in shallow water environments but are not considered for this study.

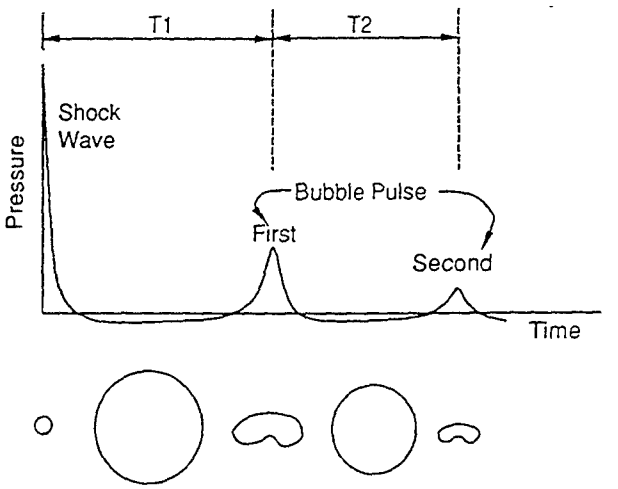

Figure 2. Gas Bubble behavior

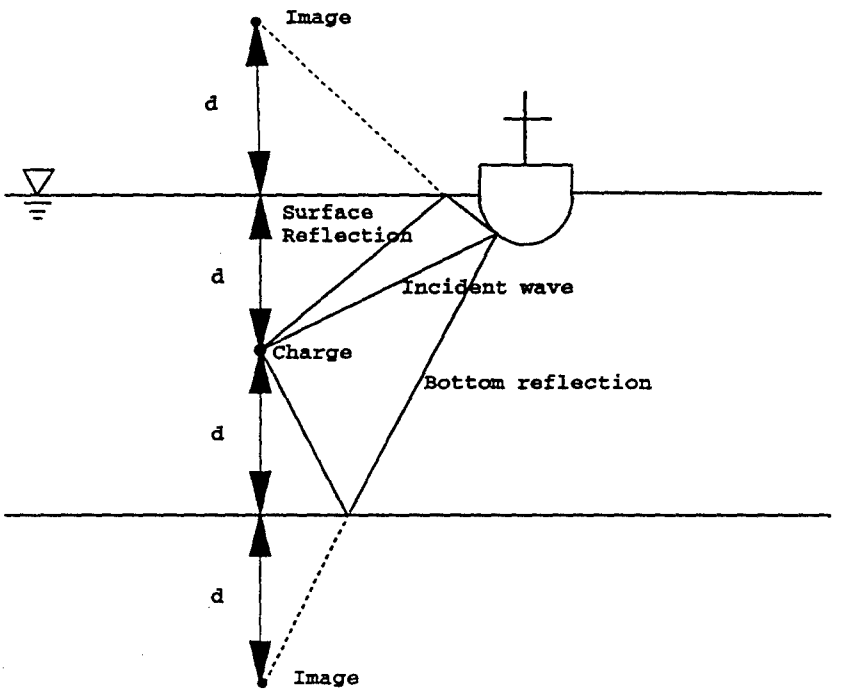

Figure 3. Pressure Wave Profiles

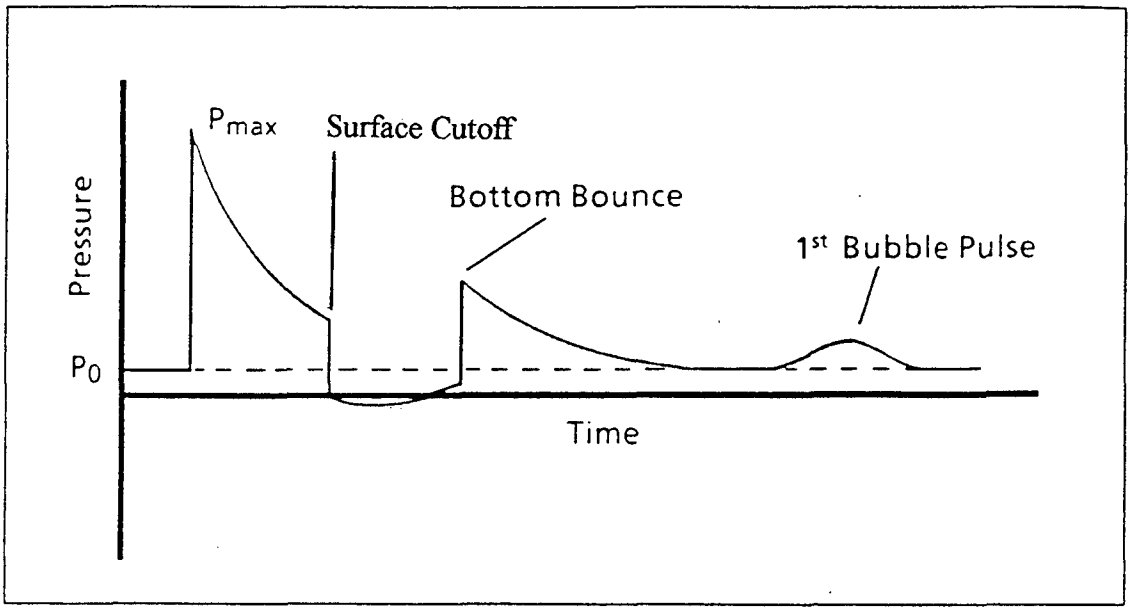

Figure 4. Combined Pressure Profile of an Underwater Explosion

The oscillating bubble pulse can also introduce a low-frequency forcing function that can resonate a ship girder frequency especially when the period of the bubble pulse is in the vicinity of the natural frequencies of the ship girder. Fig. 4 illustrates a combination of the pressure waves.

A number of empirical relationships have been derived through numerous underwater explosion tests since World War II which provide a means to calculate explosion characteristics such as incident wave pressure (P_{max}) which impinges upon a target, shock wave decay constant (θ), pressure as a function of time (P(t)), and bubble period (T) with derived constants for each respective explosive material provided:

$$P(t) = P_{max} e^{-\frac{t-t_1}{\theta}} \qquad \text{(psi)}$$

$$P_{max} = K_1 \left(\frac{W^{1/3}}{R}\right)^{A_1} \qquad \text{(psi)}$$

$$\theta = K_2 W^{1/3} \left(\frac{W^{1/3}}{R}\right)^{A_2} \qquad \text{(msec)}$$

$$T = K_5 \frac{W^{1/3}}{(D+33)^{5/6}} \qquad \text{(sec)}$$

W = Charge weight (lb)

R = Standoff distance (ft)

D = Charge Depth (ft)

t_1 = Arrival time of shock wave (sec)

t = Time of interest (sec)

K_1, K_2, K_5, A_1, A_2 = Shock wave parameters

B. STRUCTURAL BEHAVIOR

The dynamic response of a linear-elastic structure can be defined, based on the number of elements and nodes that define the structure, as

$$[M]\{\ddot{x}(t)\} + [C]\{\dot{x}(t)\} + [K]\{x(t)\} = \{F(t)\} \qquad (2.1)$$

where [M] = structural mass matrix, [C]=damping matrix, [K]=stiffness matrix, {F(t)}=applied external force, {x(t)}= general displacement vector and derivatives with respect to time. For a structure in a fluid medium, the applied external force created by an underwater explosion, is defined as

$$-[G]\,[A_{fluid}]\,(\{P_i(t)\} + \{P_s(t)\}) = \{F(t)\} \tag{2.2}$$

where [G] = the transformation matrix between structural and fluid nodes, $[A_{fluid}]$= diagonal area matrix for the elements in the fluid, $\{P_i(t)\}$= incident wave nodal pressure vector and $\{P_s(t)\}$ = scattered wave nodal pressure vector.

The USA code provides the means to model the pressures involved in an underwater shock as a "forcing function" on a fully or partially submerged model. The code also utilizes variations of the DAA (Doubly Asymptotic Approximation) method [Ref. 10] that models the surrounding acoustic medium as a membrane on the surface of the structure actually in contact with the homogeneous fluid. The effects of cavitation on a structure modeled with a surrounding fluid can be also included through the CFA. The fluid motion and structural response is linked together through a series of compatibility relations that are matrix differential equations that relate the symmetric fluid mass matrix of the model's wet surface, fluid particle velocities from the scattered wave normal to the structures wet surface, and rates of changing scattered fluid pressures. The USA code creates this matrix by utilizing an infinite, inviscid, incompressible fluid in an irrotational flow created by the structure's wet surface and then creates a virtual mass matrix which is comprised of the added mass of the fluid on the elements of the structures mass matrix which are wet. Kinematic compatibility is obtained between the fluid motion and

structural motion by an invariance of virtual work and transformation matrices that create the final interaction equations for fluid and structure motion [Ref. 10].

Hence, the final equations of structure and changing fluid pressures create a set of " augmented interaction equations" which the USA code solves, given a specified time increment, in an unconditionally stable manner.

C. CAVITATION

Two types of cavitation which can occur during an underwater explosion is that of "local cavitation" which occurs at the fluid-surface interface and "bulk cavitation" which occurs near the free surface that can extend beyond the target of interest by hundreds of feet. Utilizing Taylor flat plate theory, the particular models in this thesis will utilize only air backed plate conditions as illustrated in Fig. 5.

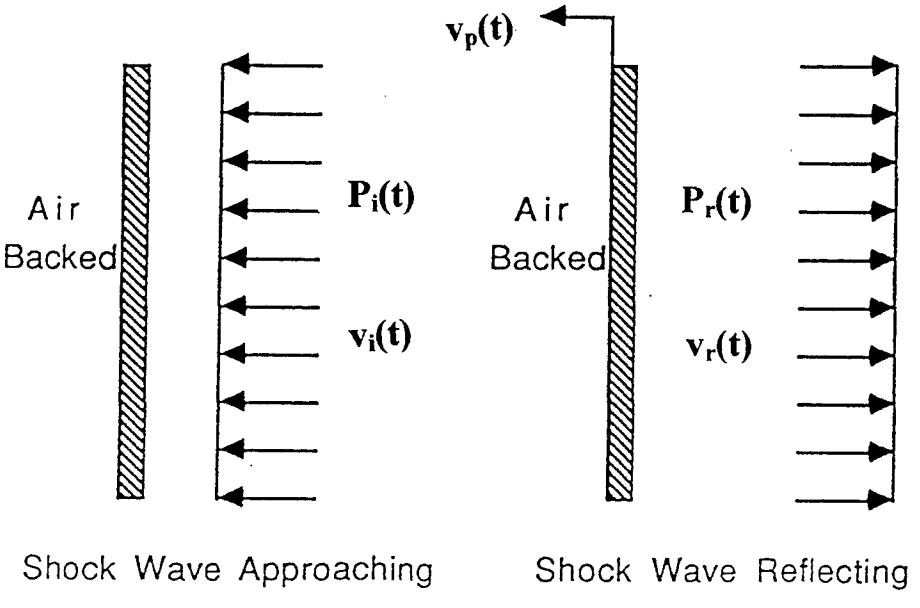

Figure 5. Taylor Plate Subjected to Plane Wave.

1. Local Cavitation

When the pressure pulse from an underwater explosion impinges upon a flexible surface such as the hull of surface ship, a fluid-structure interaction occurs which dynamically excites the ship structure. Looking at an infinite, air backed plate of mass, per unit area (m) subjected to an incident plane shock wave $P_i(t)$, a reflection wave of pressure $P_r(t)$ will come off the plate. Letting $v_p(t)$ be the velocity of the plate and applying Newton's second law of motion:

$$m \times \frac{dv_p}{dt} = P_r + P_i \tag{2.3}$$

Letting the fluid particle velocities behind the incident and reflected shock waves be $v_i(t)$ and $v_r(t)$, respectively, the velocity of the plate becomes

$$v_p(t) = v_i(t) - v_r(t) \tag{2.4}$$

Incident and reflected shock wave pressures are defined, respectively :

$$P_i = \rho C v_i \tag{2.5}$$

$$P_r = \rho C v_r \tag{2.6}$$

where ρ=fluid density and C=acoustic velocity. Substituting the pressures (2.5) and(2.6) into (2.4) and utilizing for a high explosive shock wave

$$P_i(t) = P_{max} e^{-\frac{t}{\theta}} \tag{2.7}$$

where t = time starting after the shock wave arrives at the target, one can solve for P_r:

$$P_r = P_i - \rho C v_p = P_{max} e^{-\frac{t}{\theta}} - \rho C v_p \tag{2.8}$$

Returning to the basic equation of motion (eq. 2.1) and substituting for P_i gives the following first order linear differential equation:

$$m\frac{dv}{dt} + \rho C v_p = 2P_{max} e^{-\frac{t}{\theta}} \tag{2.9}$$

The above differential equation is solved for v_p,

$$v_p = \frac{2P_{max}\theta}{m(1-\beta)}\left[e^{(-\frac{\beta t}{\theta})} - e^{(-\frac{t}{\theta})}\right] \tag{2.10}$$

where $\beta=\rho C\theta/m$ and $t>0$. Total pressure on the plate is also found to be

$$P_i + P_r = P_{max}\left[\frac{2}{1-\beta}e^{-\frac{t}{\theta}} - \frac{2\beta}{1-\beta}e^{-\frac{\beta t}{\theta}}\right] \tag{2.11}$$

Hence, as β becomes larger, representing a light weight plate becoming more flexible, the total pressure will become negative at a very early time and as the total pressure approaches vapor pressure, local cavitation occurs in front of the plate. At this point, the plate is separating from the fluid and the maximum velocity for the plate is attained [Ref. 11]

2. Bulk Cavitation

The combination of the rarefraction wave and incident shock wave near the free surface creates a region of decreasing fluid pressure that approaches the vapor pressure of water. The rarefraction wave direction is determined by an image charge located an equivalent distance from the surface boundary in the air as the actual charge in the fluid. An upper and lower boundary begins to form which defines the bulk cavitation zone (Fig. 6). The velocity of the water particle near the free surface will have primarily a vertical velocity at cavitation. As the reflected shock wave passes, the fluid is then acted upon by gravity and atmospheric pressure.

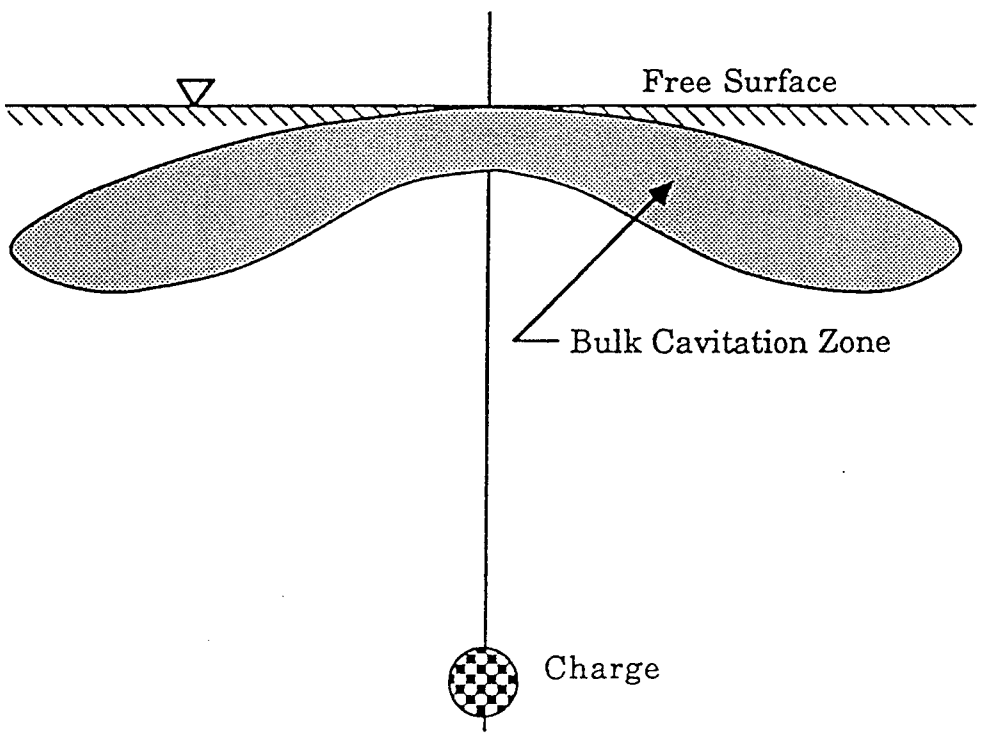

Figure 6. Bulk Cavitation Zone [Ref. 11]

The upper cavitation boundary of Fig. 6 is the set of location points where the rarefraction wave arrives and the absolute pressure drops to the cavitation pressure. The total pressure which determines the upper boundary is the summation atmospheric, hydrostatic, incident shock, and rarefraction which can be defined as

$$F(x,y) = K_1\left(\frac{W^{1/3}}{r_1}\right)^{A_1} e^{-\frac{(r_2-r_1)}{C\theta}} + P_A + \gamma y - K_1\left(\frac{W^{1/3}}{r_2}\right)^{A_1} = 0$$

$$r_1 = \sqrt{(D-y)^2 + x^2}$$

$$r_2 = \sqrt{(D+y)^2 + x^2}$$

where

x,y = horizontal range and vertical depth of point

r_1 = standoff distance from charge to point

r_2 = standoff distance from image charge to point

C = speed of sound in water

D = charge depth

θ = decay constant

P_A = atmospheric pressure

γ = weight density of water

W = charge weight

K_1, A_1 = shock wave parameters

The lower cavitation boundary is determined by equating the decay rate of the breaking pressure which is the rarefaction wave pressure that reduces a particular location of fluid to the point of cavitation pressure, approximately zero, to the decay rate of the

total absolute pressure of the fluid as illustrated in Fig. 6. This boundary can be defined as [Ref. 12]

$$G(x,y) = -\frac{P_i}{C\theta}\left\{1+\left[\frac{r_2 - 2D(\frac{D+y}{r_2})}{r_1}\right]\left[\frac{A_2 r_2}{r_1} - A_2 - 1\right]\right\} - \frac{A_1 P_i}{r_1^2}\left[r_2 - 2D\left(\frac{D+y}{r_2}\right)\right] + \gamma\left(\frac{D+y}{r_2}\right) + \frac{A_1}{r_2}(P_i + P_a + \gamma y) = 0$$

where

$$P_i = K_1\left(\frac{W^{1/3}}{R}\right)^{A_1} e^{\frac{-(r_2 - r_1)}{C\theta}}$$

$$\theta = K_2 W^{1/3}\left(\frac{W^{1/3}}{R}\right)^{A_2}$$

Hence, any point that satisfies F(x,y)=0 and G(x,y)=0 determines the upper and lower boundary points. Fig.7 and Appendix A provides a MATLAB code [Ref. 13] for bulk cavitation zones for various depths and charge weights for TNT explosive material. This particular tool was useful in modeling the 2D cross sectional hull and placing the charge in location that would minimize the effects of bulk cavitation and aid in concentrating effects of local cavitation. Fig. 7 illustrates the region of the bulk cavitation zone above the charge does not vary much with changing depth. However, the bulk cavitation zone increases in depth with appreciable increases in charge size. 30 feet below the keel (total depth of 50 feet) was used for the two dimensional study.

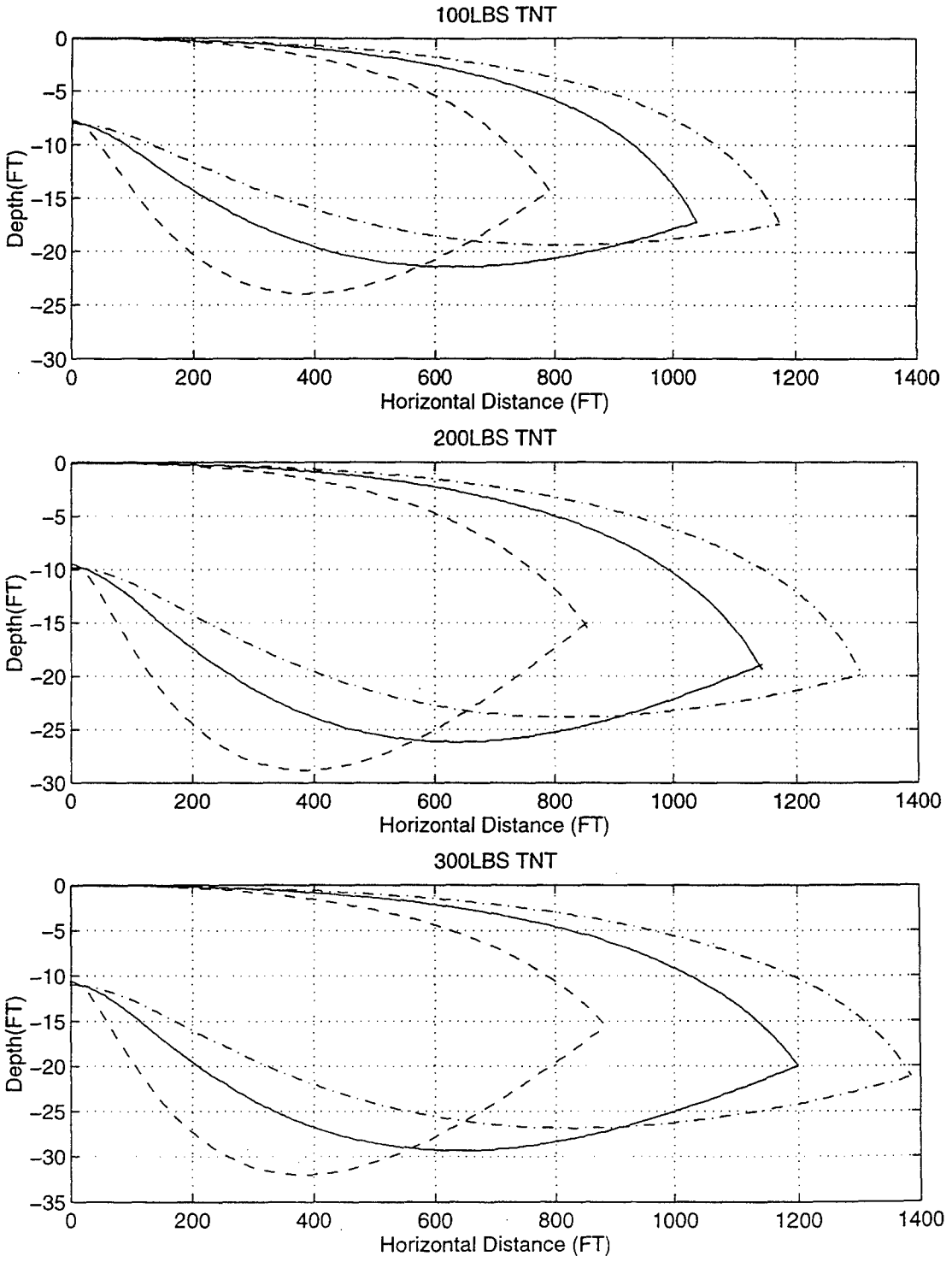

Figure 7. Bulk Cavitation Zones for a TNT charge located at the following depths: ---50ft,–100ft, -.150ft

III. COMPUTATIONAL FLOW

Model preparation, translation, calculation, and post-processing involved a number of programs which is depicted in Fig. 8. Each process involves a number of output files which are input to the next step in the process or provides the user a means to verify results from each step before proceeding.

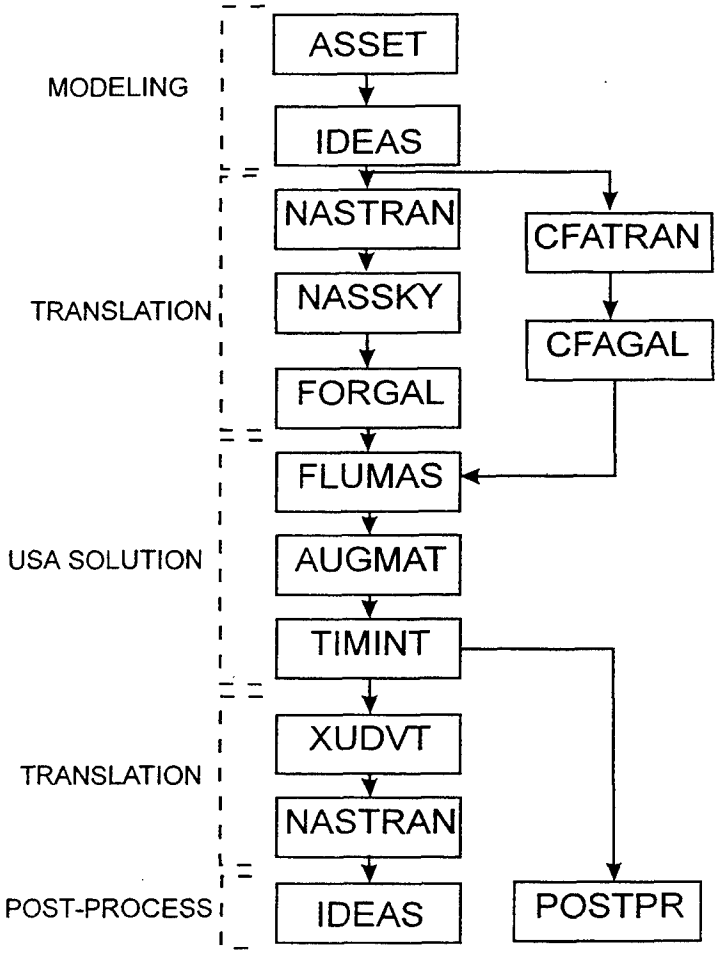

Figure 8. Computer Program Flow

A. MODELING

1. ASSET

ASSET/MONOSC (Advanced Surface Ship Evaluation Tool/Monohull Surface Combatant) [Ref.14] program is an interactive program which created the original ship dimensions for the three dimensional study. It provides a naval architectural tool to address ship design, which includes geometric definition of the hull and superstructure, hull subdivision, hull structure, resistance, appendages, equipment, and costs [Ref. 14]. An early design of the DDG 51 class destroyer with general weights of equipment groups and hull structure requirements based on inputs from designer imposed needs or mission requirements was exported out of ASSET in an IGES (Initial Graphics Exchange System) file format which included general ship offsets which can be imported into IDEAS through the IGES translator. Although general bulkhead, deck, superstructure design was provided, no further details to subcompartmentized spaces, specific weights and locations of internal equipment, sonar dome offsets, and any other explicit details of the notional ship design was available. Appendix B provides a summary of the DDG 51 notional model.

2. IDEAS

IDEAS, Master Series 2.0, [Ref. 5] was utilized to model all three cases of study. The IDEAS program is comprised of a large number of applications such as design,

modeling, testing, manufacturing, and simulation, each with a large group of subtasks for the user to utilize in icon panel form or menu driven selection. The program is also a "team concept" software which allows a number of users in a design or analysis team to take individual parts of the whole model to be designed, modified, or analyzed. For each model, the Simulation Application and all its respective subtasks were utilized to create (e.g. surfacing) and mesh the finite element model for export.

a. One and Two Dimensional Models

For the one dimensional and two dimensional cavitation study, one model was required to be created which included the structure and surrounding fluid. Fluid mesh thickness could not exceed the following requirement due to numerical stability of the CFA code:

$$\frac{2\rho_w D}{\rho_s t_s} \leq 5$$

where ρ_w =density of water, ρ_s =density of steel, t_s =thickness of steel plate, and D= width of fluid elements. For example, utilizing $\rho_s/\rho_w \approx 8$, if the thickness of the plate or hull t_s =0.5 in, D ≤ 10 in. After creating all structure and fluid model regions, the following order for meshing was conducted due to the order that the CFATRAN and CFAGAL program organizes particular fluid nodes and elements:

1. Fluid volume elements (brick elements)
2. DAA boundary (thin shell elements)
3. Hydrostatic boundary (thin shell elements)

4. Specified Pressure regions (not utilized for this study, thin shell elements)

5. Wet structural surfaces (thin shell elements)

6. Remaining structural surfaces

The thin shell elements for the DAA boundary, hydrostatic boundary, as well as for the specified pressure regions if used, provide a means to select the nodes in these particular regions that the CFA requires for numerical solution. The thin shell elements do not become a part of the soluiton process but act as "markers" in the CFATRAN program for the boundary element nodes which are specifically associated by the MAT field in the NASTRAN ASCII input file. Because of the numerical processing in the USA code, node numbering needs to be described in a counter-clockwise manner looking from the fluid towards the structure. Color coding particular surfaces and their respective elements or by creating specific groups of surfaces or elements in the meshing subtask-grouping icon greatly aids in changing particular characteristics such as the node numbering.

A one psi pressure vector outward from the structure into the fluid is applied to all structural wet elements to act as a marker for the USA code fluid matrix development and restraint set conditions set for symmetric boundaries are created in the BOUNDARY CONDITION subtask.

After meshing, two copies of the global mesh are made. One FEM model will be structure only with the one psi pressure, deleting fluid elements and nodes and one FEM model will be the fluid volume elements with the DAA, hydrostatic, and wet structure thin shell elements, deleting the other dry structural nodes and elements. These two FEM models are then exported out of IDEAS and import to MSC/NASTRAN.

b. Three Dimensional Ship Model

Prior to the IGES translator task, modifications needed to be made to the actual IGES ASCII file for the correct unit system, ensuring IDEAS was preset to the same units (feet, inches, meters, etc.).

Offset points and lines.were utilized as "wire guides" to recreate the model in IDEAS for creating all surfaces through lofting, mesh of curves, or planar creation shown in Fig. 9. The following sequence proved to be the best option in creating a complete three dimensional ship model in IDEAS, Simulation, Master surfacing task:

1. HULL
2. BULKHEADS
3. DECKS
4. SUPERSTRUCTURE:

After all the surfaces have been created, all the edges must be connected or STITCHED in order for meshing to be successful and a check for free edges is performed in preparation for meshing. Any new surfaces that need to be created, such as internal bulkheads or connecting the superstructure to the hull, can be done through a surface bound by a combination of edges and three dimensional lines connecting those opposing edges.

The required thin shell element properties are applied and a one psi pressure vector must be applied to all the wet surfaces through the BOUNDARY CONDITION subtask as well as any symmetry condition through the RESTRAINT SET

icon. IDEAS provides a full series of element checks (warping, distortion, interior angles, and normal directions) which must be done for proper solution processing. Only one FEM model was required for export since the CFA program was not applied to this particular model.

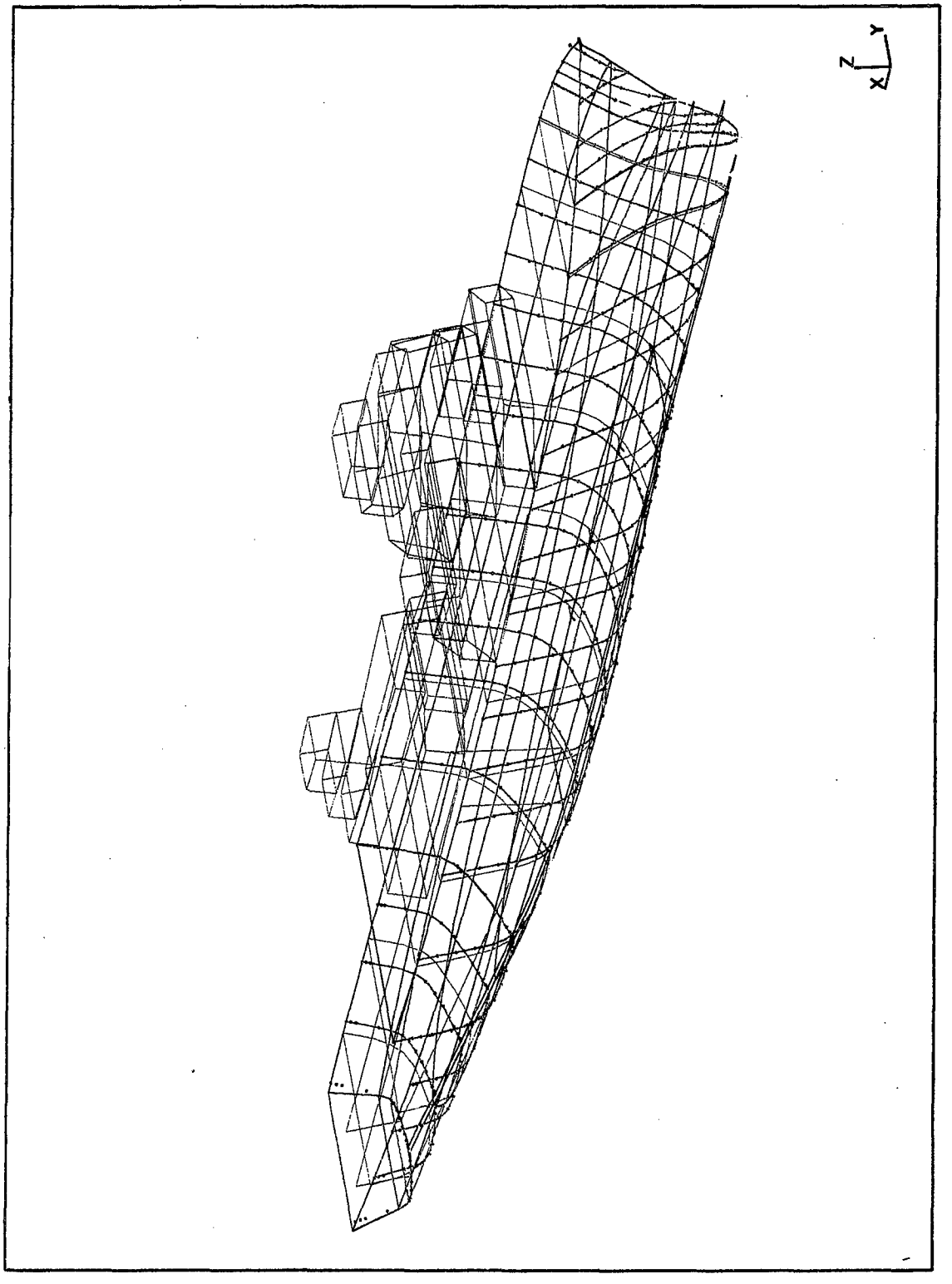

Figure 9. Imported ASSET DDG 51 Model

B. TRANSLATION

Each of the following steps allows for output files to be viewed, verifying that information (number of nodes, eigenvalues, etc.) is being properly computed and created in the unformatted fortran files for the next step.

1. MSC/NASTRAN 67.5

The MSC/NASTRAN structure database is the required format for this particular version of the USA code during the initial start and restart. The USA code itself is conducting the solution process which would normally be a SOL 109 transient analysis process in MSC/NASTRAN. Appendix B provides the DMAP alters for IDEAS post processing which is attached to the beginning of the exported file out of IDEAS and for the MSC/NASTRAN restart, deleting unnecessary and unneeded lines up the bulk data section. This process generates the geometry information and the structure's M, C, and K matrices

2. CFATRAN/CFAGAL

CFATRAN is a program modified from [Ref. 15] that takes the MSC/NASTRAN file of the fluid mesh model and groups the elements, nodes, and nodal connectivity in the required format for the CFAGAL program. CFAGAL will read the CFATRAN output and create a global access library of the fluid model and its

boundaries, just as the program FORGAL does for the structure model. This library will then be accessed during the FLUMAS process.

3. NASSKY/FORGAL

Nassky prepares the NASTRAN UT1 output file which contains the geometry and matrix data of the structure into "skyline" matrix format , a generic Fortran unformatted file. FORGAL then converts this generic file data into a GAL file (Global Access Library) database which the USA code will access for structure related data.

C. UNDERWATER SHOCK APPLICATION AND SOLUTION

Appendix B provides sample inputs for the following programs which were utilized for the two-dimensional study.

1. FLUMAS

This is the first step in the USA code which creates the fluid mass mastrix of a structure wet surface in an infinite, inviscid, incompressible fluid by the boundary element technique. The key inputs here are the following [Ref. 16,17]:

1. Mesh Geometry: fluid wet-surface and structure wet-surface mesh
2. Element definitions: general curved surface or surface of revolution
3. Material Property: mass density, speed of sound, DAA2 parameter
4. Constraint options: location of free surface, half model, quarter model, long

cylinder, node reassignment in fluid-structure transformation if needed.

For cavitation studies, the CFA is activated and the fluid volume database created by CFAGAL is incorporated with the FLUMAS output. Care should be exercised here during CFA solutions. The NCAV field refers to the number of elements on the wet structure plus the DAA boundary. During non-CFA runs, the NCAV field refers only to the wet elements on the structure since this defines the DAA boundary.

2. AUGMAT

This process in the USA code utilizes the equations specified earlier as the "augmented equations" by utilizing the data in the GAL file and FLUMAS output to construct the specific matrices. The key inputs are the following [Ref. 16,18].

1. Fluid and Structure mass matrices
2. Structural DOF correspondance table
3. Fluid mesh geometry
4. Fluid/Structure DOF transformation coefficients
5. Type of solution to be conducted: plane wave, DAA2 options

3. TIMINT

This step constitutes the most time consuming step depending upon on the number of nodes, elements, and requested length of time to be studied. The

unconditionally stable staggered soluiton technique is utilized which basically involves the following [Ref. 16,19]:

1. Estimating the unknown structural restoring force $[K_s]\{x(t)\}$ at $t + \Delta t$ from the extrapolation of current and passed values.
2. Solve the fluid equation and obtain a preliminary estimate of the total pressure vector at $t + \Delta t$.
3. Solve the structural equation for the displacement and velocity vectors at $t + \Delta t$.

Other steps are involved between these particular steps for matrix transformations and improved accuracy. General inputs from the user involve the following:

1. Incident wave characteristics: location and type of charge source, standoff, specified pressure profile, exponentially decaying wave.
2. Time step information: start and finish times, increments.
3. Display data of particular nodes for checking output results in the solution file:desired node number and freedoms for displacement, velocities, or pressures on the DAA boundary.

Although unconditionally stable, the user should utilize small enough time steps to capture accurate model behavior. Solution time history responses of all structural nodes and fluid nodes for all runs are stored in the file designated POSNAM in the TIMINT input.

D. POST-PROCESSING

Two methods of post processing was done due to the growing amounts of required memory for larger models such as the three dimensional ship hull.

1. XUDVT

This second interface program converts the USA solution history in the corresponding MSC/NASTRAN data block, UDVT, a file format readable by MSC/NASTRAN. The initial MSC/NASTRAN job is restarted at the point just before the NASSKY translation, allowing MSC/NASTRAN to continue to a normal conclusion. The USA solution replaces that which would normally be generated by MSC/NASTRAN in a transient analysis.

During CFA studies, the number of wet points required to be entered are those wet points totals generated by NASSKY which can be found in the nassky.out file. However, during non-CFA studies, the wet points refer to the total number of wet element faces. If the incorrect number of wet points or wet elements are entered, translation will fail or data history for some nodes will not be translated. XUDVT also allows displacement, velocity, acceleration, and pressure histories to be extracted in ASCII table format and placed in the PLT file for X-Y plotting by other programs (e.g. MATLAB).

2. POSTPR

This is a USA postprocessing program which allows extraction of particular node displacement, velocity, or pressure histories. Although not needed for non-CFA studies, this is the only current method which one can extract pressure history profile of fluid nodes during a CFA study. The data is placed in ASCII column tables which can be plotted by other programs such as Matlab. Due to the large solution files generated by the three dimensional ship model and the growing size of files during the XUDVT-MSC/NASTRAN-IDEAS translation and final post-processing, POSTPR proved to be a memory saving tool. The user must ensure the original UT1 file name is either deleted or changed in order to prevent a XUDVT failure since this process produces a UT1 file for the MSC/NASTRAN restart.

3. MSC/NASTRAN (restart)

Appendix B illustrates the required fields needed to restart MSC/NASTRAN with a new UT1 file created by the XUDVT process. This process utlizes the original model.MASTER file originally created by the initial MSC/NASTRAN run and creates a solution file for IDEAS to import (model.OP2) which contains all or selected time histories of displacement, velocity,acceleration, and stress. The user should utilize a different .OP2 file name from that of the .OP2 file created in the first MSC/NASTRAN run. Files usually triple in size compared to the POSNAM file output from TIMINT.

4. IDEAS

The final .OP2 file can be imported into IDEAS through the FILE IMPORT-MSC/NASTRAN process. IDEAS will create a universal file (.unv) prior to actually creating a model file database. This unversal file is usually three times the memory file size of the .OP2 and model.POS file due to being in ASCII format. Model file database size (file.sf1 and file.sf2) become approximately the same size as the universal file. Hence, a user should ensure plenty of hard drive memory is available during this translation phase, especially for large models (> 2000 elements).

IV. ONE-DIMENSIONAL ANALYSIS

A. PLATE MODEL

A one dimensional study was conducted utilizing the case defined by [Ref. 7] which involved modeling a floating plate on the surface of a bilinear fluid. The goal of this model was to accomplish the same results shown in [Ref. 7] by creating a finite element model and solving with the USA code. Follow-on study was performed by Newton [Ref. 20] in area of cavitation in support of developing a "shock shield," a gas-filled cushion that was to surround the exterior of a submarine hull and reduce the magnitude of underwater shock loads transmitted through the hull.

Fig. 10 and Table 1 describe the particulars of the Bleich-Sandler case.

1 thin shell element, 4 nodes, 1" thick
Symmetry on all four edges
Dimensions: 1.5"x 1.5"
E=30.0 x 10^6 psi
Poisson's ratio=0.3
Mass density=5.32986 x 10^{-4} lb_f/in^3

Table 1. Plate Characteristics

Fluid Depth: 150.0 in
100 volume elements, 8 nodes, 1.5"X1.5" 1.5"
404 total fluid nodes
Mass density= 9.3455 x 10^{-5} lb s^2/in^4
Speed of sound= 5.712 x 10^4 in/sec

Table 2. Fluid Characteristics

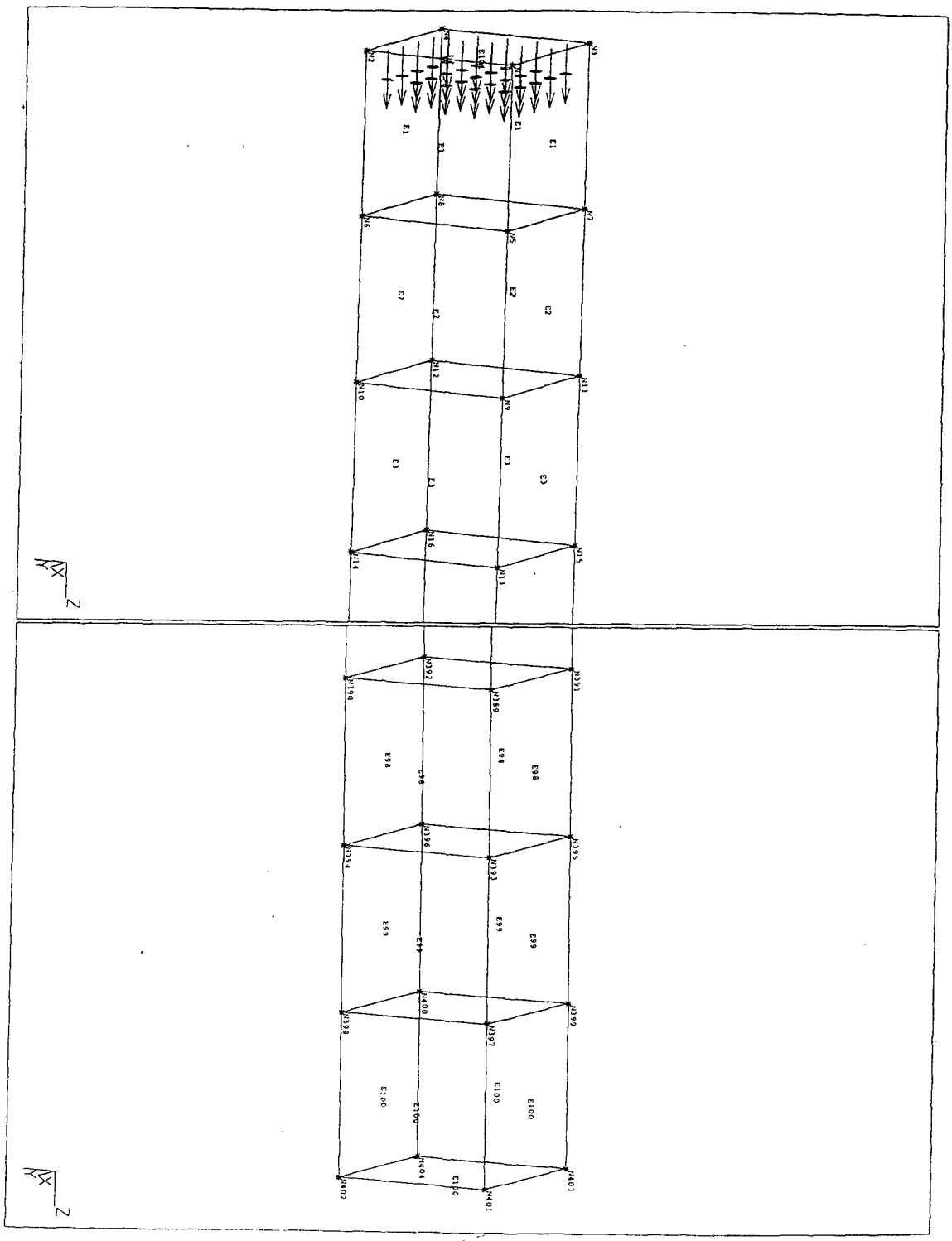

Figure 10. IDEAS Bleich Plate and Fluid

Peak pressure =103 psi Decay time= 9.958 E-4 sec Charge depth = 1.0 E7 in, centered on the center of the plate

Table 3. Incident Pressure Characteristics

B. RESULTS

Utilizing a time step size of 1.313 x 10^{-5} sec, 1200 time steps were collected. With the CFA interface turned on with the USA, program Fig. 11 depicts the computed velocity and pressure at the plate. Fig. 12 depicts pressures at specific locations along the column of fluid. Because of the numerical computation scheme within the USA code, time zero noted on each pressure figure refers to the point in time that the incident pressure wave arrives at that particular fluid node and not the global time of plate motion. Total pressures at time zero for each fluid node is the sum of the atmospheric, hydrostatic, and incident pressure wave at that point of arrival from the initial charge location and applied exponential decay. Fig. 11 illustrates that the cavitation region does not touch the interface boundary between the fluid and the plate. Node 401 in Fig 12 confirms the cavitation region is captured by the fluid FEM and does not extend beyond the DAA boundary. Fig. 13 depicts the plate velocity and pressure with CFA OFF.

Calculated time periods of zero pressure or cavitation occurrence grow to a period of .008 sec half-way through the column and stay approximately the same to the end of the fluid column. In addition, the CFA captured the cascading effects of cavitation closure which occured at similar times following incident pressure wave arrivals at each

fluid node and closure pressures became larger at deeper depths than at the surfaces. This closure phenomenon begins at the point t=.0108 sec at which the plate experiences an immediate velocity cutoff of the downward direction back to zero by the arrival of this "secondary shock" at the plate. Pressure at this particular time jumps to approximately 14% of the peak pressure and creates an upward velocity of approximately 16% which brings the plate velocity back to zero. Multiplying time by 1004.22 to get it in terms of decay time units of the incident wave and normalizing velocity to 1/1000 of the speed of sound with a sign change due to the z-axis for verical displacement being defined downward into the fluid, calculated results match those (Fig.14) with Bleich and Sandler as shown in Fig. 15 and 16.

Hence, the finite element modeling approach with the USA/CFA code produced identical results as those shown by Bleich and Sandler through the method of characteristics [Ref. 7]. In addition to the pressure history profile of Fig. 15, USA postprocessing was able to display the cavitation closure anywhere in the fluid column.

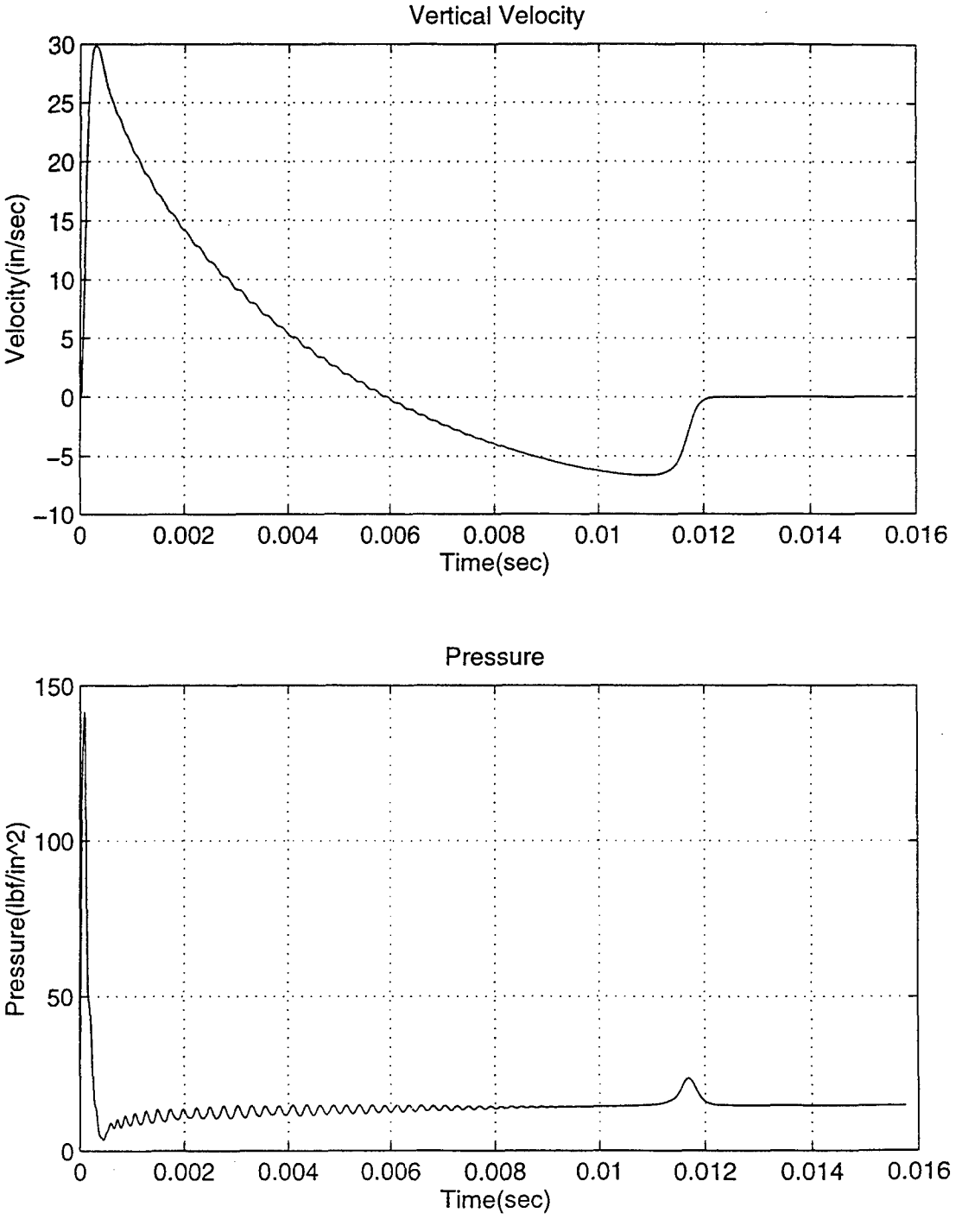

Figure 11. Bleich Plate Velocity and Pressure (CFA ON)

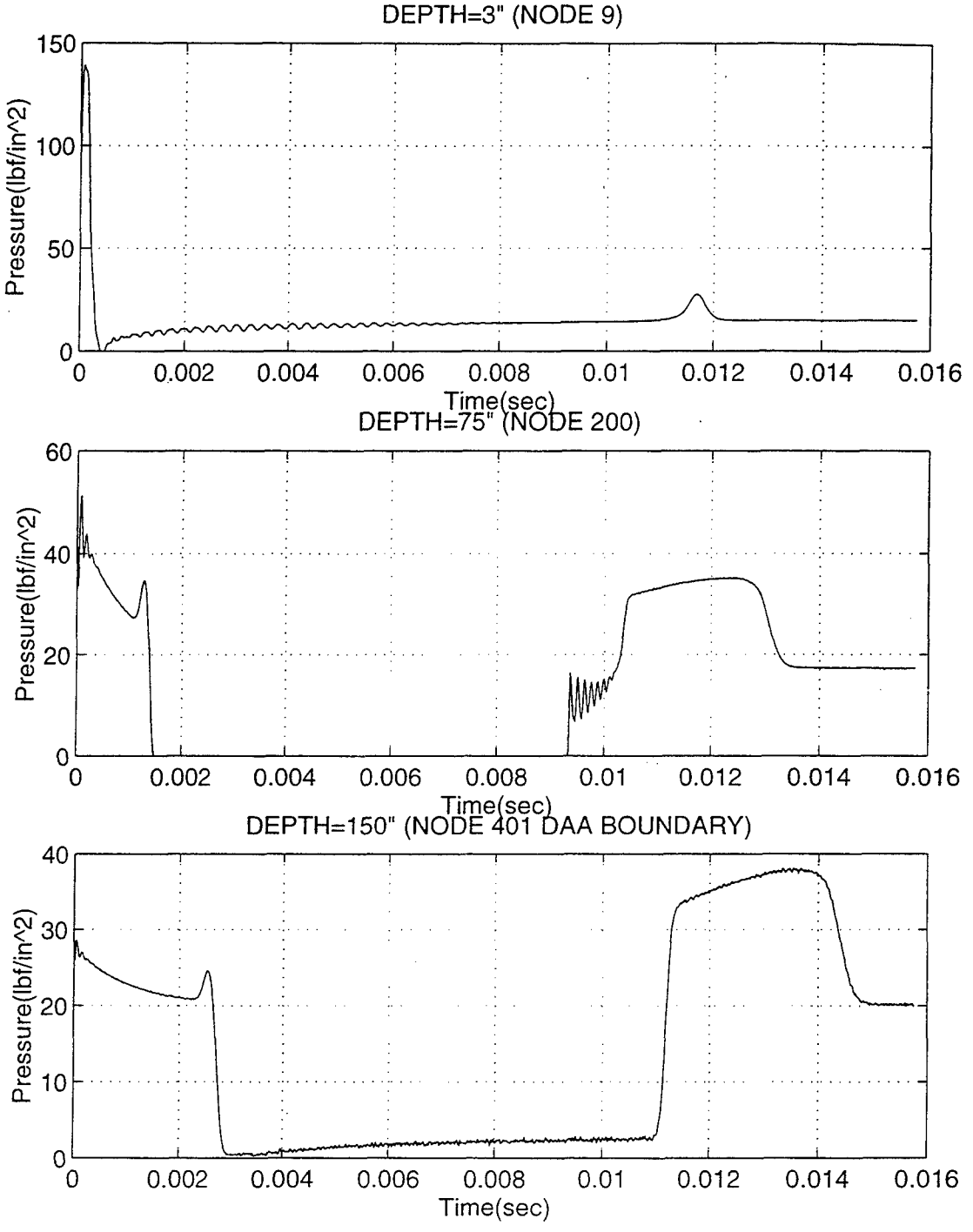

Figure 12. Bleich Fluid Pressure at Nodes 9, 200, and 401. (CFA ON)

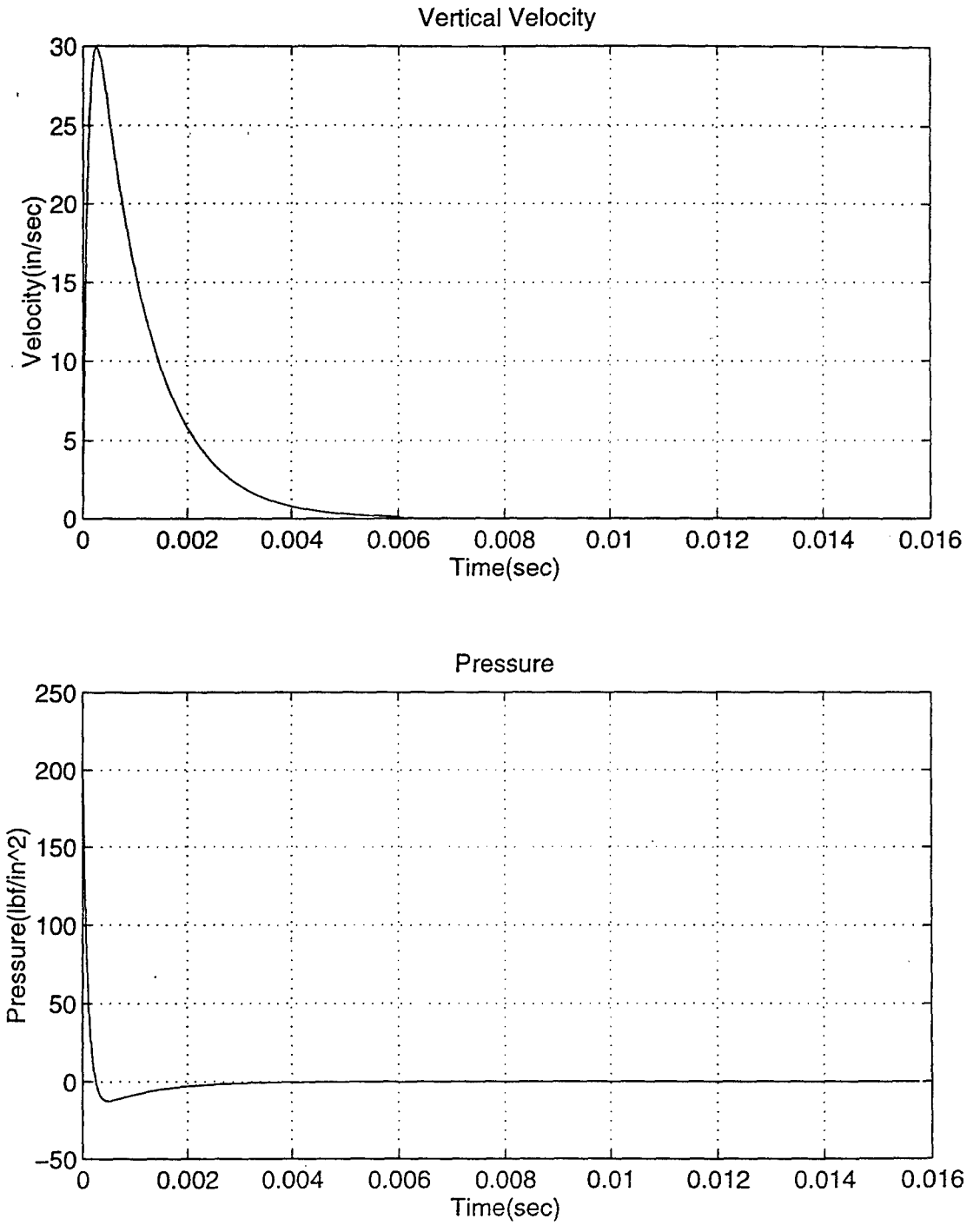

Figure 13. Bleich Plate Velocity and Pressure (CFA OFF)

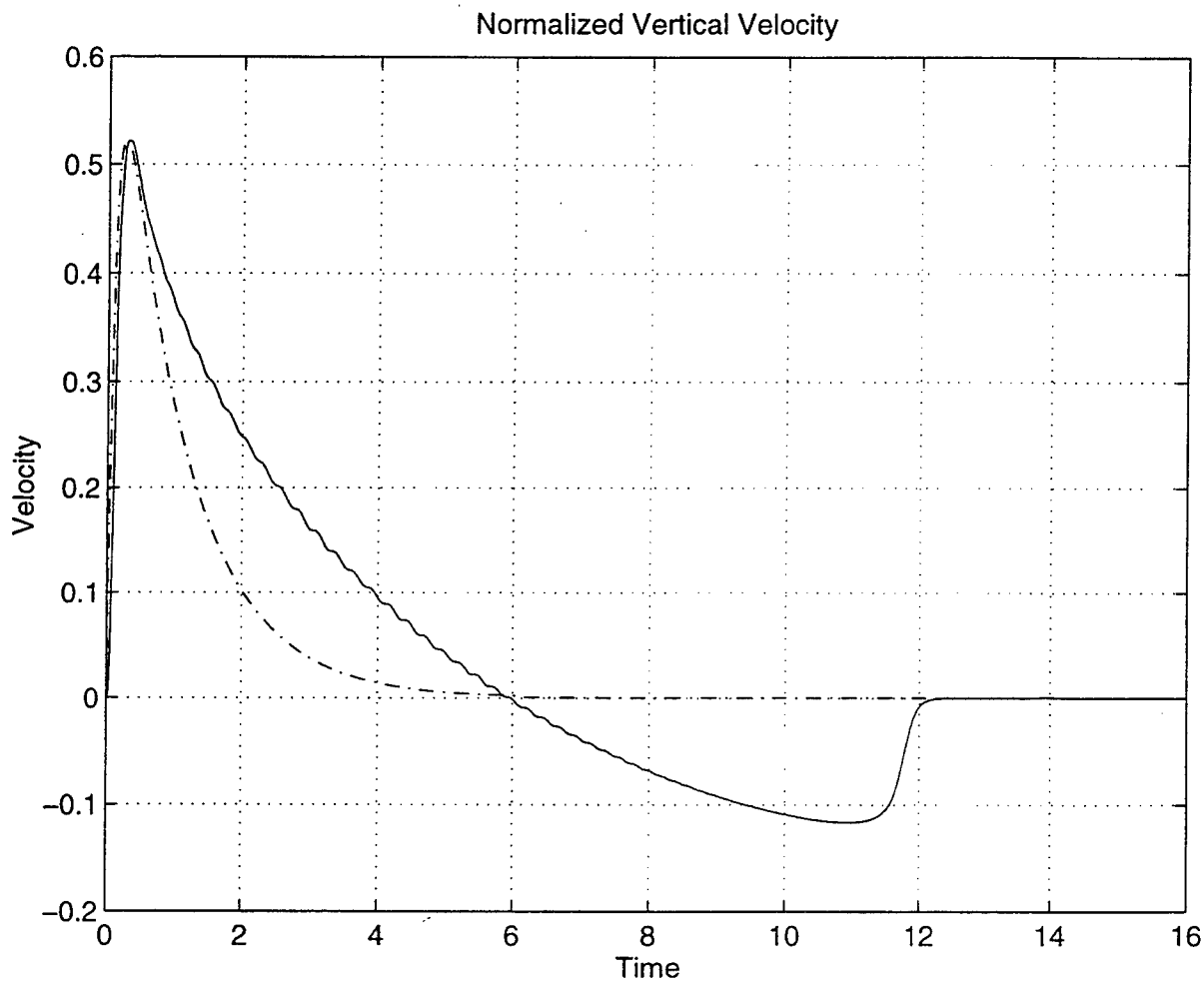

Figure 14. Normalized Vertical Velocity (–CFA ON, -. CFA OFF)

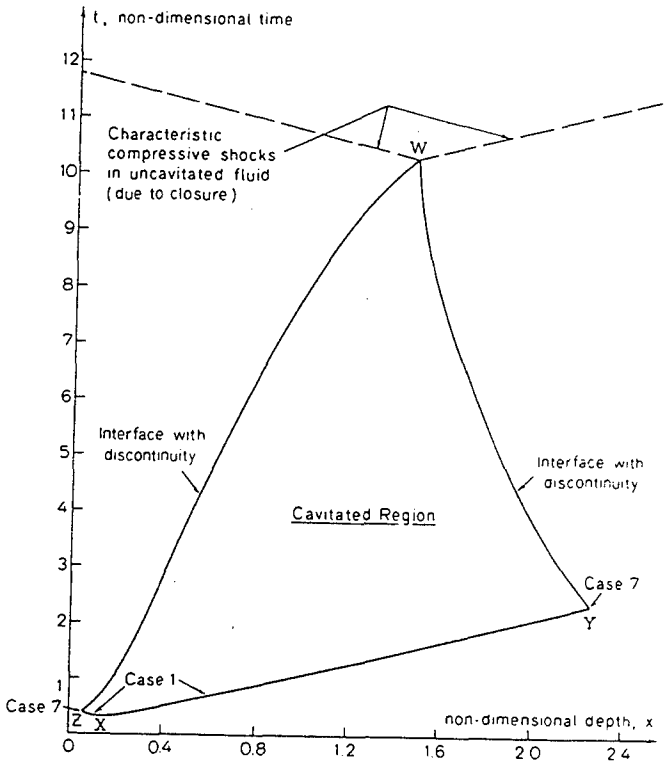

Figure 15. Time history of cavitated region [Ref. 7]

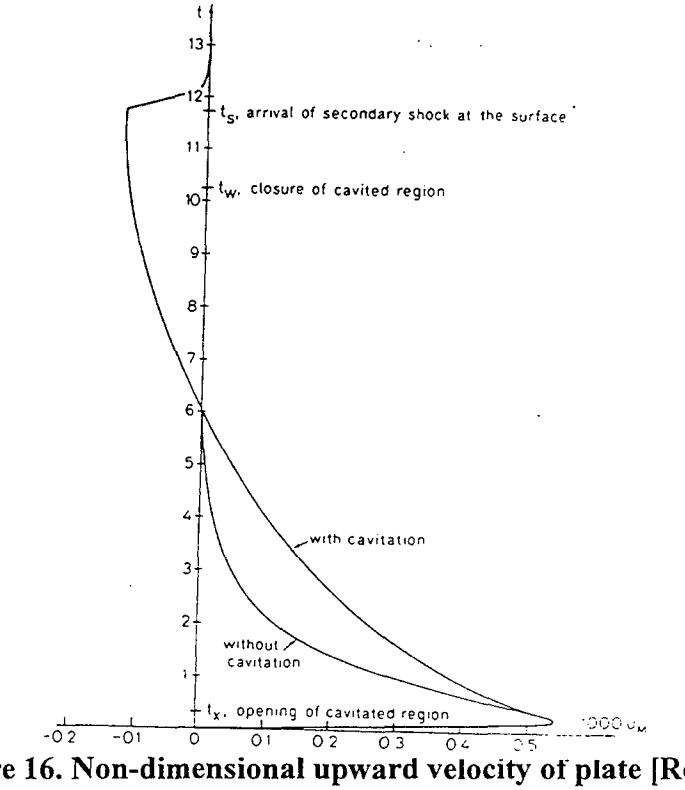

Figure 16. Non-dimensional upward velocity of plate [Ref. 7]

V. TWO DIMENSIONAL PROBLEM

A. CROSS-SECTIONAL HULL

The mid-section of the imported wireframe hull of the DDG model was utilized for this particular study, assuming structural properties remain linear throughout the process. Previous work conducted by Newton [Ref. 21] in the area of a two dimensional study involved a symmetric cylinder submerged underwater exposed to a plane wave incident shock front, utilizing earlier Fortran finite element programs for meshing, propagation of underwater shock, and transient response calculations.

The goal in this particular model is to study responses, specifically peak velocities, with and without cavitation effects, of a surface ship model with a draft of 20 feet. The time frame was limited to the first 30 msecs, in an attempt to eliminate the effects of the bubble pulse while comparing plane wave modeling and DAA2 spherical.

Utilizing the USA code, Fig. 17 illustrates location of cross section in the global ship wireframe, 1 foot in depth, and Fig.18 to Fig. 20 illustrate the meshed model. In Fig. 18, red donotes the structure mesh while green denotes the fluid mesh. Fig. 20 depicts the outer DAA, hydrostatic, and structural interface elements mentioned previously. Tables 4-6 provide specific model characteristics.

TOTAL NUMBER OF GRID POINTS	452
TOTAL NUMBER OF THIN SHELL ELEMENTS	230
THICKNESS OF ELEMENTS	0.5 in
TOTAL NUMBER OF WET ELEMENTS	40

Table 4. Structure Characteristics

MODULUS OF ELASTICITY (ksi)	29600.0
DENSITY (lbm/ft^3)	489.02
YIELD STRENGTH (ksi)	51.00
POISSON'S RATIO(ν)	.3

Table 5. Element Properties

NUMBER OF FLUID NODES	3034
NUMBER OF FLUID VOLUME ELEMENTS	1440
NUMBER OF DAA FACE ELEMENTS	40
NUMBER OF HYDROSTATIC PRESSURE FACE ELEMENTS	72
NUMBER OF PRESCRIBED PRESSURE FACE ELEMENTS	0
FACE ELEMENTS CONTACTING STRUCTURE	40
MAXIMUM NUMBER OF FLUID VOLUME NODES	8
MAXIMUM NUMBER OF FACE ELEMENT NODES	4

Table 6. Fluid Characteristics

Utilizing the bulk cavitation program to determine the extent of various bulk cavtiation zones of a TNT explosion, the smallest region of bulk cavitation takes place directly above the charge at the surface. Therefore, a charge location directly beneath the hull at 100 feet standoff (depth = 120 feet) would minimize effects of the bulk cavitation zone in the general vicinity of the hull model and provide a means for setting the lower edge of the DAA boundary just beyond the cavitating region at a depth of 50 feet, 30 feet under the keel.

B. RESULTS

Fig. 21 to Fig. 30 record the velocities at the locations in the structure and time varying pressures at locations in the fluid volume region for the CFA analysis noted on Fig. 19. Fig. 31 to Fig. 33 provide a comparison of keel velocities and accelerations. The

pressure profiles, like that seen in the one-dimensional analysis, reflect a respective time zero which starts at the point of incident pressure wave arrival at that particular node and not the initial time of structure motion. Structure motion is derived from the cumulative integration of all the pressure profiles in the fluid region superimposing each pressure profile at different spatial locations in time.

The introduction of a fluid mesh beneath the structure and the turning on CFA captured the pressure varying fluid under the hull (Fig. 21 and 24) which significantly effected the velocity response of the hull. The cavitation effects on the hull during plane wave and DAA2 calculations produced almost identical results in the early time phase of hull velocity at the keel (node 42) which was the closest to the charge location. As expected in late time response, the plane wave solution begins to slightly vary from the DAA2 calculations. However, peak velocity response are the same in early time.

Pressure profiles at the keel for both CFA models (Fig. 21 and 24), which are practically identical, indicate the first signs of cavitation closure pressure occurring at a much earlier time compared to the Bleich-Sandler case with an appreciably larger pressure peak, 41% of the initial pressure wave. Numerous other cavitation closure events occur at the keel with decreasing max pressures. This observed behavior was also an event reported in the DDG-53 USS John Paul Jones Live Fire and Testing Shock Post report [Ref. 22] which may have contributed significantly to large accelerations at particular electrical switchboards following the incident pressure wave.

Keel velocities in the plane wave (CFA OFF) and DAA2 (CFA OFF) analysis, which places the DAA boundary at the ship's wet hull surface, did not capture the

detailed high frequency response of the structure exposed to identical underwater explosion conditions (Fig. 27 and 29). Peak keel velocities were identical in magnitude and occurrence in time but greatly diverged past reaching the peak velocity of 162 in/sec. Pressures along the keel during both CFA OFF calculations were found to include only the large initial pressure wave arrival and small variations in the pressure later in time along the wet hull, while those in the DAA2 calculation being slightly larger.

Internal deck velocities, however, revealed velocities greater during the plane wave modeling with a surrounding fluid mesh and CFA ON (Fig. 22). The pressure and corresponding variations along the wet surface of the hull caused internal velocities to be greater than those seen in the DAA2 CFA ON solutions (Fig. 25), primarily due to the less accurate calculations late in time for the plane wave equations and higher velocity response calculations. Both CFA OFF runs (Fig. 28 and 30) reveal small variations in velocity, the greatest occuring at the lowest deck. These small velocites could be attributed to the simplified cross sectional hull model which does not include any internal longitudinal or transverse bulkheads. If these particular bulkheads were modeled between decks, the transit velocity responses of the keel could have been transmitted to the upper decks instead of the bending the outer hull only.

Fig. 31 depicts the overlay of velocities of all 4 models (plane wave with and without CFA, DAA2 with and without CFA) at the keel, illustrating the larger velocities of the CFA OFF calculations for both plane wave and DAA2 modeling. Plane wave modeling of the underwater explosion incident pressure wave without a fluid mesh provides for a conservative approach in calculating the peak velocity of the structure at

the fluid structure interface. A shift to a higher velocity at an earlier time was more pronounced during this particular CFA study in comparison to the Bleich-Sandler case with a 22 % increase in peak velocity. Appreciable differences in acceleration were noted between CFA ON and CFA OFF calculations (Fig. 32 and 33). CFA OFF results reflected initial accelerations 3.5 times larger than CFA ON results but with no following variations.

Peak velocities in each case are provide in Table 7.

LOCATION	Node	Plane wave (CFA ON)	DAA2 (CFA ON)	Plane wave (CFA OFF)	DAA2 (CFA OFF)
Keel	42	124	124	162	162
Inner Bottom	3209	Increasing	Increasing	Increasing	4.3
Deck 3	3234	Increasing	Increasing	.094	.13
01 Level	3162	Increasing	Increasing	2.7E-4	Increasing

Table 7. Maximum Velocities (in/sec)

The responses labeled "increasing" in Table 7 reflect increasing values at the end of the time period studied.

Fluid pressures at nodes 3021, 1600,and 2994 during both plane wave and DAA2 CFA ON calculations (Fig.23 and 26) show similar relative patterns of growing numbers and durations of cavitation periods as depth decreases. The magnitude of peak pressures following initial cavitation in the DAA2 results tended to be 15-20% larger than the plane wave peak pressures. Node 3021 pressures during both CFA ON calculations at t=.0025 secs captured the largest peak pressure, followed by Node 2994 at t=.0047 secs.

Hence, based on the results, the best conservative approach to modeling a surface ship exposed to an underwater explosion would be to apply the plane wave incident pressure wave in a fluid mesh that surrounds the entire wet surface of the ship.

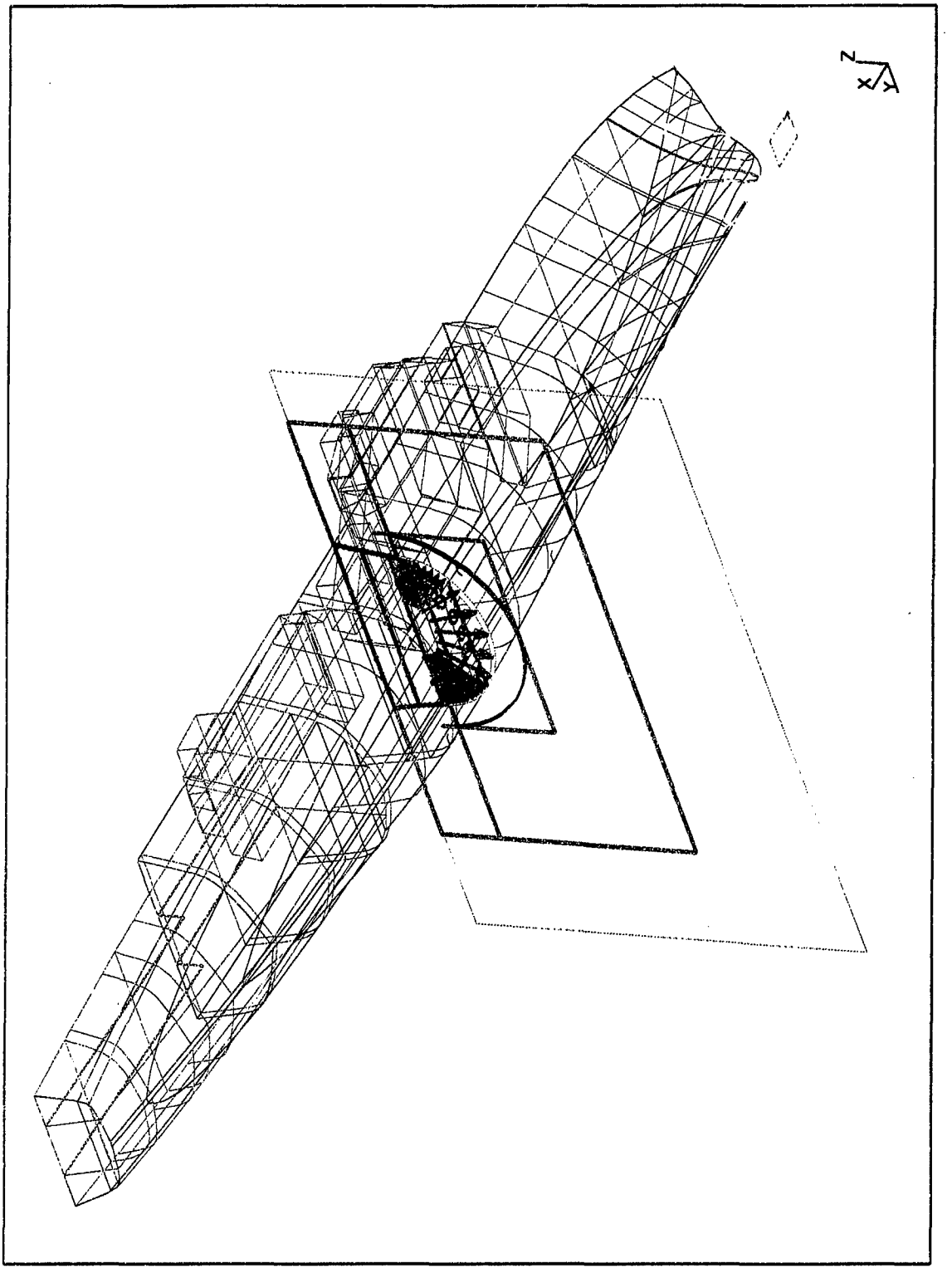

Figure 17. Wire Cross Section

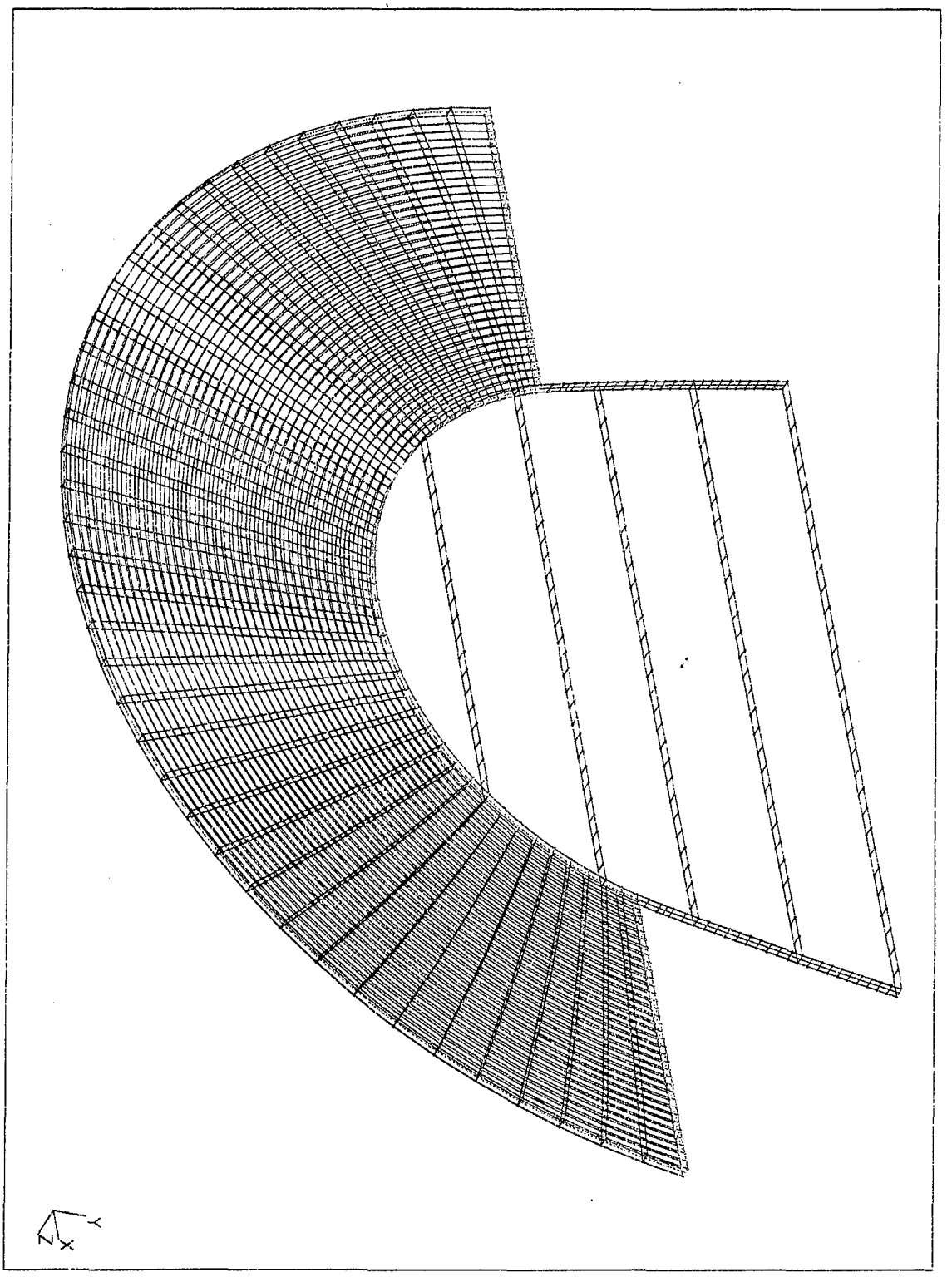

Figure 18. Structure and Fluid FEM

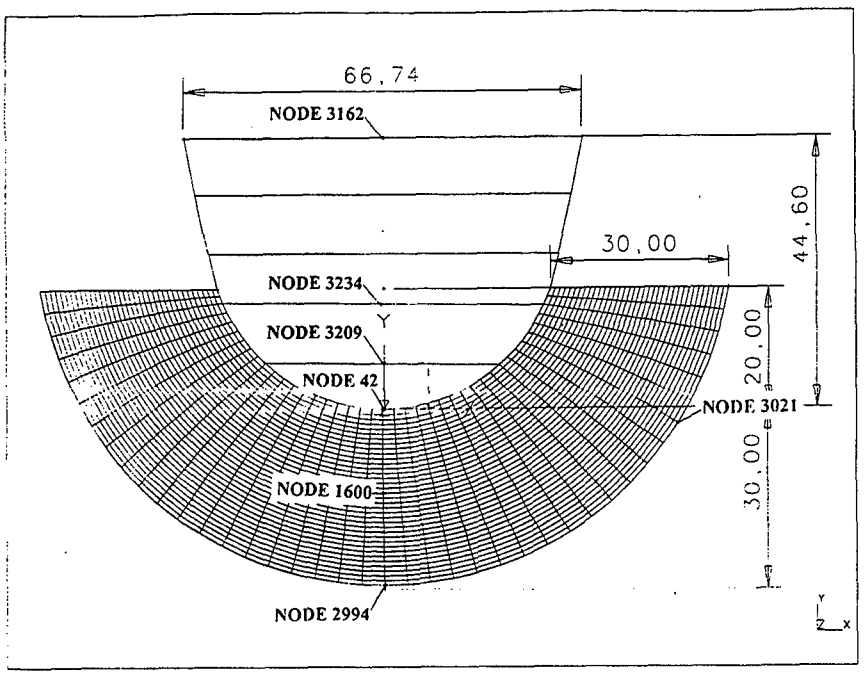

Figure 19. Cross Section Dimensions

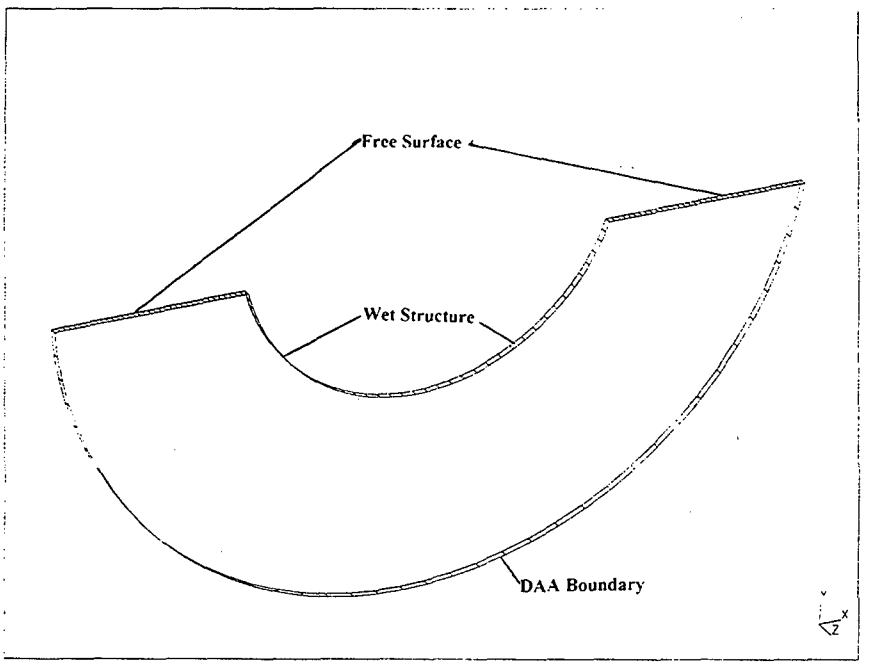

Figure 20. DAA, Hydrostatic, and Wet Structure Boundaries

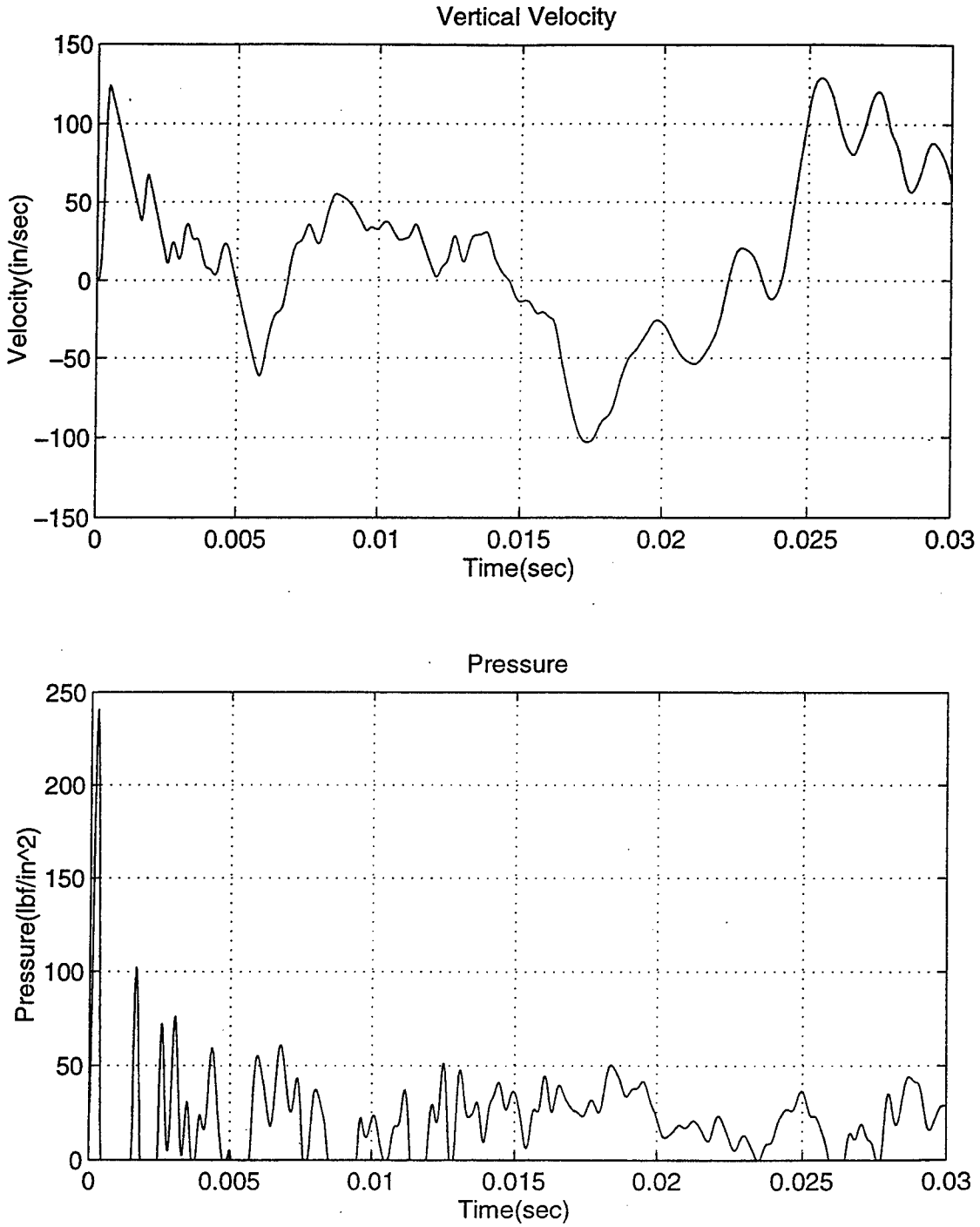

Figure 21. Velocity and Pressures at the Keel (Node 42)-Plane wave, CFA ON

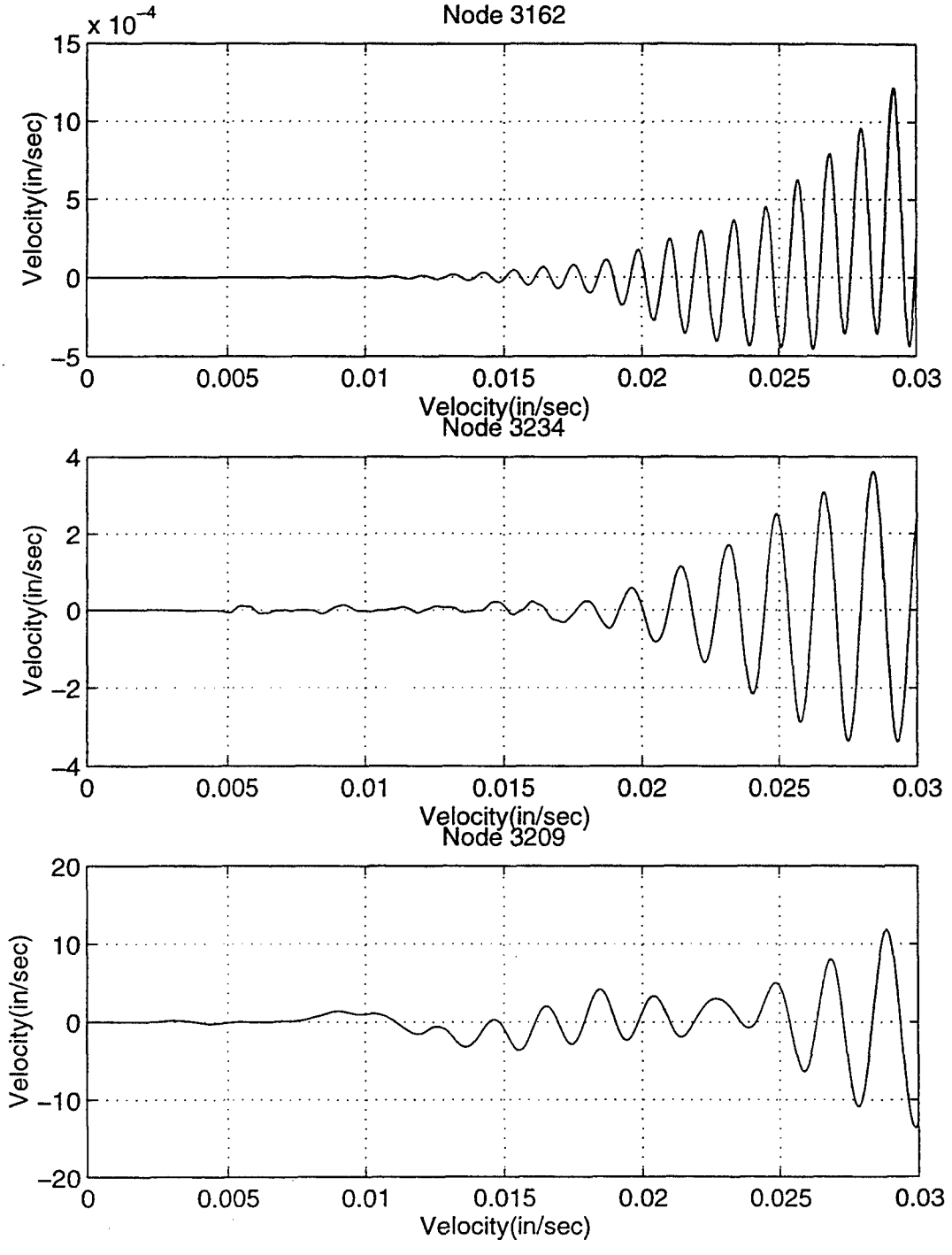

Figure 22. Internal Deck Velocities-Node 3162(top), Node 3234 (middle), Node 3209 (bottom).Plane wave, CFA ON

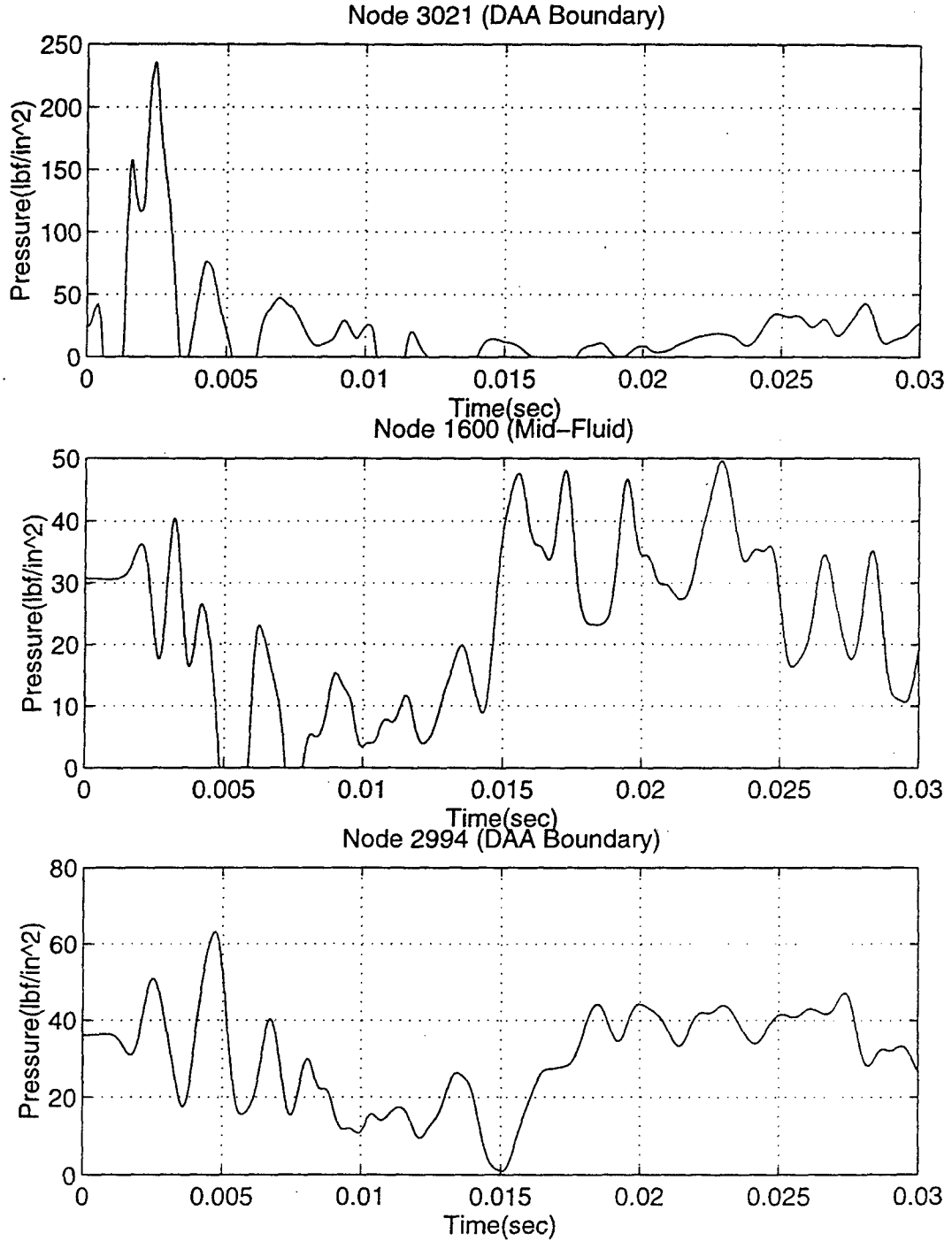

Figure 23. Fluid Pressures-Node 3021 (top), Node 1600 (middle), Node 2994 (bottom). Plane wave, CFA ON

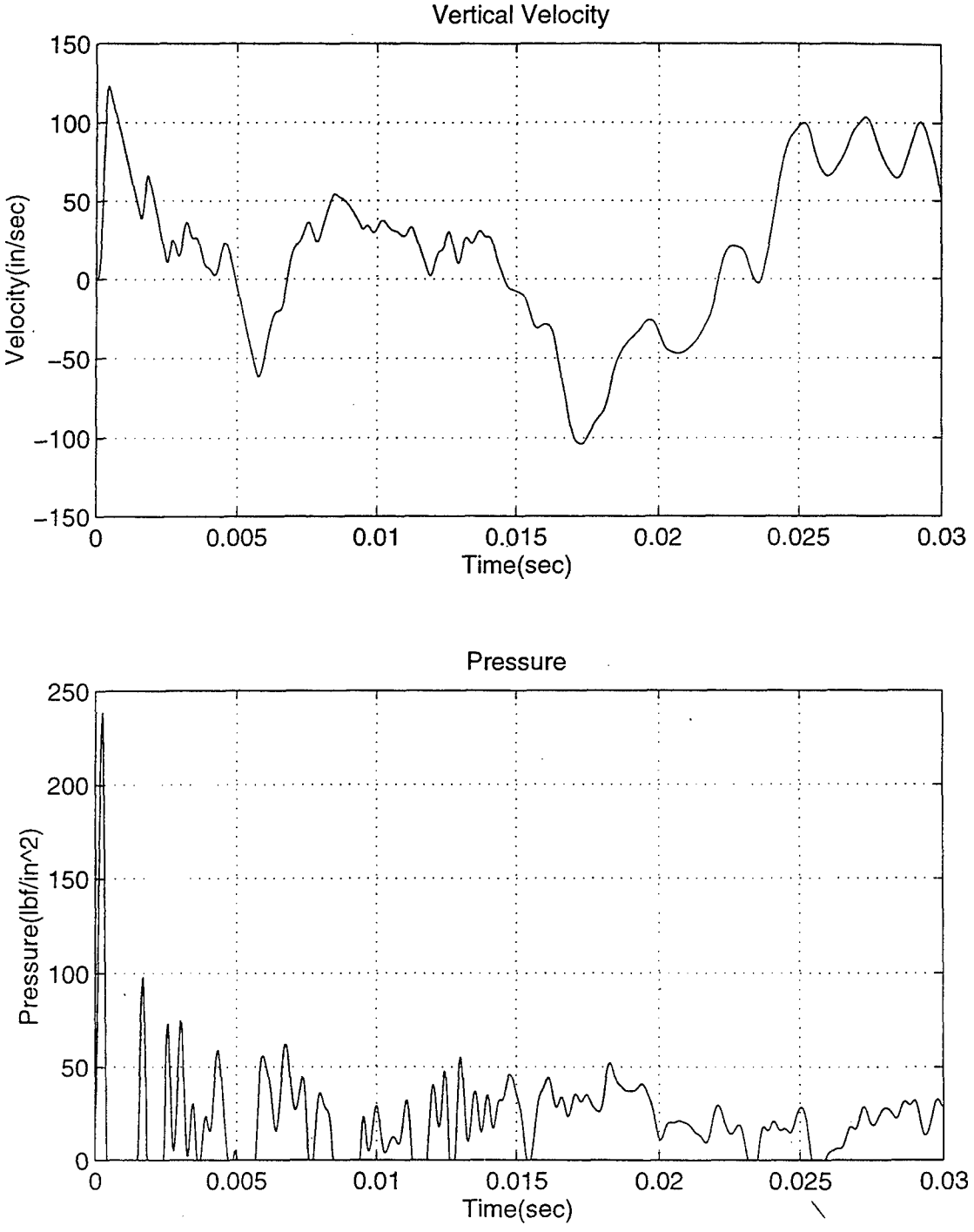

Figure 24. Velocity and Pressure at the Keel (Node 42)- DAA2, CFA ON

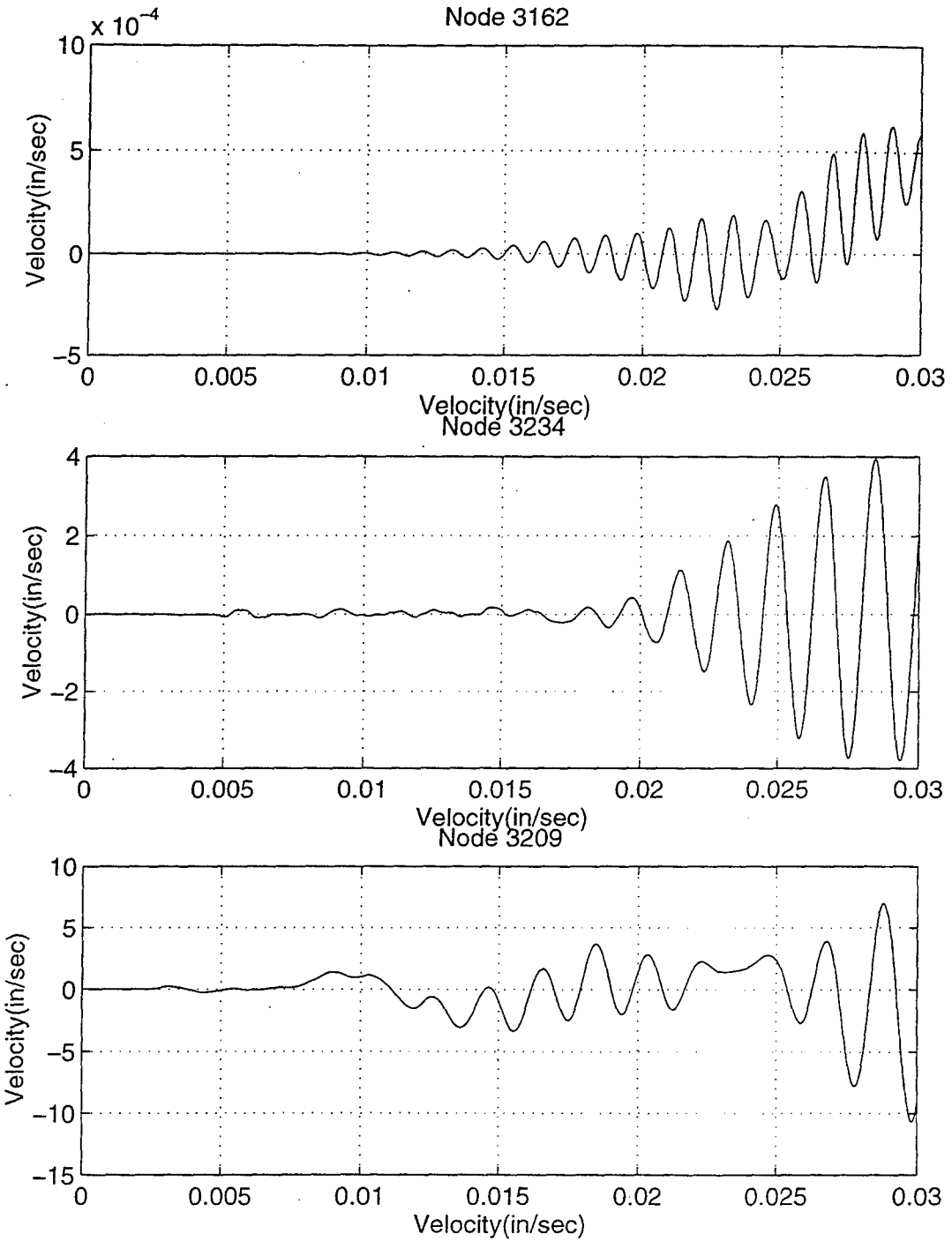

Figure 25. Internal Deck Velocities- Node 3162 (top), Node 3234 (middle), Node 3209 (bottom). DAA, CFA ON

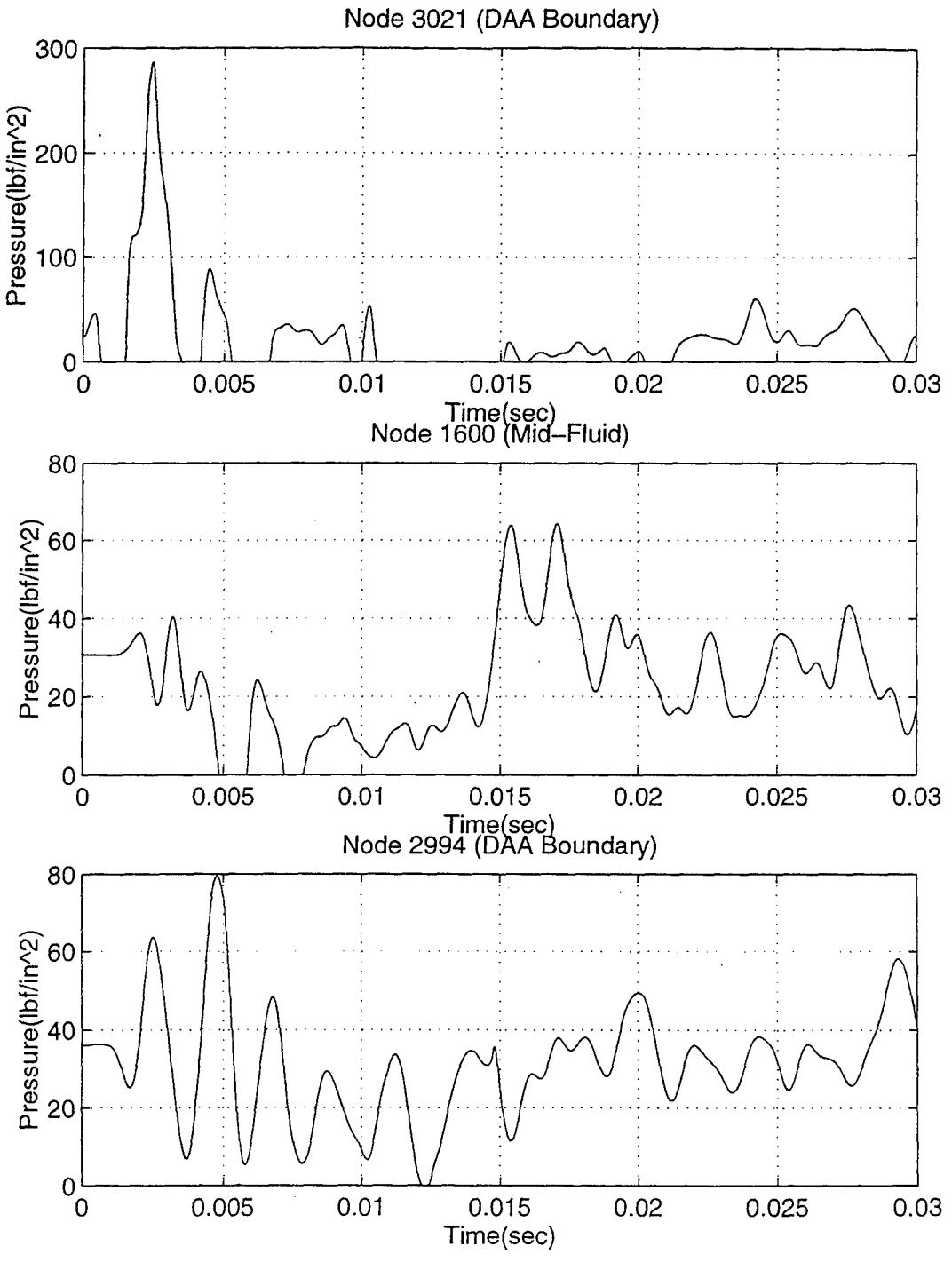

Figure 26. Fluid Pressures-Node 3021 (top), Node 1600 (middle), Node 2994 (bottom). DAA2, CFA ON

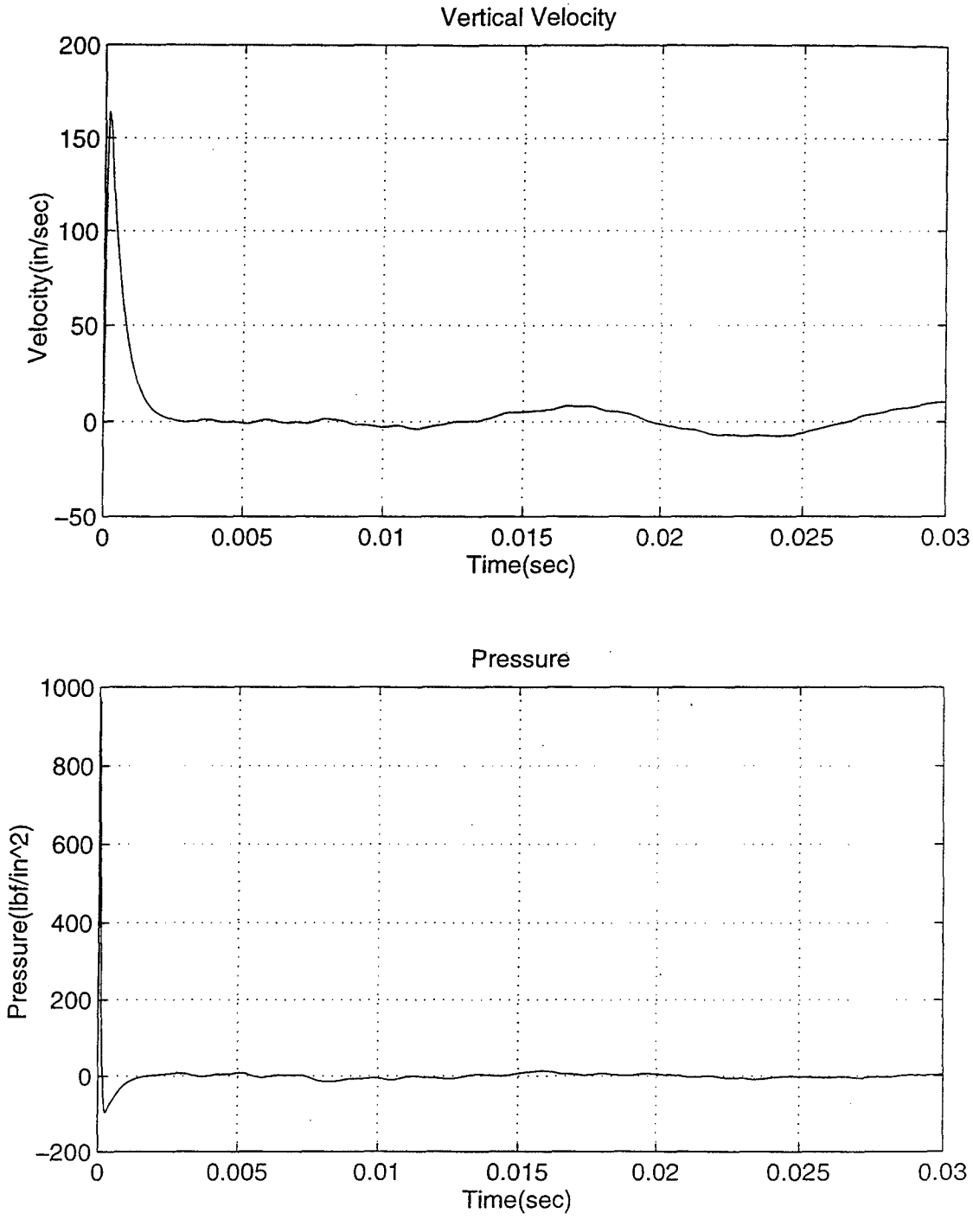

Figure 27. Velocity and Pressure at the Keel (Node 42)-Plane wave, CFA OFF

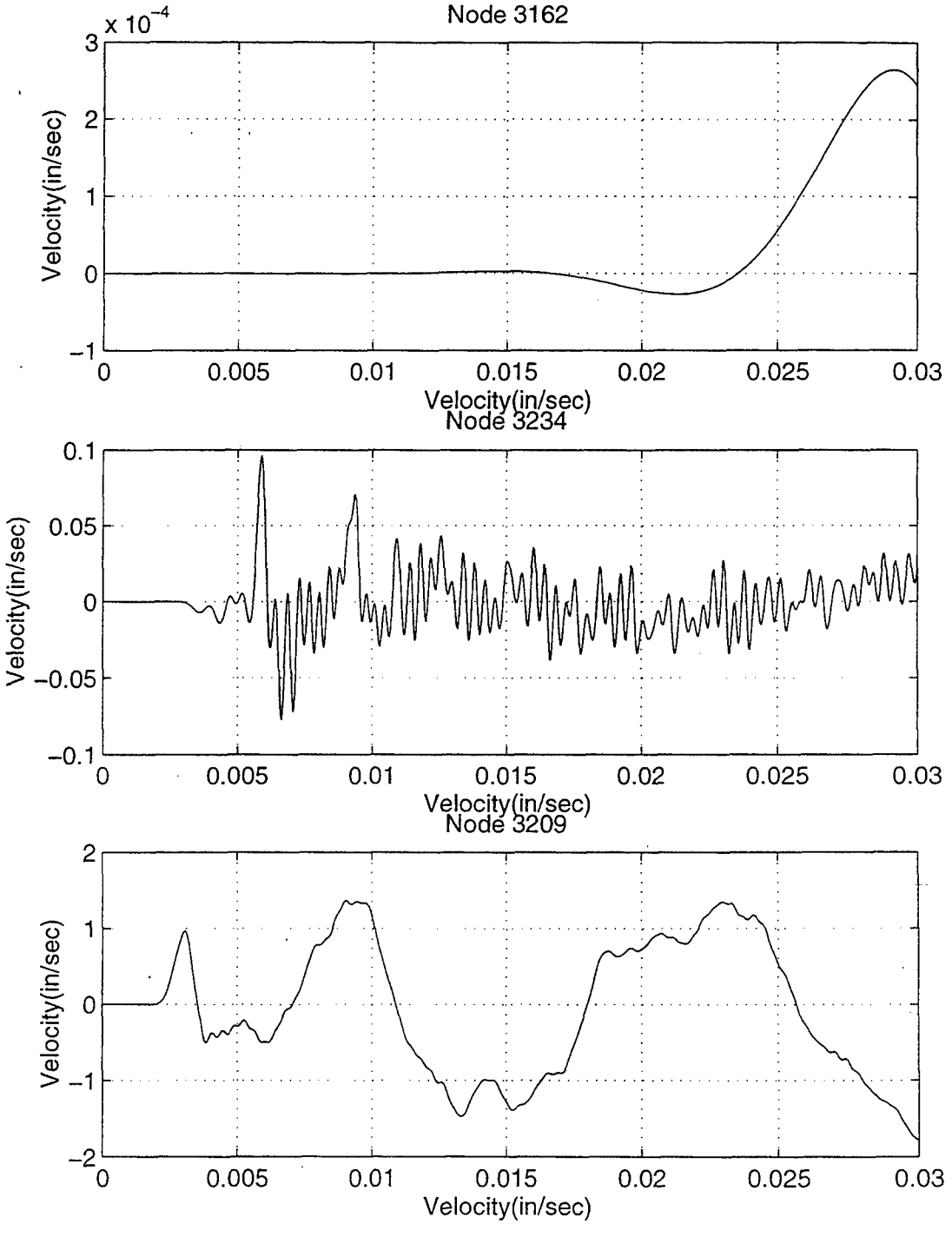

Figure 28. Internal Velocities-Node 3162 (top), Node 3234 (middle), Node 3209 (bottom). Plane wave, CFA OFF

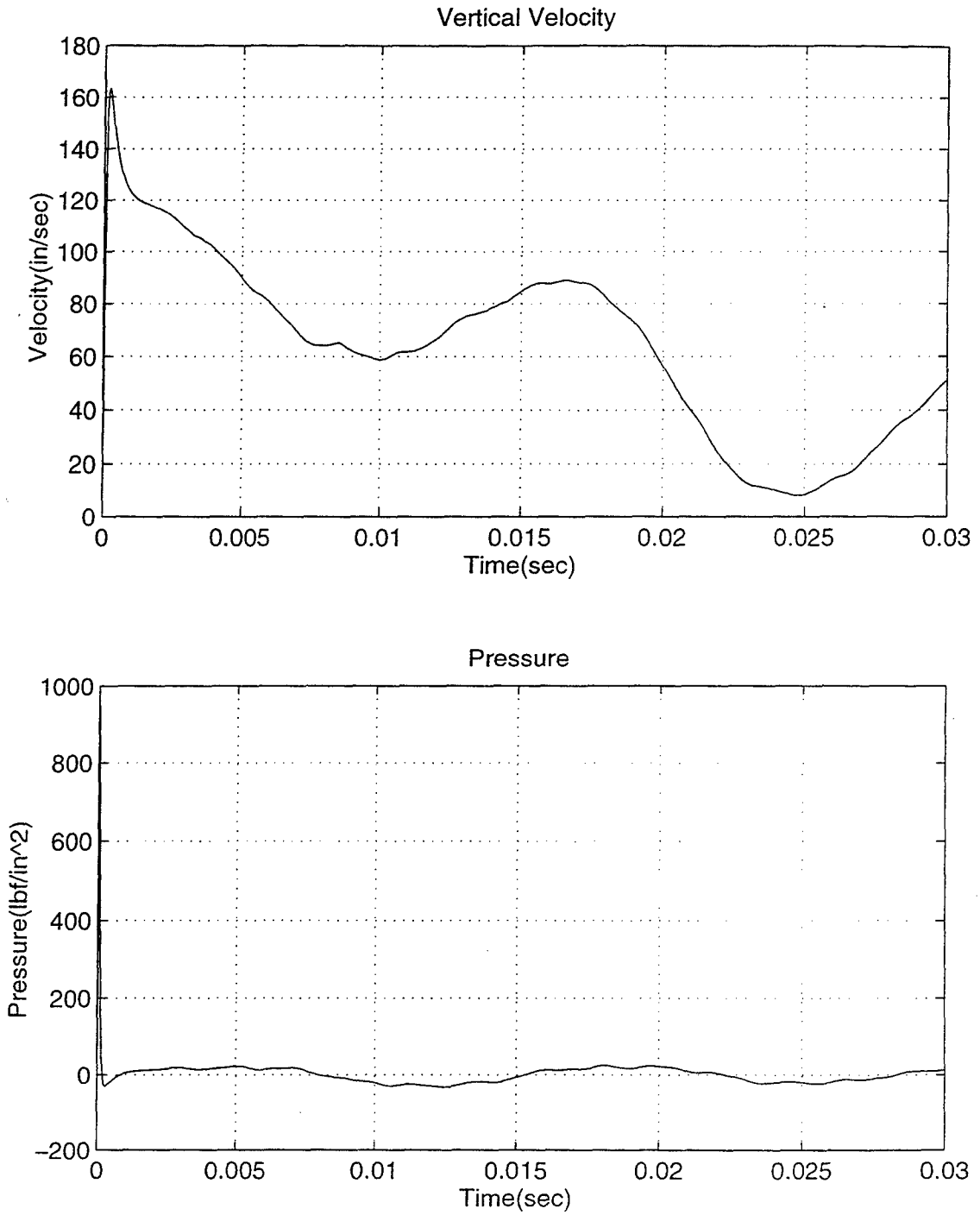

Figure 29. Velocity and Pressure at the Keel (Node 42)-DAA2, CFA OFF

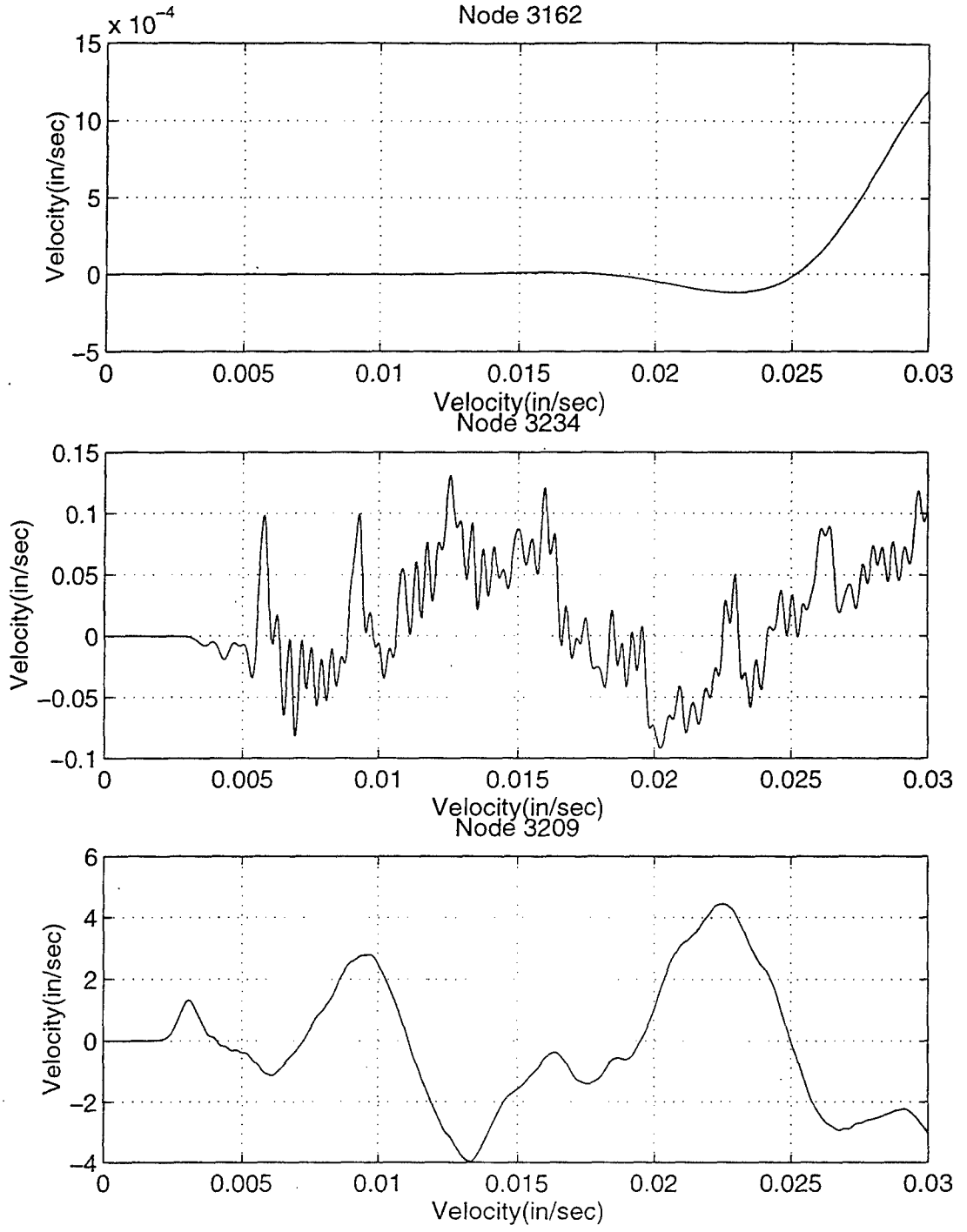

Figure 30. Internal Velocities-Node 3162 (top), Node 3234 (middle), Node 3209 (bottom). DAA2, CFA OFF

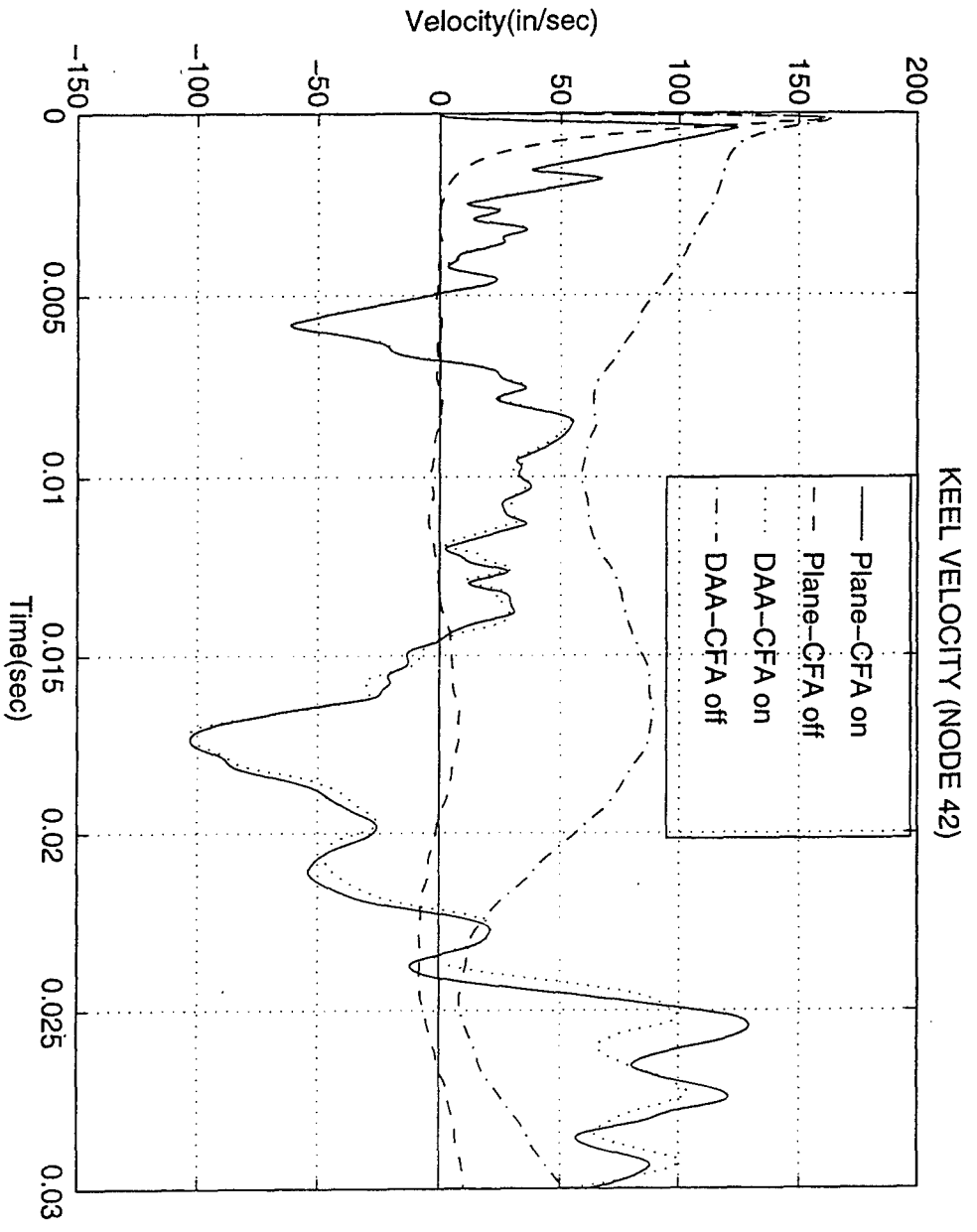

Figure 31. Comparison of Keel Velocities.

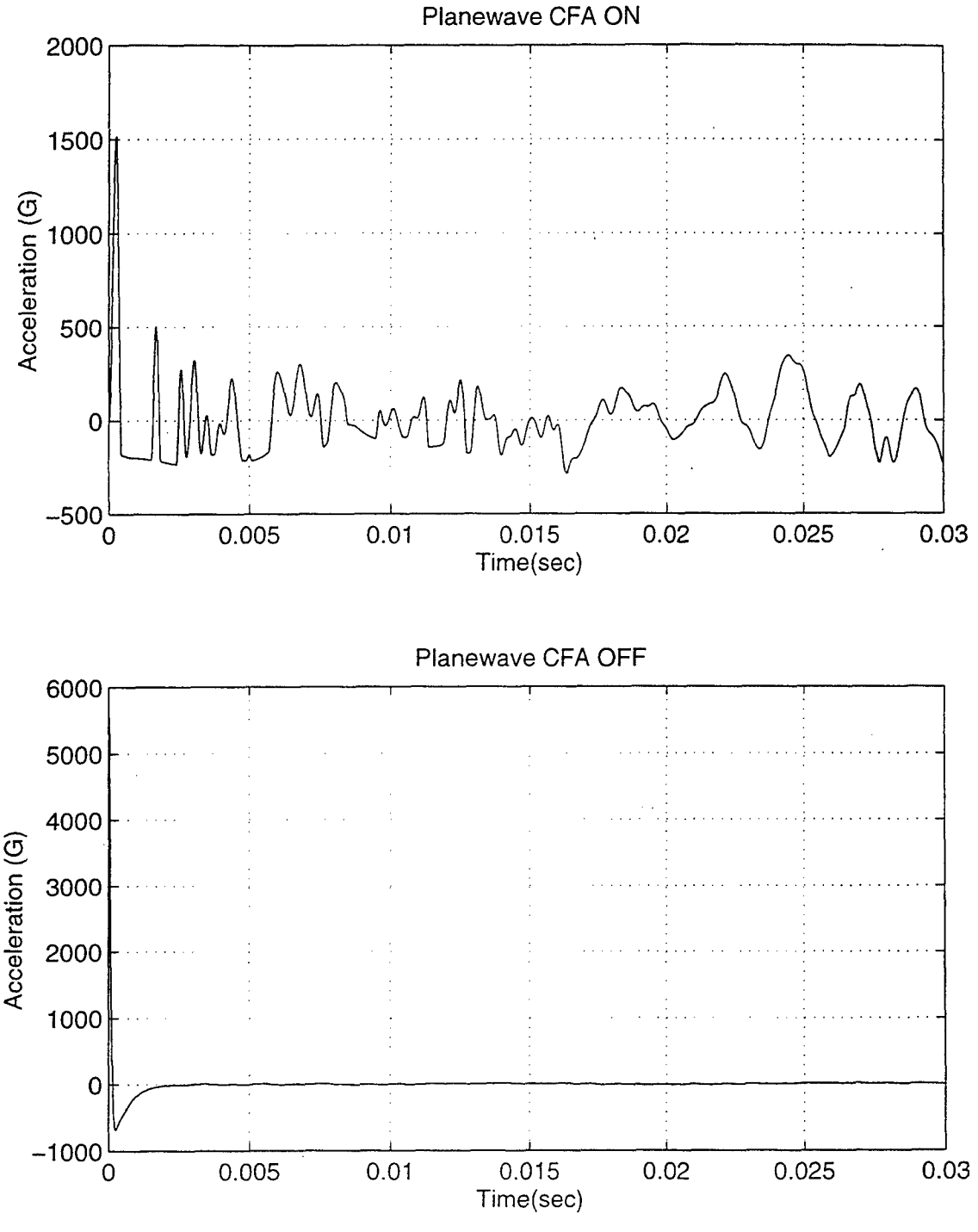

Figure 32. Comparison of Keel Accelerations-Plane wave

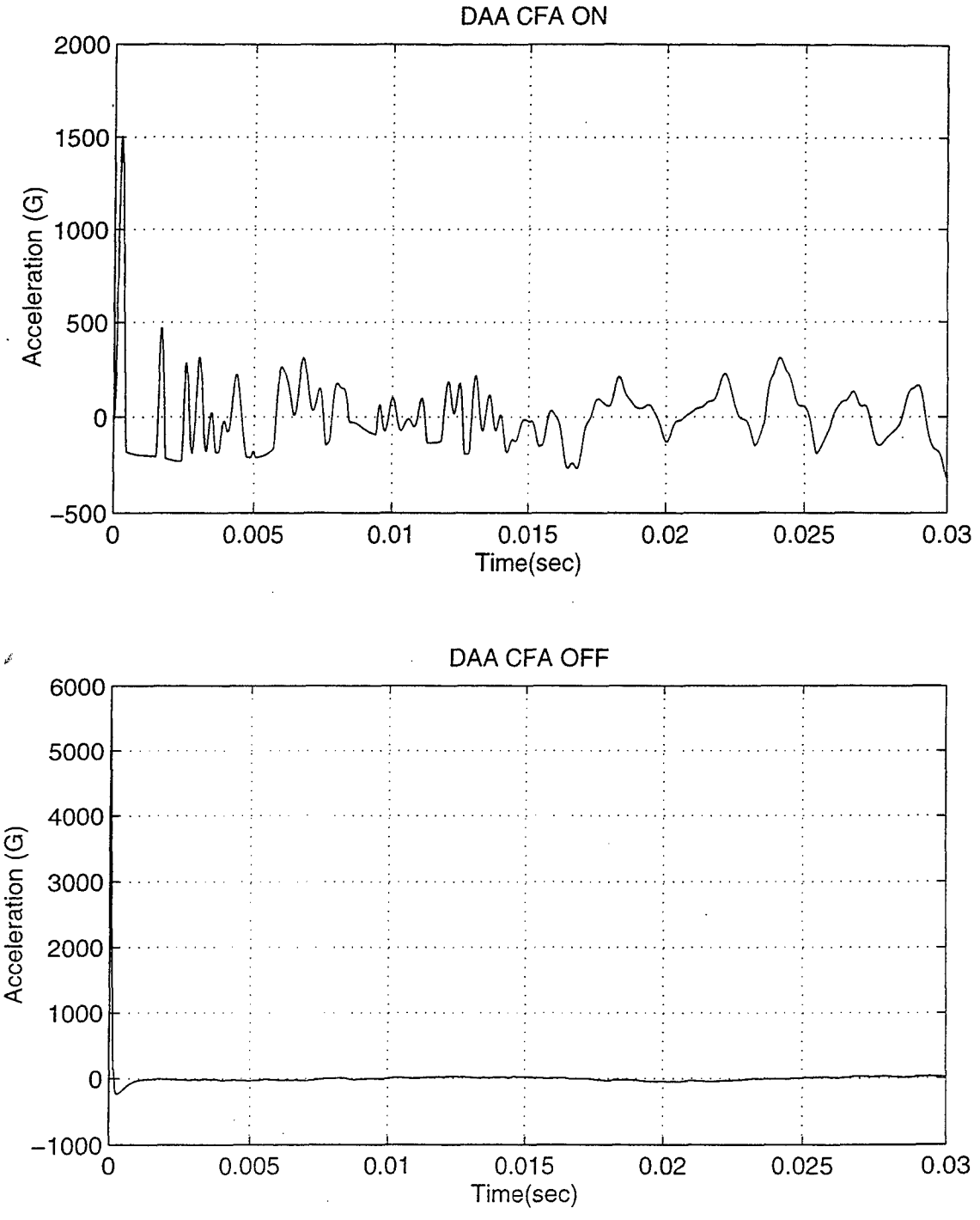

Figure 33. Comparison of Keel Accelerations- DAA2

VI. THREE DIMENSIONAL MODEL

The ideal three dimensional ship analysis would include:

1. A detailed ship model which included specific hull and equipment characteristics (locations, weights, etc.)
2. A fluid mesh model of the surrounding ocean that captures the cavitation region in three dimensions, as seen in the one and two dimensional analysis.
3. A computer hardware that can handle the detailed processing and large solution database.

Due to the complexity of a global ship model and the time integration required, a simplified "notional" ship design was utilized which was part of an earlier model of the Arleigh Burke Destroyer. Based on the results obtained with the two-dimensional model and the requirements for conditions 2 and 3 stated above, a plane wave/CFA OFF analysis was utilized for the three-dimensional ship model which sets the DAA boundary at the wet surface of the hull. Table. 8 provides general characteristics of the DDG model [Ref. 23].

Length Between Perpendiculars (LBP)	466.0 ft
Length Overall (LOA)	492.1 ft
Beam, Weather Deck	66.5 ft
Draft to Keel	20.7 ft
Lightship weight	6327 LTON
Full Load displacement	8000.3 LTON

Table 8. DDG-51 ASSET Design Summary [Ref. 23]

Fig. 34 and 35 depict solid modeling of the imported DDG model and specific charge locations for the two models created. Fig. 36 illustrates locations of the following

major areas of interest were selected for their general purpose of holding vital pieces of equipment such as the AEGIS weapon system components and main propulsion units: node closest to the charge, bow, stern, Main Engineering Rooms (MER 1 and 2), Combat Systems Equipment Rooms (CSER 1, 2, and 3), and the general location of th SPY radar room in the superstructure.

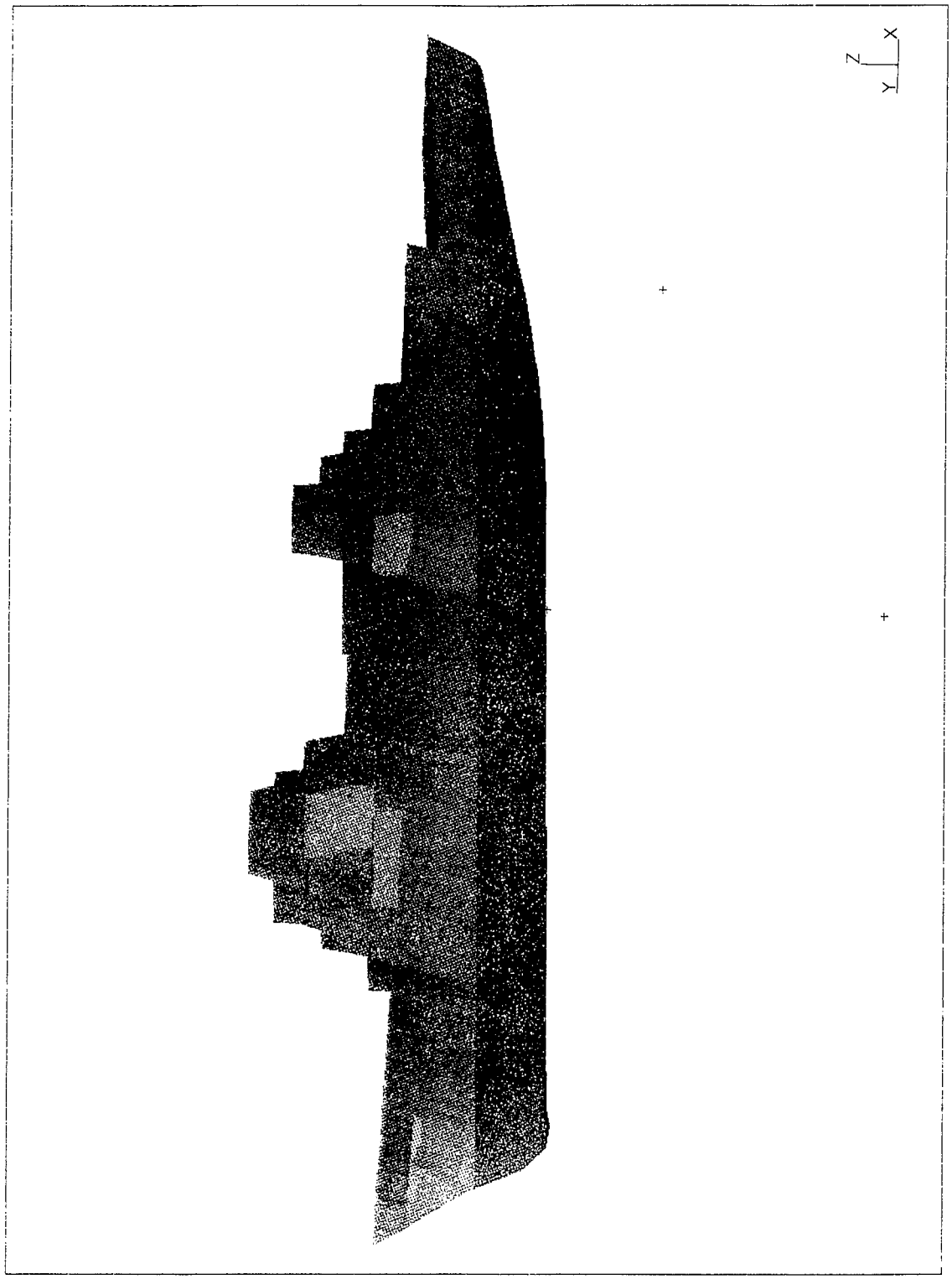

Figure 34. Solid Modeling of ASSET DDG-51.

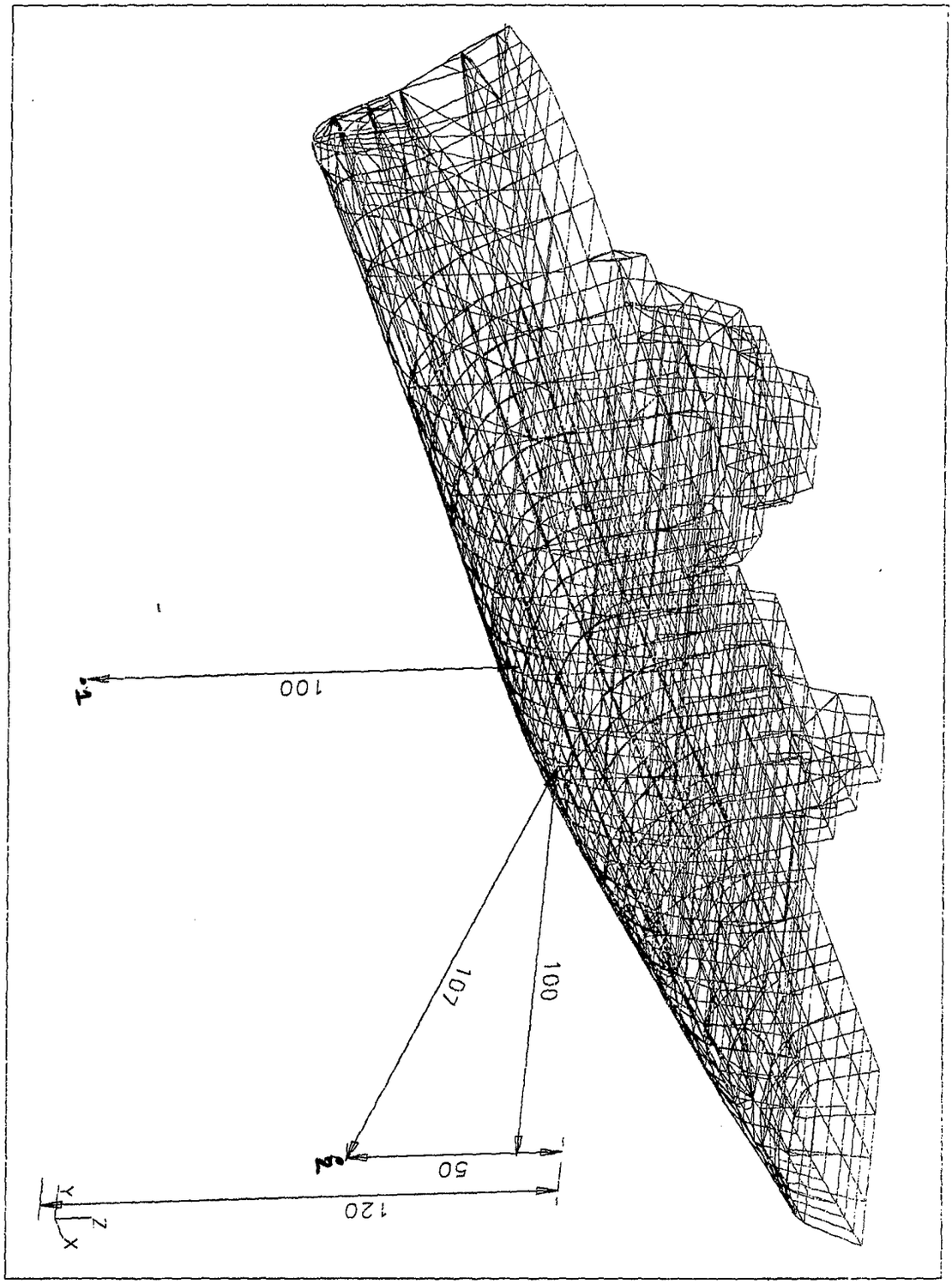

Figure 35. Charge Locations Below the Keel (1) and Offset (2).

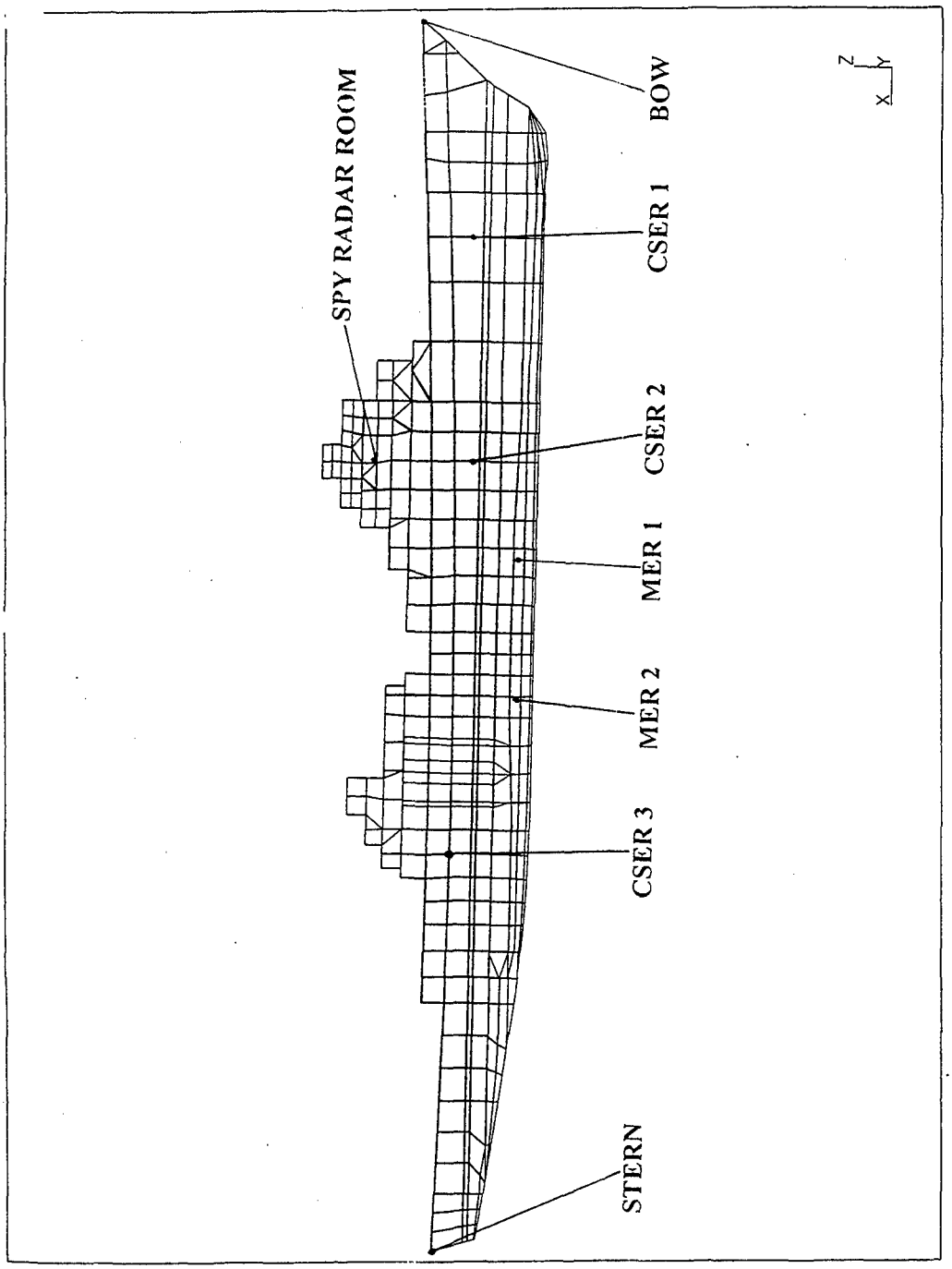

Figure 36. General Space Locations.

A. 1962 FINITE ELEMENT MODEL

1. Modeling

This initial model utilized a general plate thickness of 0.4 inches of similar material qualities used in the two dimensional model throughout the entire ship. Inner bottom stiffeners and heavy equipment locations were not constructed in the original IGES model out of ASSET but were later created in IDEAS for the 5682 element model study. Fig. 35 illustrates the 1962 element model which includes 348 wet elements. In order to capture peak velocities, damping coefficients were not applied to the model.

Explosive charge conditions were the same as those utilized for the two dimensional analysis:

CHARGE TYPE	TNT
WEIGHT	100 LBS
LOCATION (relative to ship)	MIDSHIPS, CENTERLINE, 100 ft beneath the keel
DEPTH	120 feet

Table 9. Charge characteristics

2. Results

The whipping motion of this particular model exhibited the expected basic motion of a simple free-free beam excited by a forcing function in the middle of the model. The highest velocities and accelerations occurred at the node (Node 42) closest to the charge (Fig. 37 and 38) due to an unsmeared and unstiffened keel and outer hull. The

unsmeared and unstiffened keel also experienced high frequency oscillations in comparison to other areas of the model. The bow and stern experienced the second largest maximum vertical velocities and accelerations (Fig. 39 to 42) which occurred approximately 45 msec and 32 msec, respectively, after the peak keel velocity.

Peak velocities at the bow,stern, and closest point to the charge at the keel indicate the greatest magnitude in velocities to be in the vertical direction, followed by fore and aft motion, and the athwartships direction to be the lowest. However, internal deck locations exhibited the greatest peak velocities in the fore and aft direction, followed by athwartship, and vertical velocities to be the lowest because of their general locations close to the incident shock wave arriving midships in the model. Both MER spaces (Fig. 43 to 46) experienced the largest internal accelerations, specifically in the fore and aft direction followed by CSER 3 (Appendix C) with almost equal velocites and accelerations in the fore and aft and athwartship directions. MER 2 experienced the largest fore and aft motions in comparison to the other internal spaces studied, largely due to its close location to the initial shock wave. Amongst the combat systems spaces, the SPY radar room (Appendix C) had the highest fore and velocity (9 in/sec) but with similar accelerations. The asymmetry of the aft super structure arrangement places a majority of the structure to port. This asymmetric condition in the DDG-51 model contributed to the athwartship velocities and accelerations in all areas of the ship.

Modeling the ship globally without a fluid volume mesh and exposing it to a plane wave underwater explosion captured the high frequency vibration or "ringing" in

the hull which was not observed in the plane wave/CFA OFF two dimensional cross-sectional hull model. Table 10 summarizes maximum velocities and accelerations:

Location	Node	Fore and Aft		Athwartships		Vertical	
		V(in/sec)	A(G)	V(in/sec)	A(G)	V(in/sec)	A(G)
Keel	42	10.2	47.1	3.3	20.8	176	2210
Bow	842	13.1	9.2	9.1	4.3	27.2	10.1
Stern	2157	13.4	10.1	3.8	1.33	20.1	12.2
MER1	1933	7.2	12.1	2.6	2.2	.7	.058
MER2	1895	12.3	9.92	4.6	3.8	4.2	.13
CSER1	1649	5.5	3.6	2.5	1.3	.17	.019
CSER2	1748	6.5	5.1	1.33	1.1	.16	.025
CSER3	1990	6.1	7.1	6.8	5.03	.135	.08
SPY Radar Room	2534	9	4.8	2.6	1.8	.055	.0088

Table 10. Maximum Absolute Velocity and Acceleration (1962 Elements)

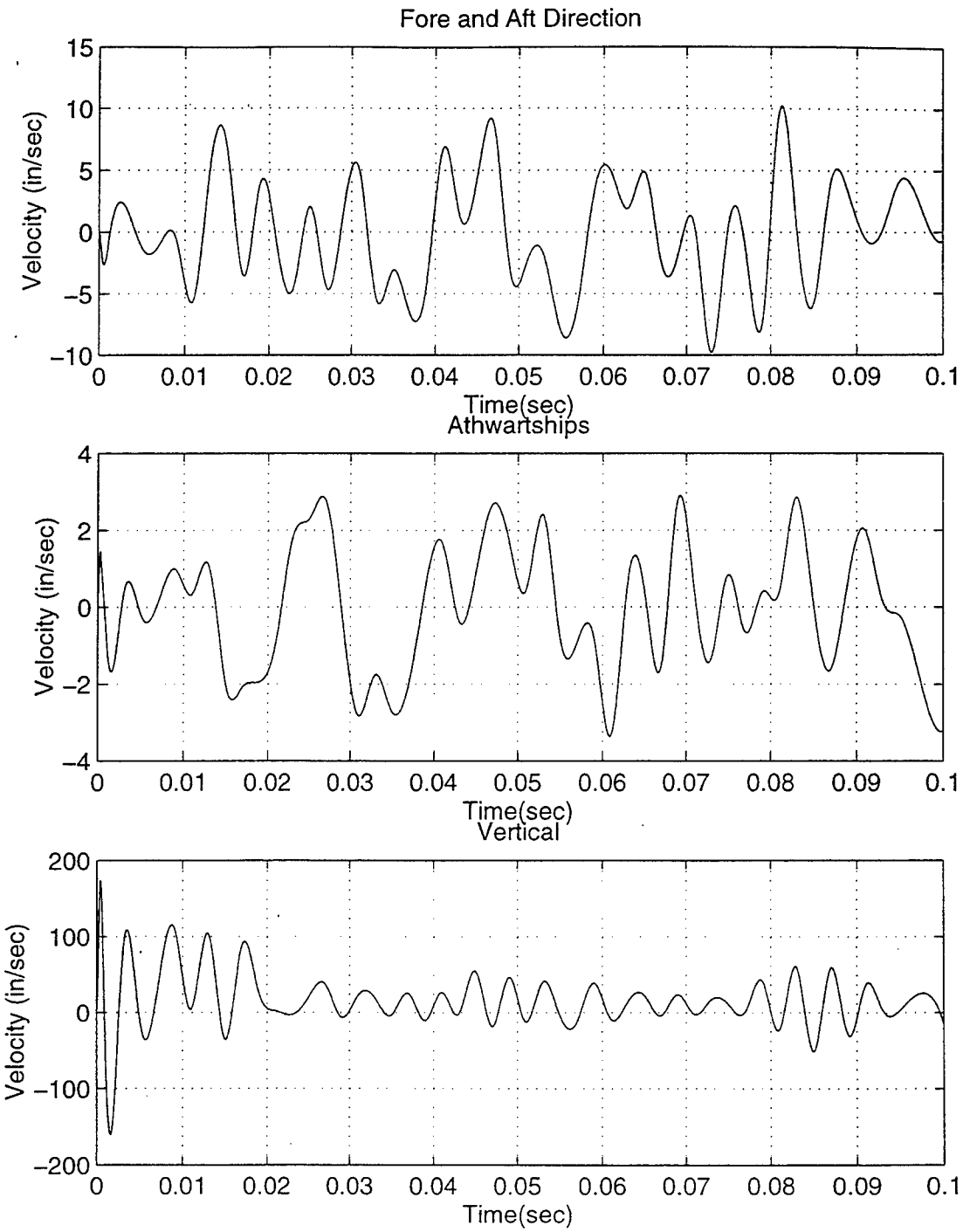

Figure 37. Keel Velocity (Node 43)

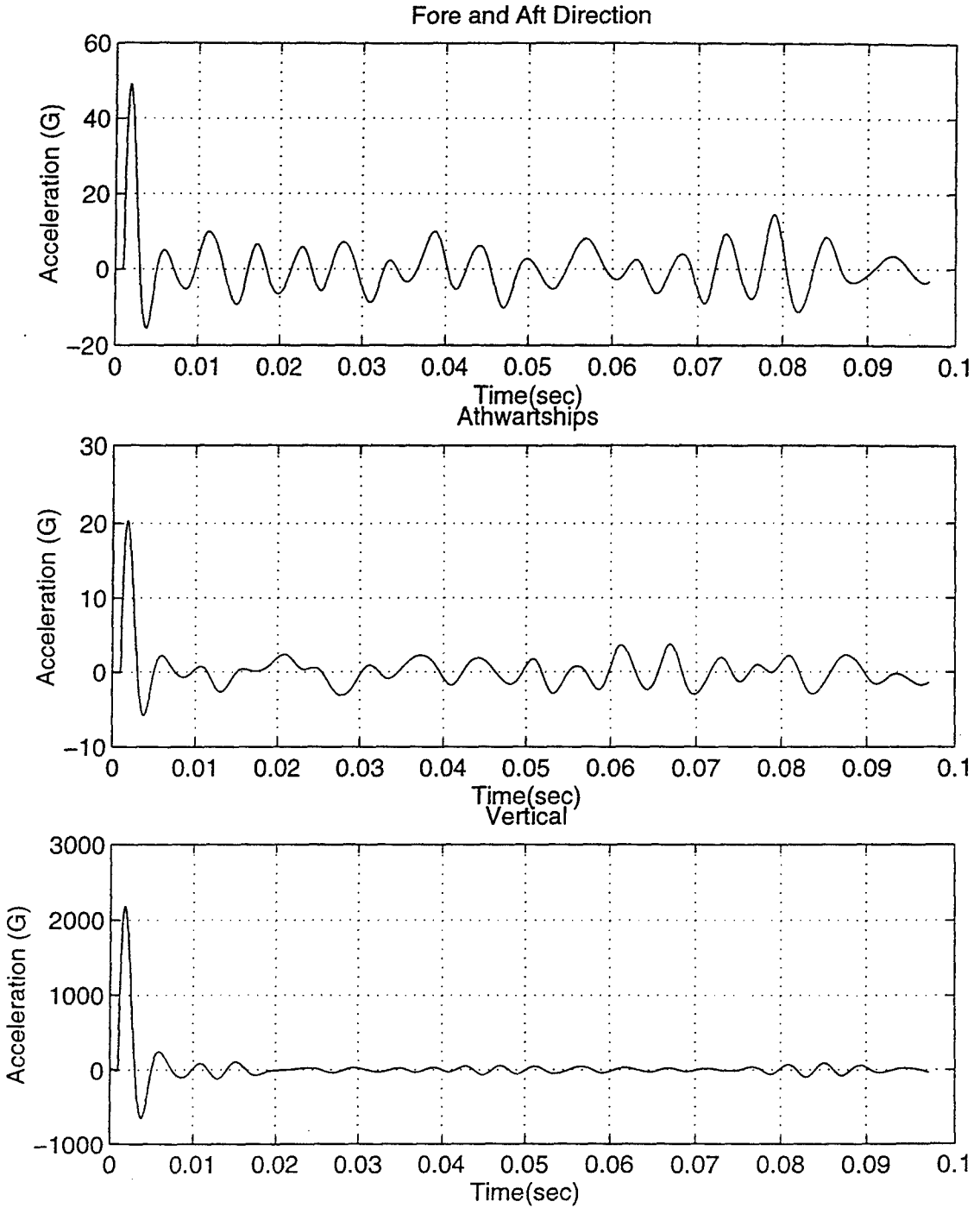

Figure 38. Keel Acceleration (Node 43)

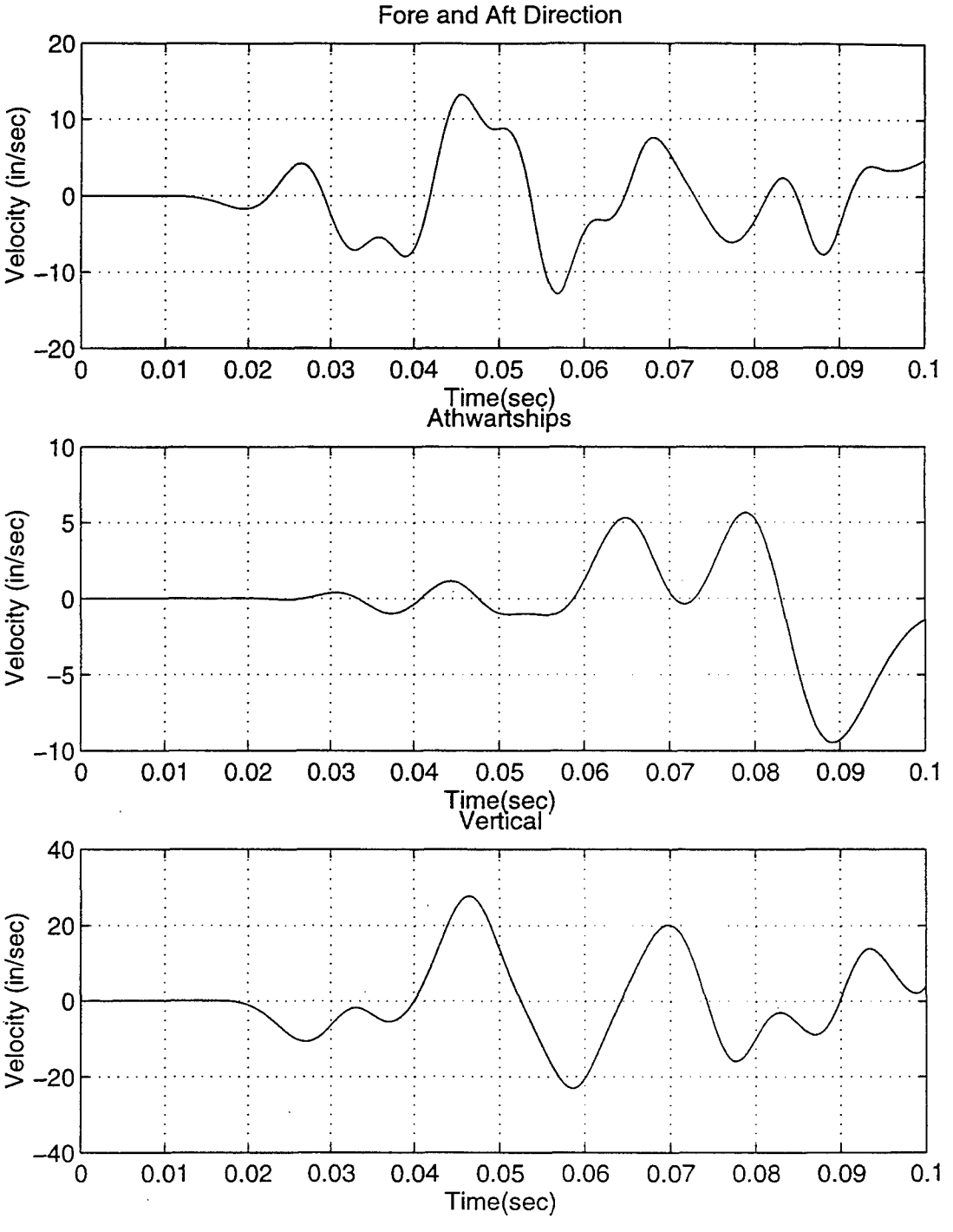

Figure 39. Bow Velocities (Node 842)

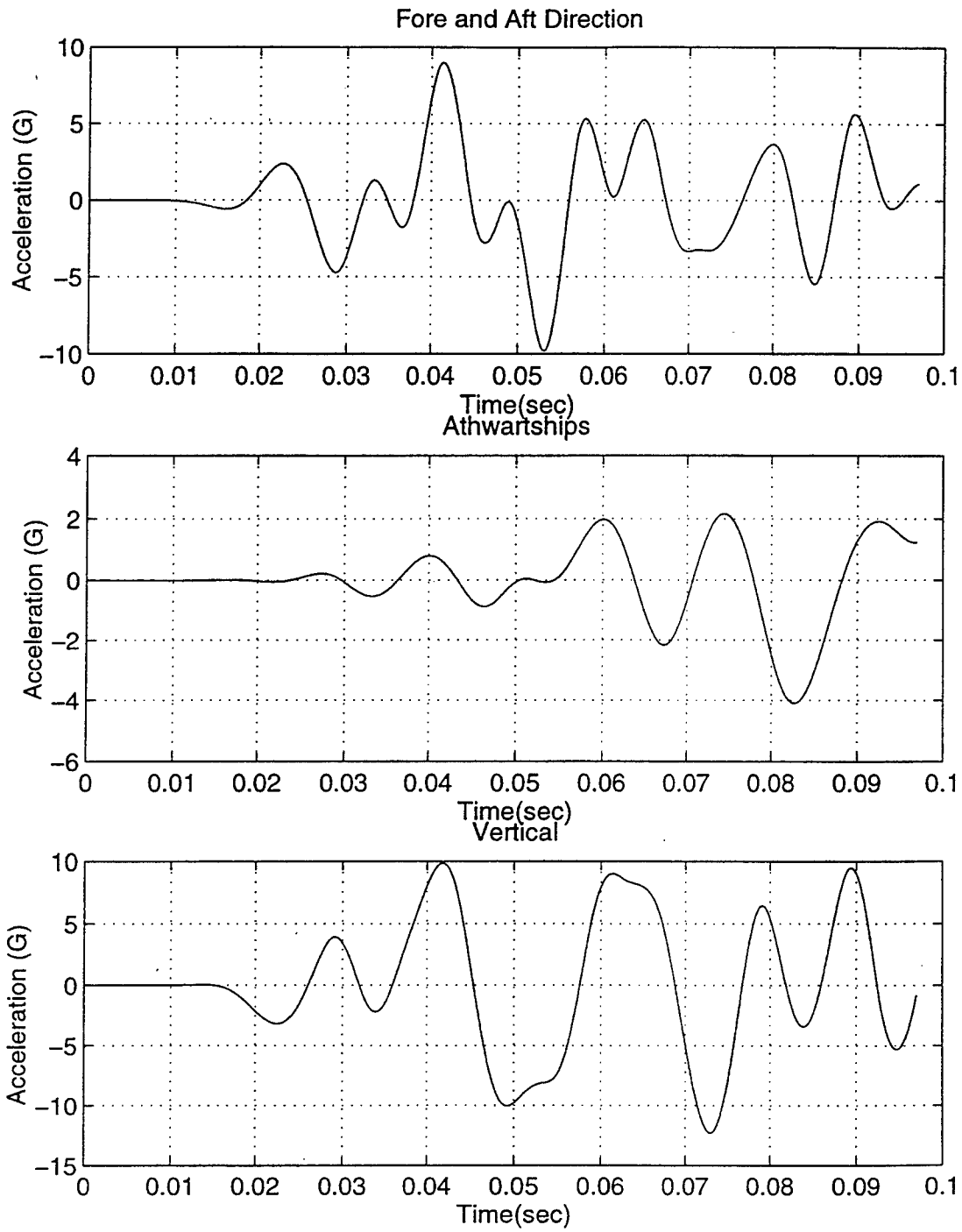

Figure 40. Bow Accelerations (Node 842)

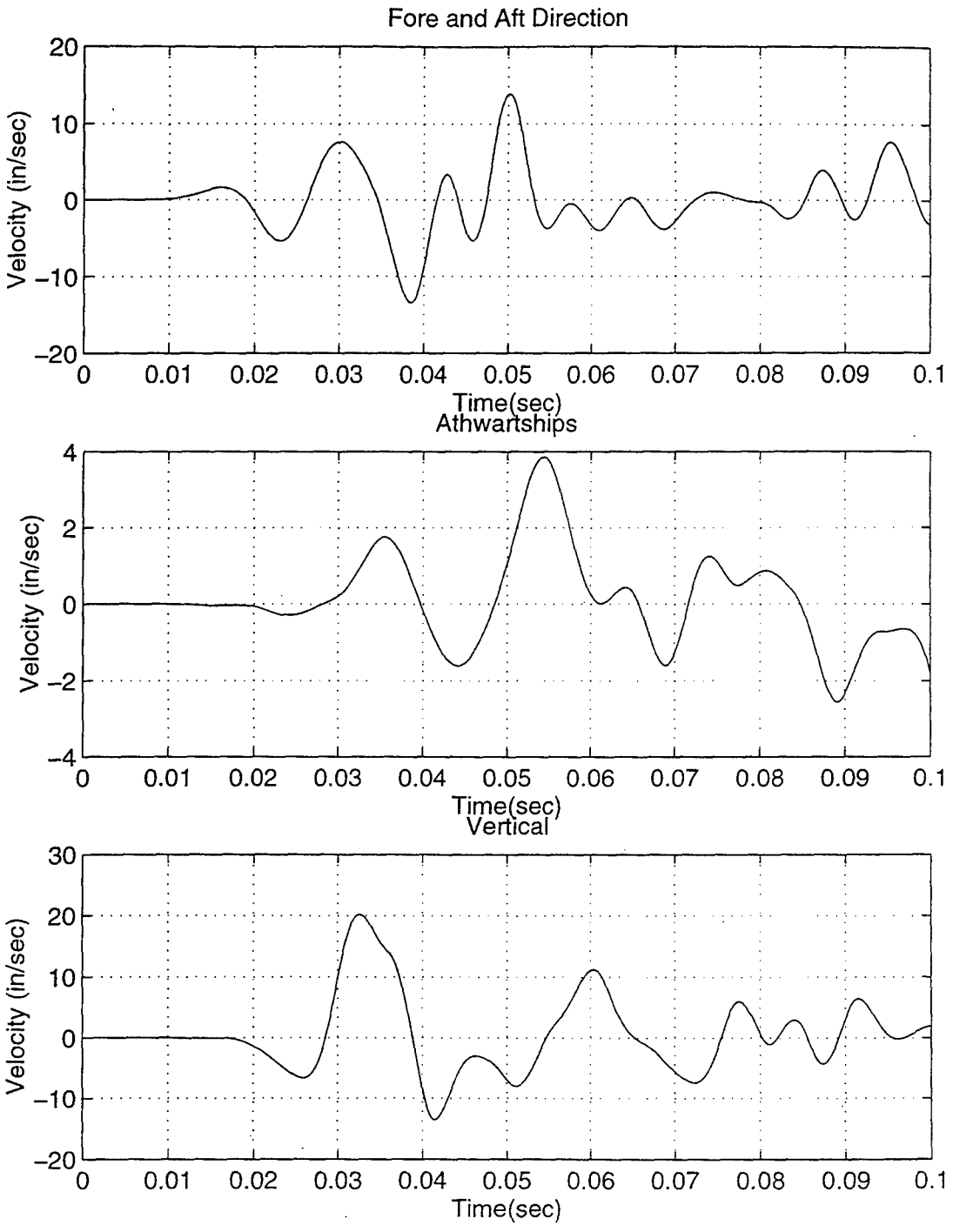

Figure 41. Stern Velocities (Node 2157)

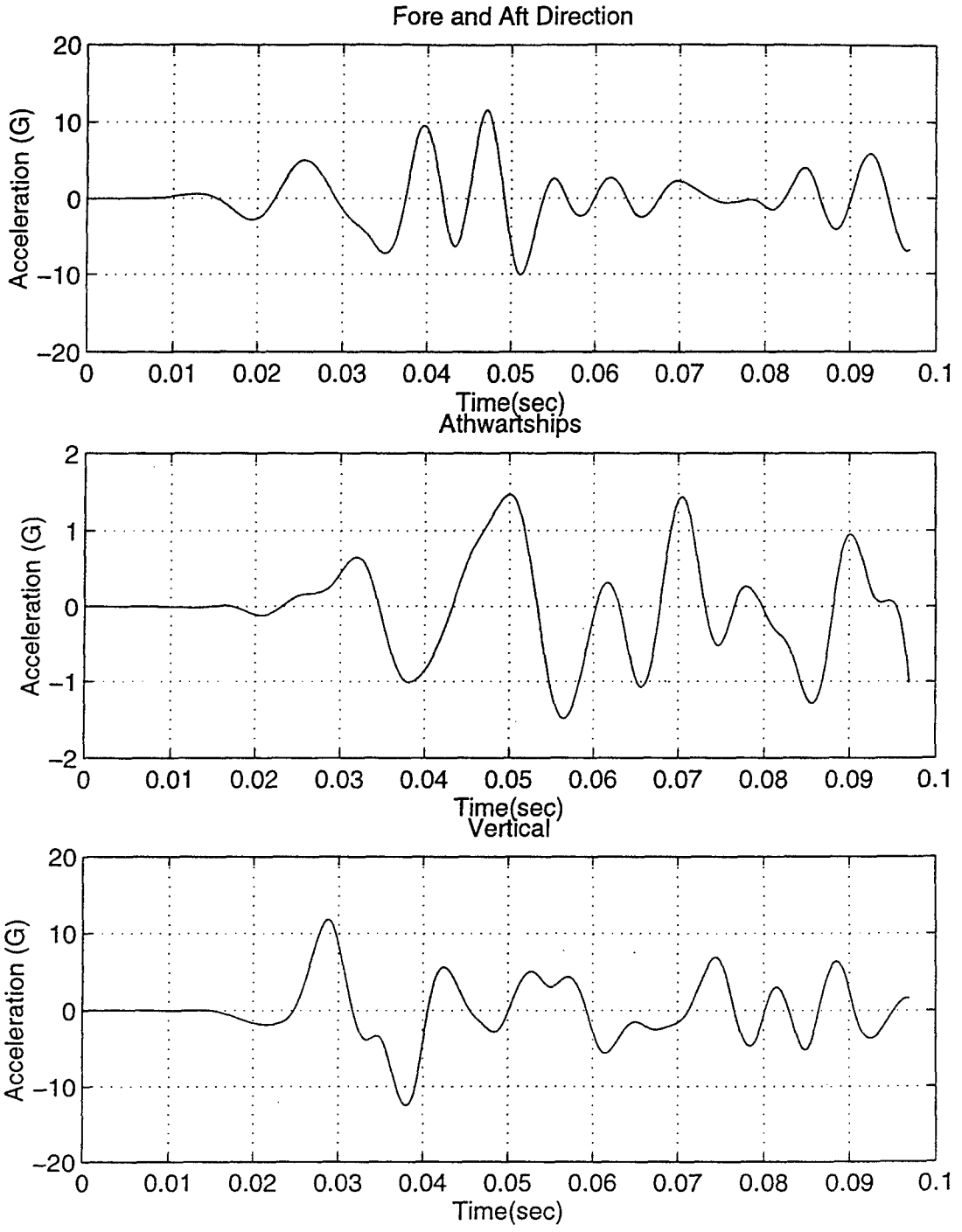

Figure 42. Stern Accelerations (Node 2157)

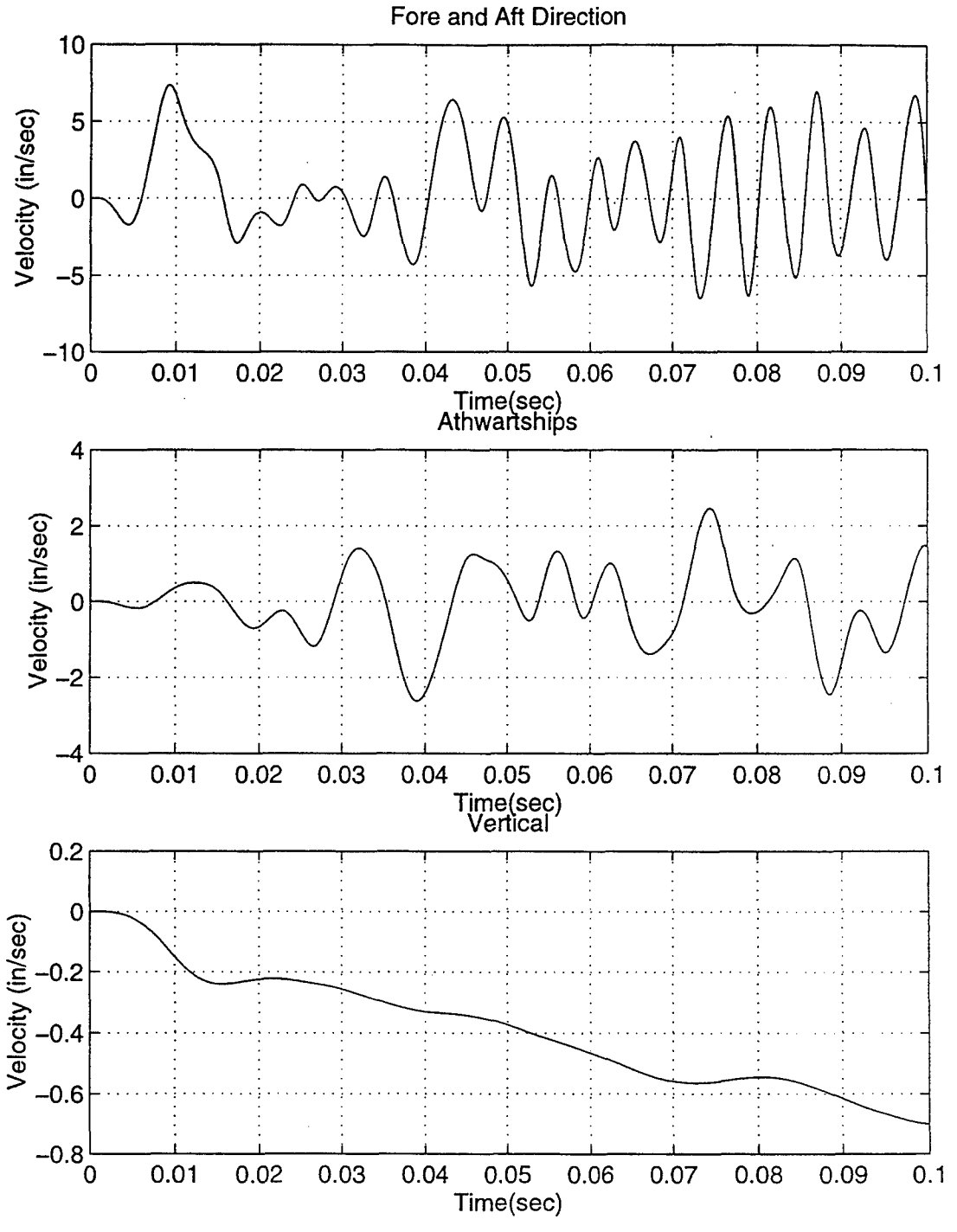

Figure 43. MER 1 Velocities (Node 1933)

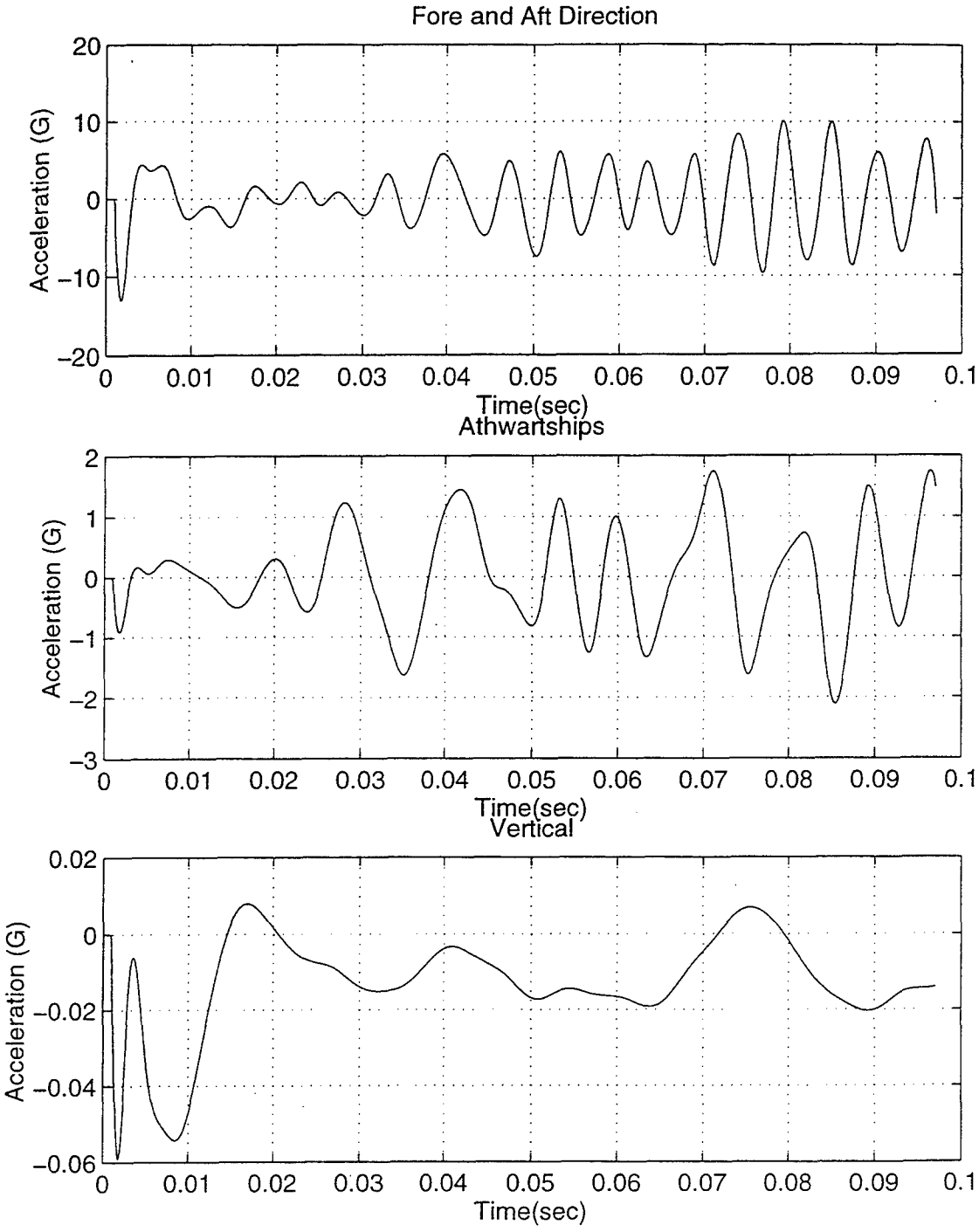

Figure 44. MER 1 Accelerations (Node 1933)

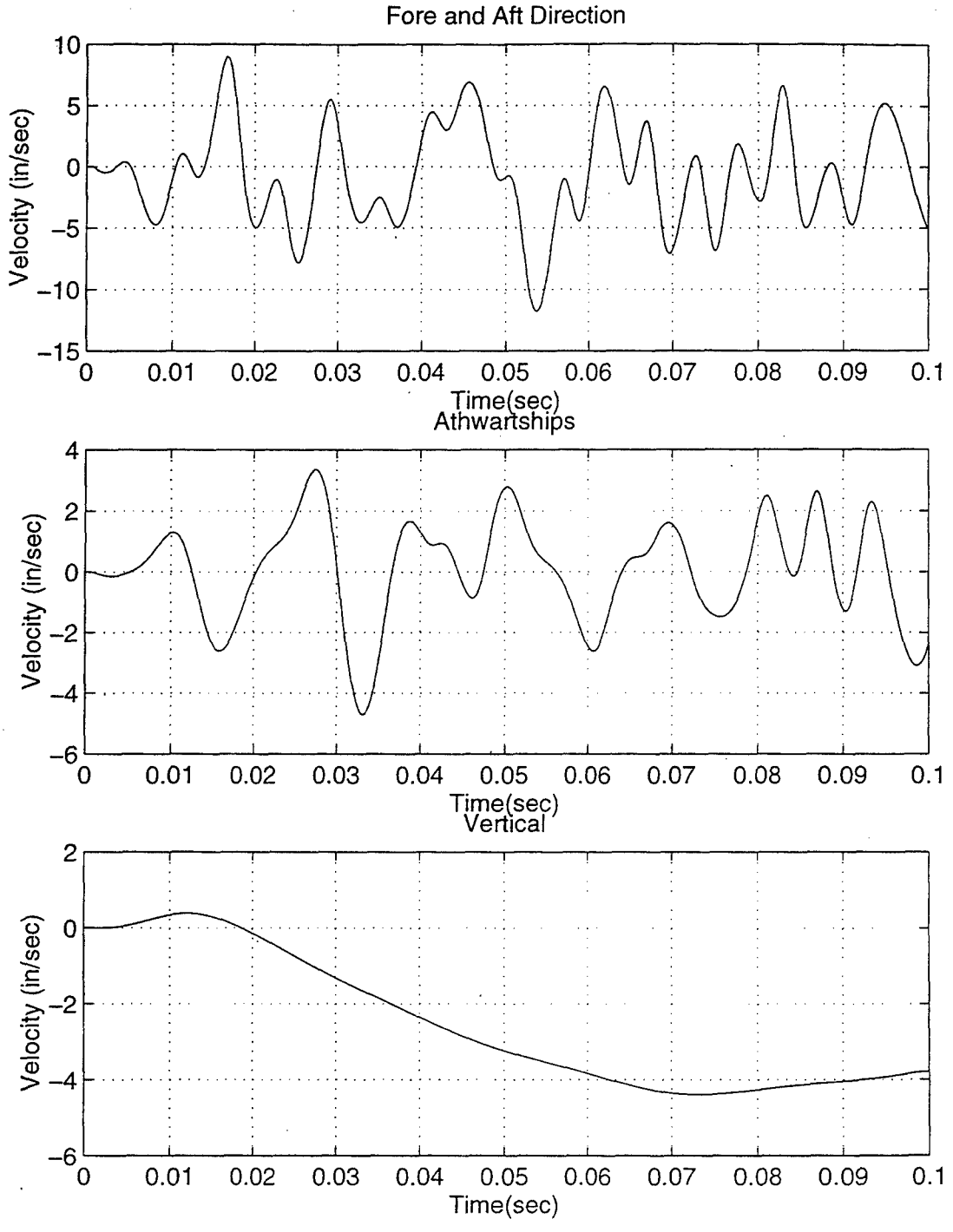

Figure 45. MER 2 Velocities (Node 1895)

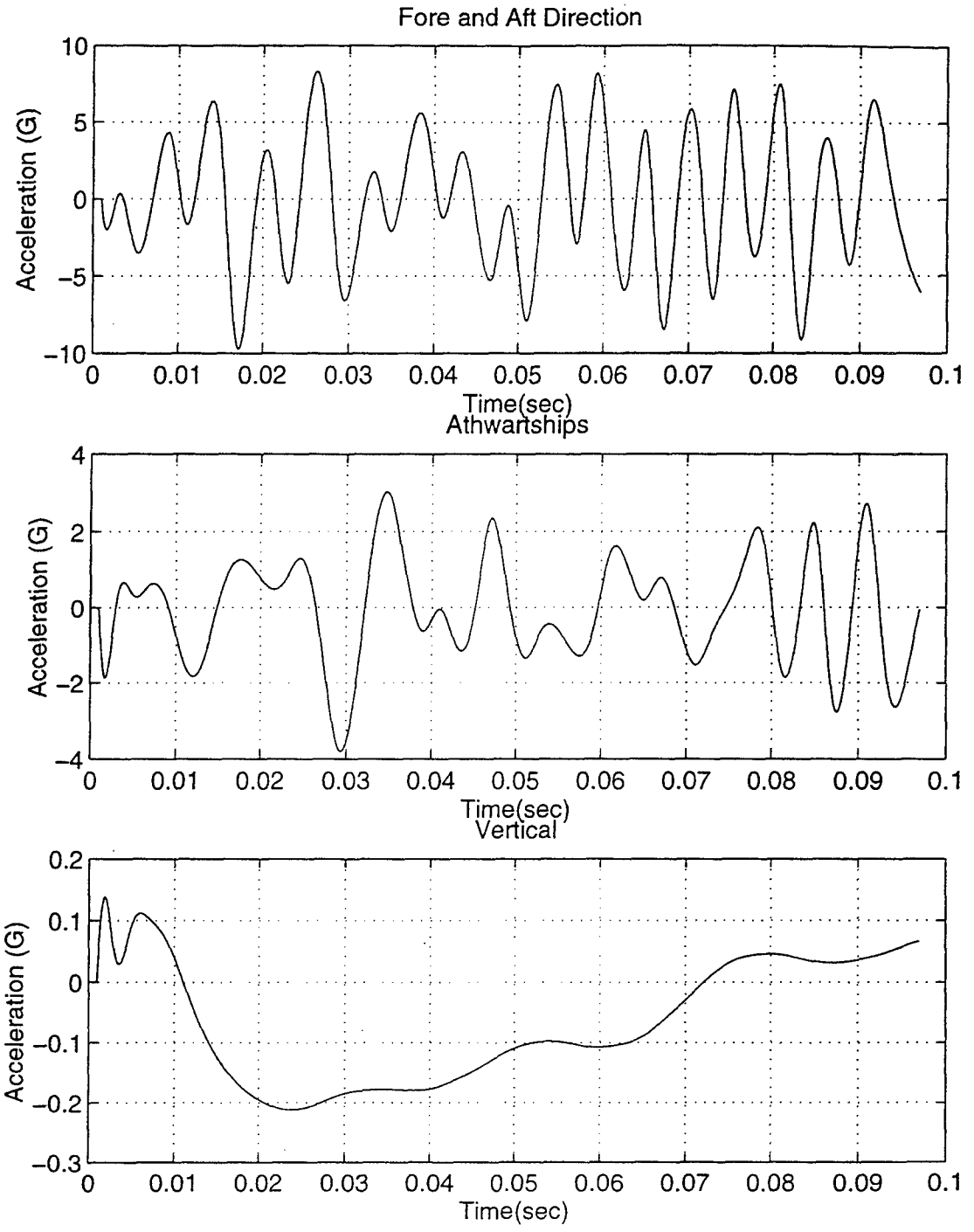

Figure 46. MER 2 Accelerations (Node 1895)

B. 5682 FINITE ELEMENT MODEL

1. Modeling

In order to provide a detailed mesh for the wet surface of the hull and improve equipment locations, a finer mesh was created of the same model which included inner bottom stiffeners and 955 wet elements, Fig. 47. Utilizing the available ASSET data on main engineering equipment [Ref. 23], early Flight II/IIA study drawings [Ref. 24], and DDG combat system equipment data [Ref. 25], large groups of heavy equipment were lump massed in their respective areas.

The detailed requirement for longitudinal and transverse stiffners was simplified by the smearing technique utilized in ASSET (APPENDIX D). Although previous work by Cunningham [Ref. 26] revealed the limitations in local and global smearing, the ASSET technique sizes stiffeners to provide a T-section with reasonable proportions that meet strength and geometric constraints. The stiffener cross-sectional area is smeared into the plate cross sectional area, creating a smeared plate thick than the standard plate by a factor of (1 + smear ratio(S)). Based on the data for the notional DDG design which included intitial plate thickness and stiffener smearing ratios, the following plate thicknesss were used in this particular model:

Structure Location	Smeared Plate Thickness (in)
BOTTOM SHELL	.57
INNER BOTTOM	.42
DECK 1	.51
DECK 2	.54
DECK 3	.49
DECK 4	.48
MAIN DECK	.55
TRANSVERSE BULKHEADS	.33
OUTER HULL	.47
SUPERSTRUCTURE	.33

Table 11. Smeared plate thicknesses (inches)

In addition to Appendix E which denotes general weights and locations of combat system equipment that were lump massed, the following specific engineering room equipment was used with respect to their locations derived from [Ref. 24].

GAS TURBINES (4)	84.7
GAS GENERATORS (3)	94.2
REDUCTION GEARS (2)	109.5

Table 12. Engineering Equipment Total Weights (LTON)[Ref. 23]

The net weight of the entire model was 3598 Lton, 43% lighter than the original "light weight" DDG ASSET model.

Charge location was placed in an offset position utilizing only 120 lbs TNT at a standoff distance of 107 feet and a depth of 50 feet .

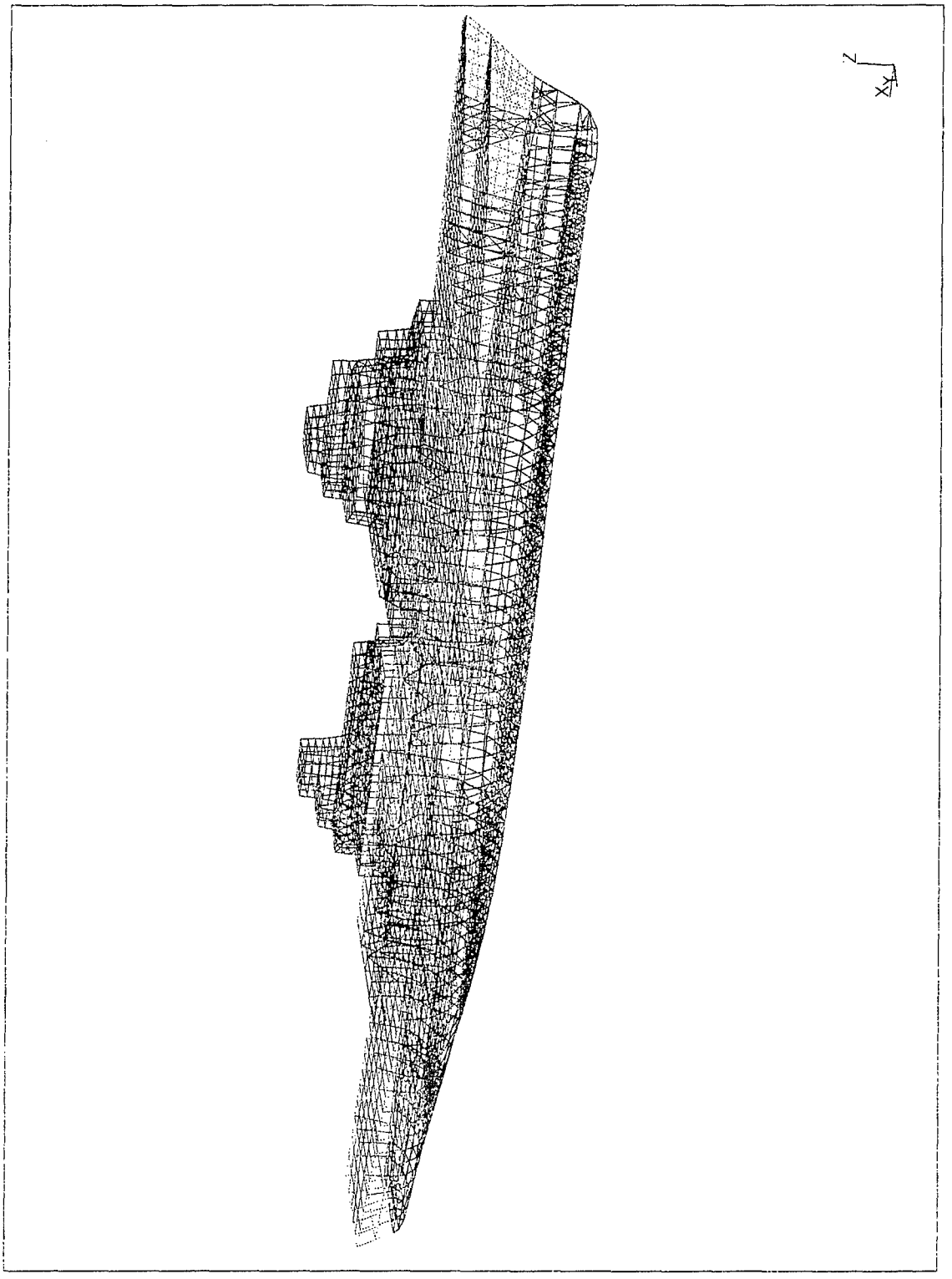

Figure 47. DDG 5682 Finite Element Model

2. Results

Due to the increased complexity of the meshed model, post processing of this particular model became quite difficult during the MSC/NASTRAN restart which prevented further post-processing into IDEAS. Fig. 48 to 51 depict the greatest velocities and accelerations occuring midships of this model, specifically at the point along the hull closest to the charge (Node 393) and at the node along the keel with the same axial distance from the bow (Node 397). These two locations coincide with those same points on the hull noted previously in Fig. 35 with charge 1 for node 397 and charge 2 for node 393.

Bow and stern reactions (Fig. 52 to 55) were noted higher than those seen in the 1962 element model due to the majority of concentrated masses being located in central locations of the ship (i.e. aft of the forward VLS and forward of CSER3) as well as the spaces of interest (Fig. 36) and the lack of masses in the general area of the bow and stern. Peak bow and stern vertical reactions occurred 40 msec and 30 msec, respectively, later relative to midships reactions (Node 393 and 397) with high frequency oscillations. MER 1 (Fig. 56 and 57) exhibited lower velocities and accelerations relative to MER2 (Fig. 58 and 59) which can be contributed by the asymmetry between the two engineering rooms. The gas turbine modules and reduction gear masses were located on the port side of the engine room of MER 2 which was the same side as the charge location and, as seen in the 1962 element model, MER 2's location was closer to the incident shock wave arrival point along the hull. Bow,stern, and both MER spaces tended

to have reactions in the following order of highest to lowest magnitude: vertical, fore/aft, and athwartships. Combat system equipment rooms (CSER 1,2 and 3) and the SPY radar room (Appendix F) showed very little motion in the fore/aft and athwartships direction with practically zero vertical motion.

For this particular tactical scenario and model, the only shipboard internal space which experienced the highest acceleration was MER 2 with large magnitudes of oscillations in the fore and aft direction as well as athwartship (Fig. 58 and 59). All other internal spaces encountered low accelerations which did not seriously introduce severe shock loadings upon their respective equipment. The effect of smearing and lump massing groups of large pieces of internal equipment created dramatically different results compared to the 1962 unsmeared, unlumped element model. In addition to these structural differences, the low charge weight and offset distance of the underwater explosion did not produce appreciable effects on internal ship behavior. Table 12 provides a summary of the maximum velocities and acclerations in each area:

Location	Node	Fore and Aft		Athwartships		Vertical	
		V(in/s)	A(G)	V(in/s)	A(G)	V(in/s)	A(G)
Standoff Point	393	17.1	64.1	53.2	172	58.9	210
Keel	397	10	52	30.2	110	28.8	106
Bow	1554	13.2	42.3	12.1	44	21.2	58
Stern	2281	13.8	23.1	10.8	30.1	12.2	35.6
MER 1	4448	.33	.18	2.1	.67	2.23	1.08
MER 2	4543	8.8	42.4	9.2	44.5	39.3	133
CSER 1	3567	.013	1.9E-3	.012	1.3E-3	6.4E-4	5.1E-5
CSER 2	3669	.19	.023	.78	.07	7.7E-4	1.48E-4
CSER 3	3541	.15	.19	1.4	.23	7E-3	1.5E-3
SPY Radar Room	6955	.59	.071	.15	.019	3.2E-4	4.3E-3

Table 13. Maximum Absolute Velocities and Accelerations (5698 element model)

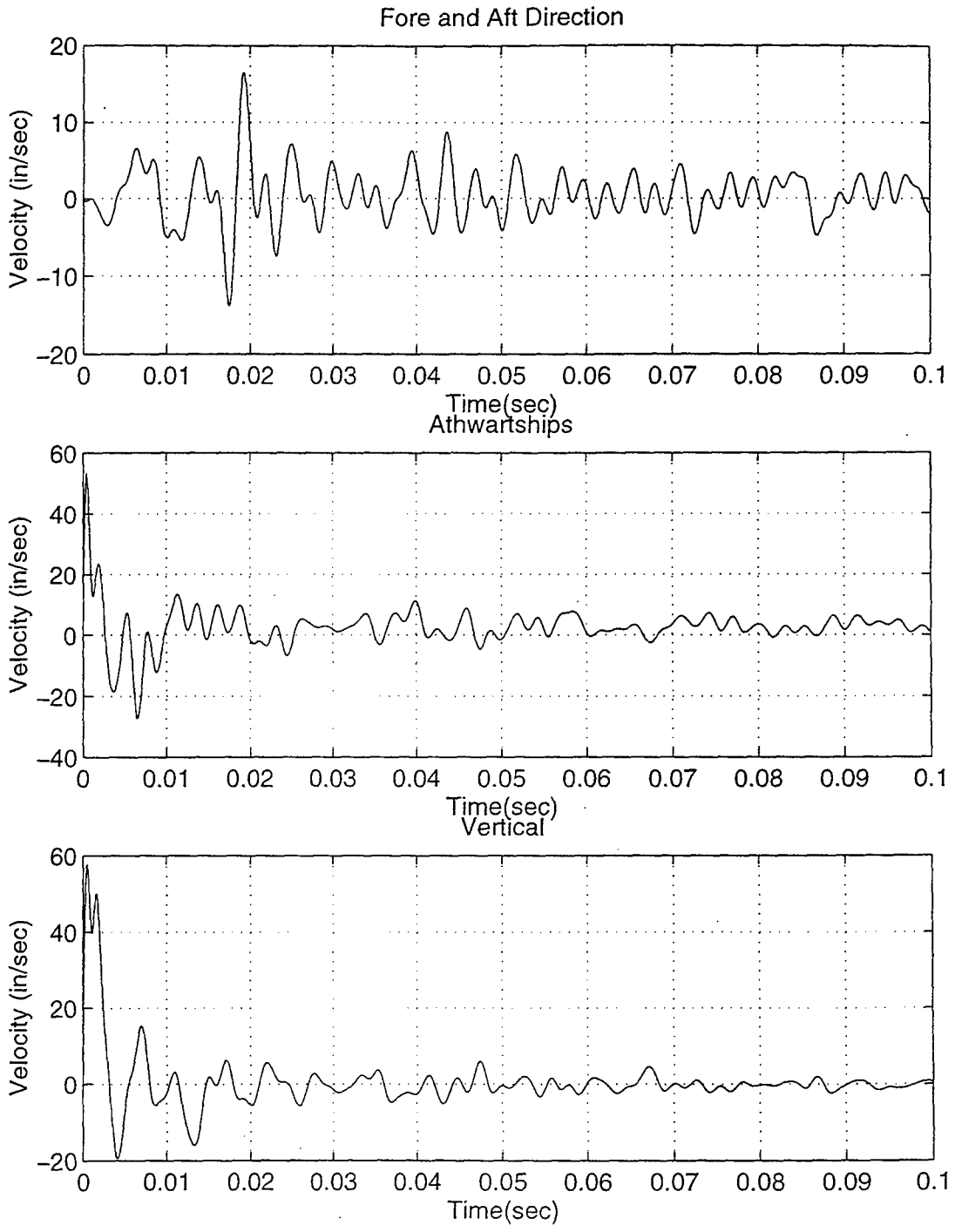

Figure 48. Hull Standoff Point Velocities (Node 393)

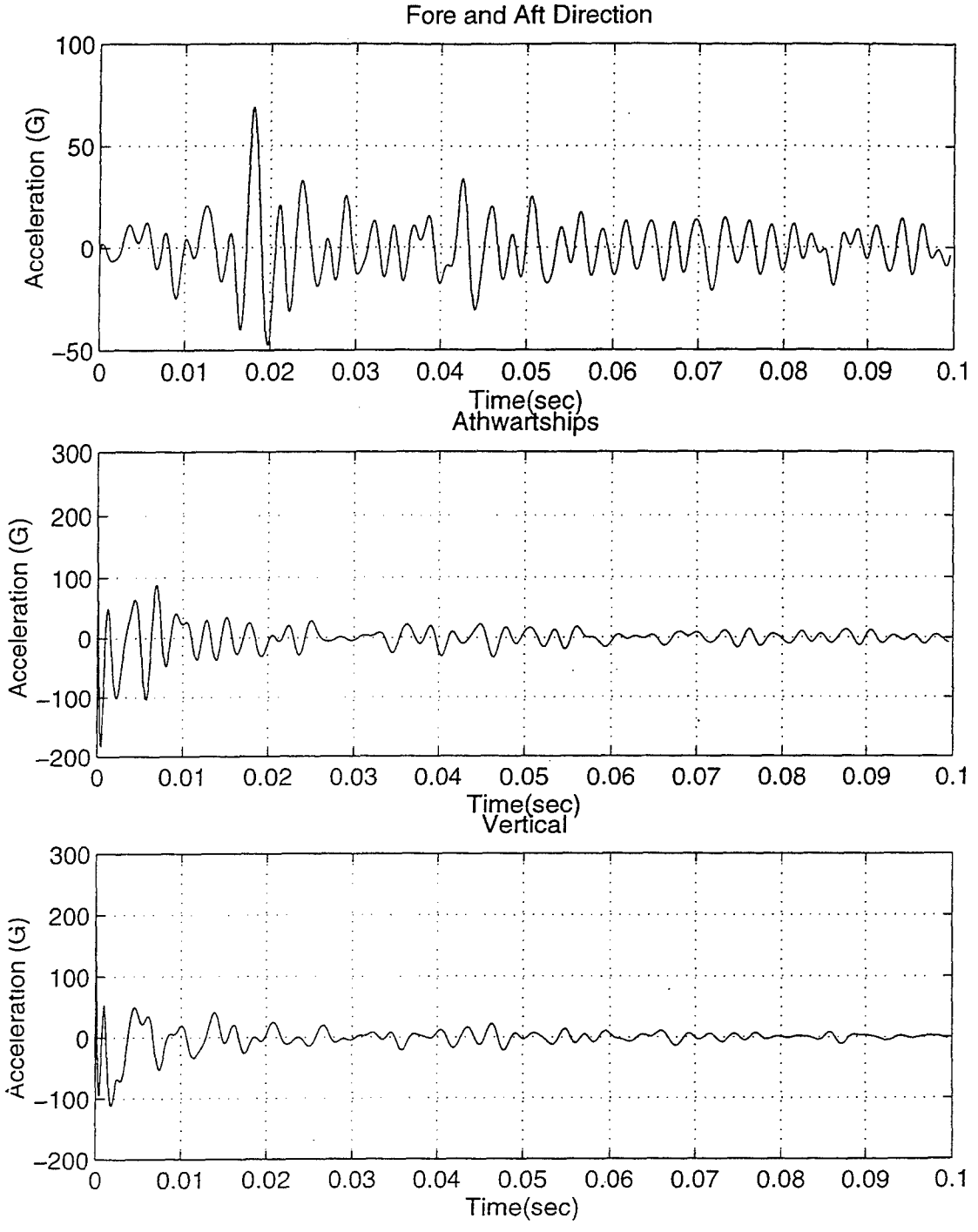

Figure 49. Hull Standoff Point Accelerations (Node 393)

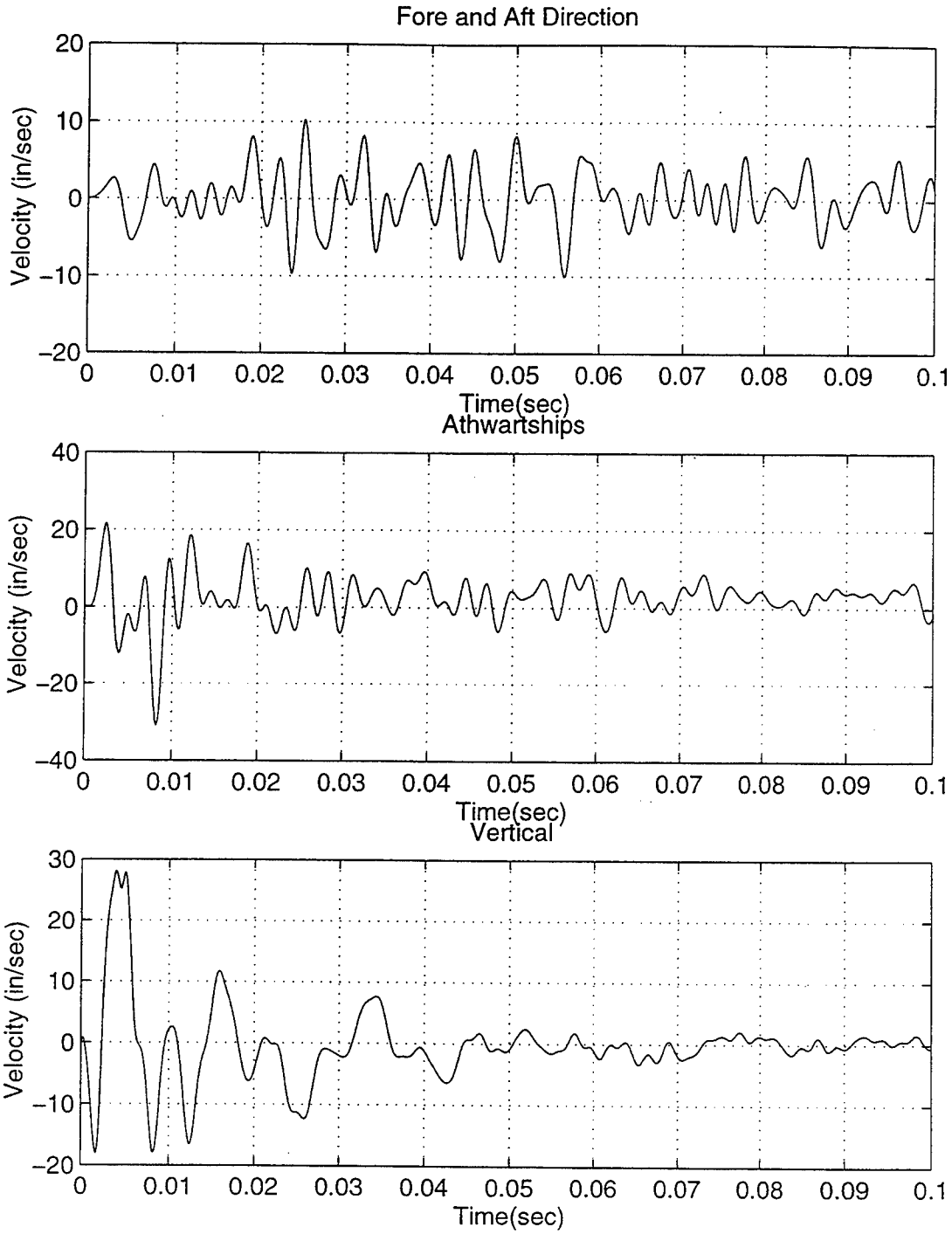

Figure 50. Keel Velocities (Node 397)

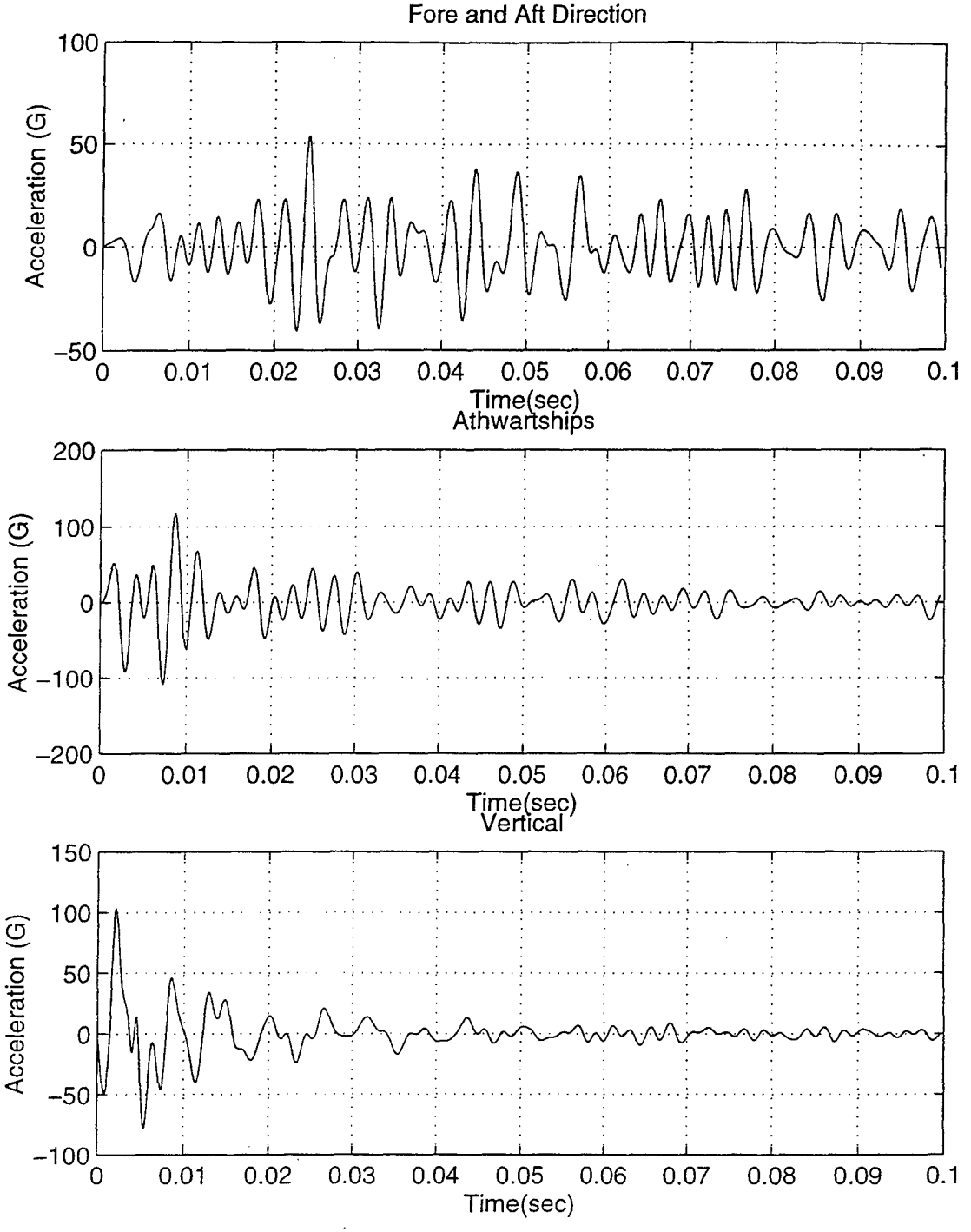

Figure 51. Keel Accelerations (Node 397)

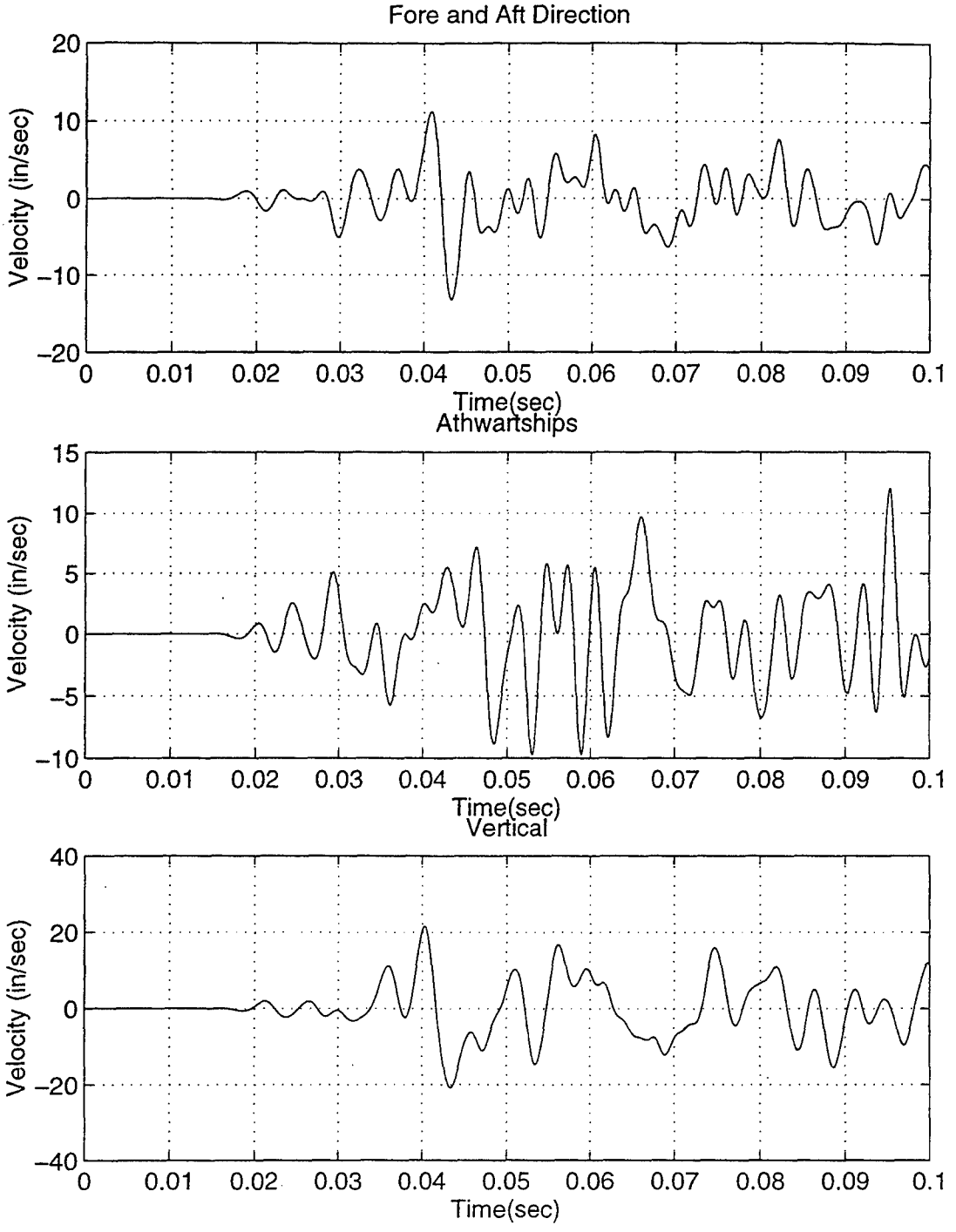

Figure 52. Bow Velocities (Node 1554)

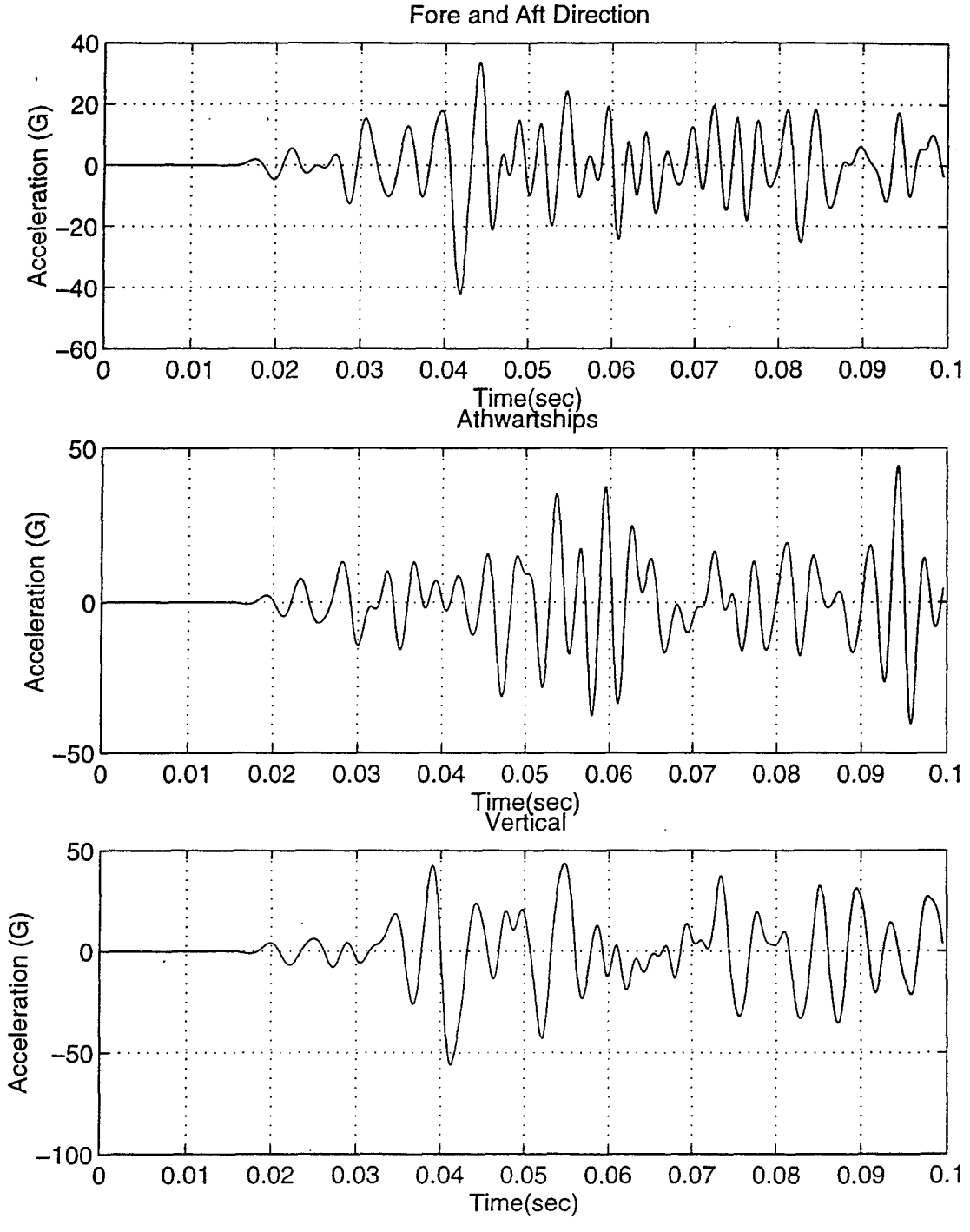

Figure 53. Bow Accelerations (Node 1554)

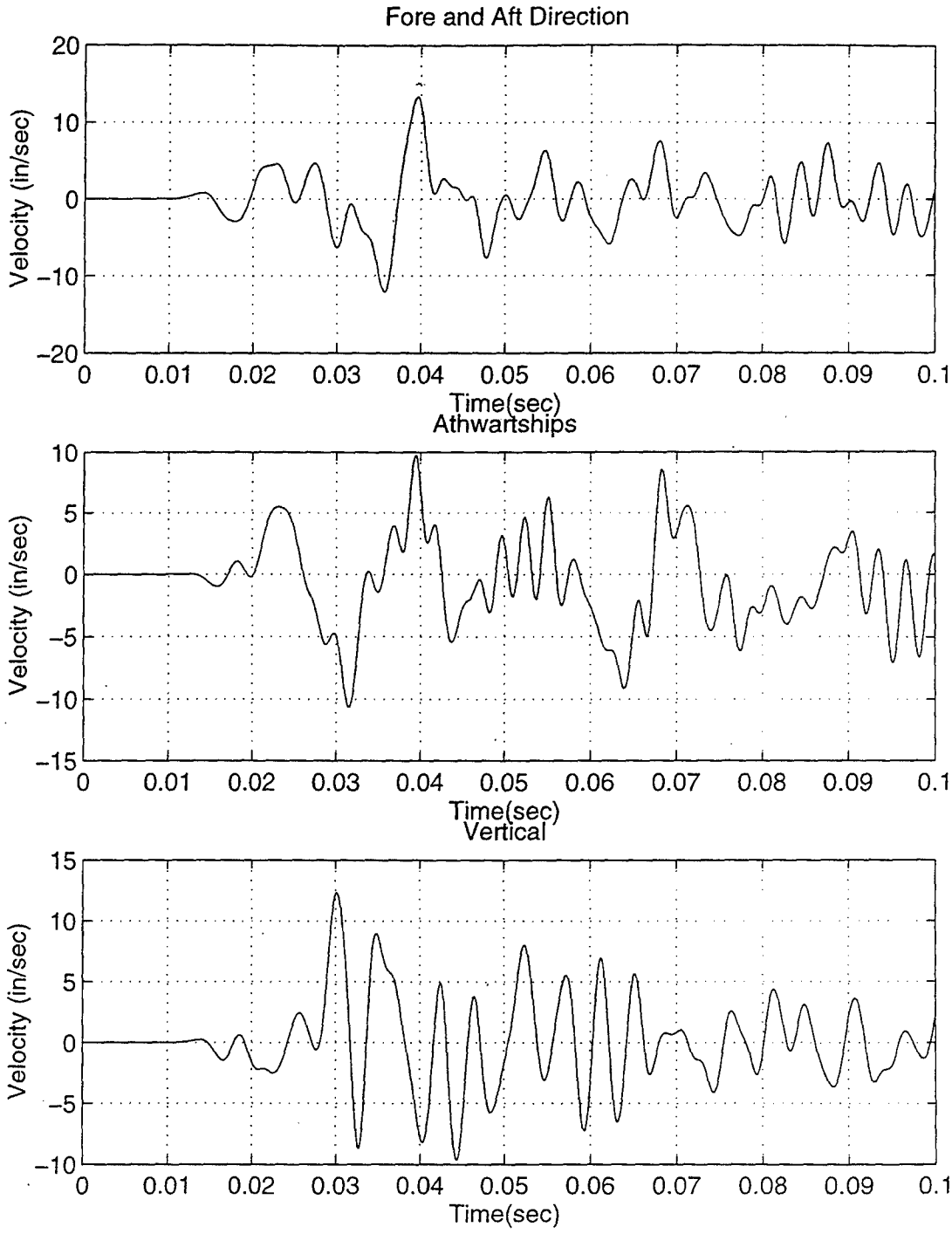

Figure 54. Stern Velocities (Node 2281)

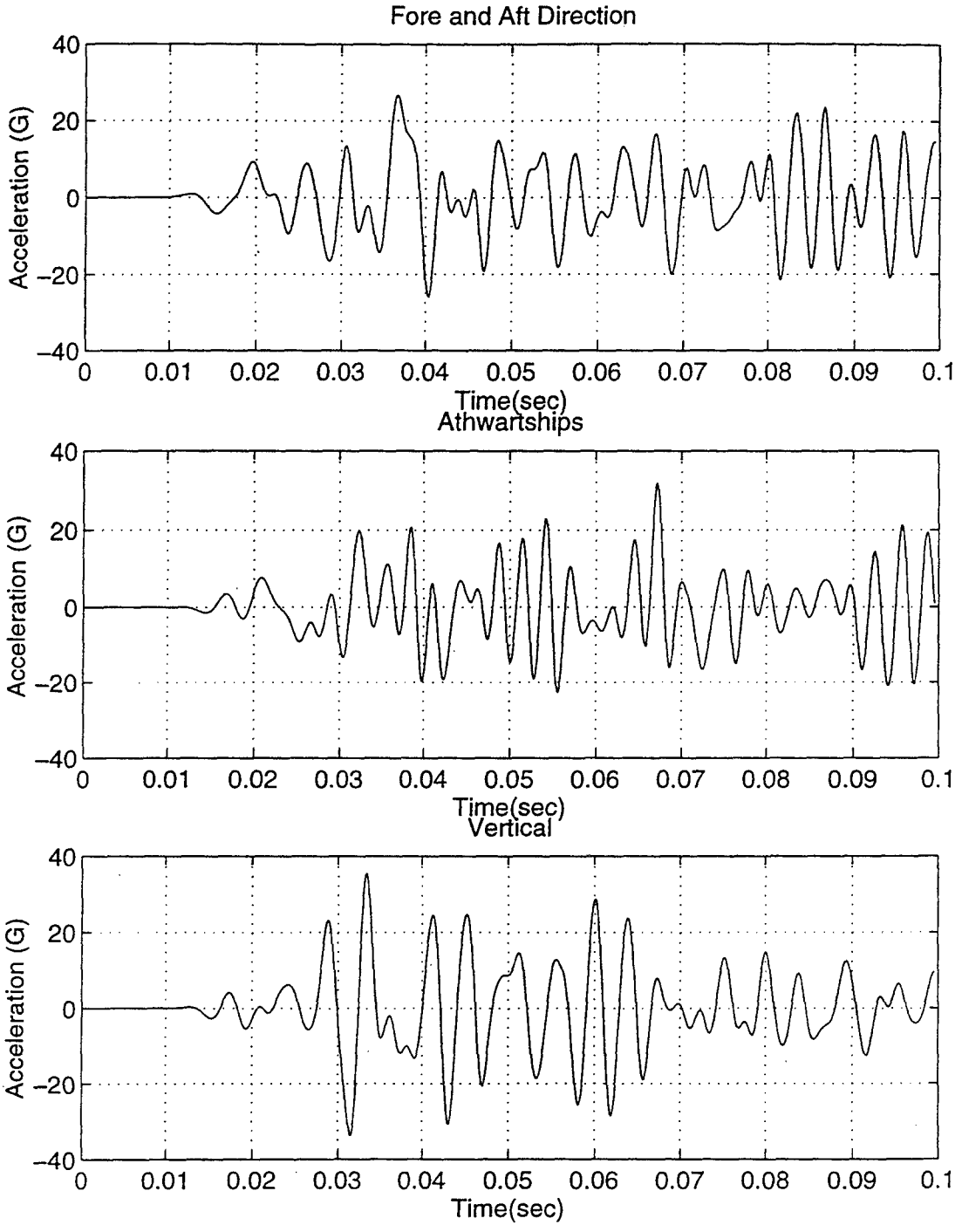

Figure 55. Stern Accelerations (Node 2281)

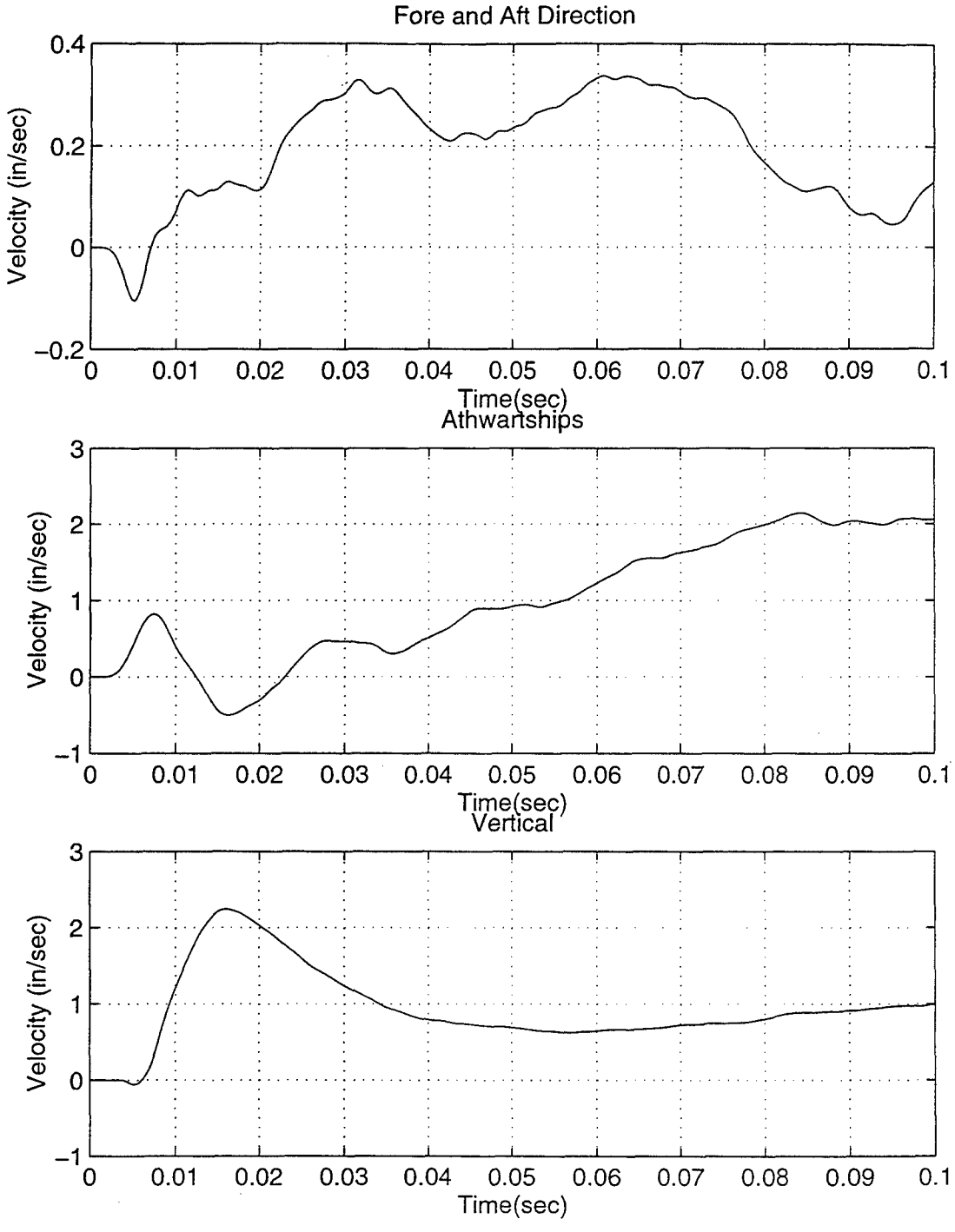

Figure 56. MER 1 Velocities (Node 4448)

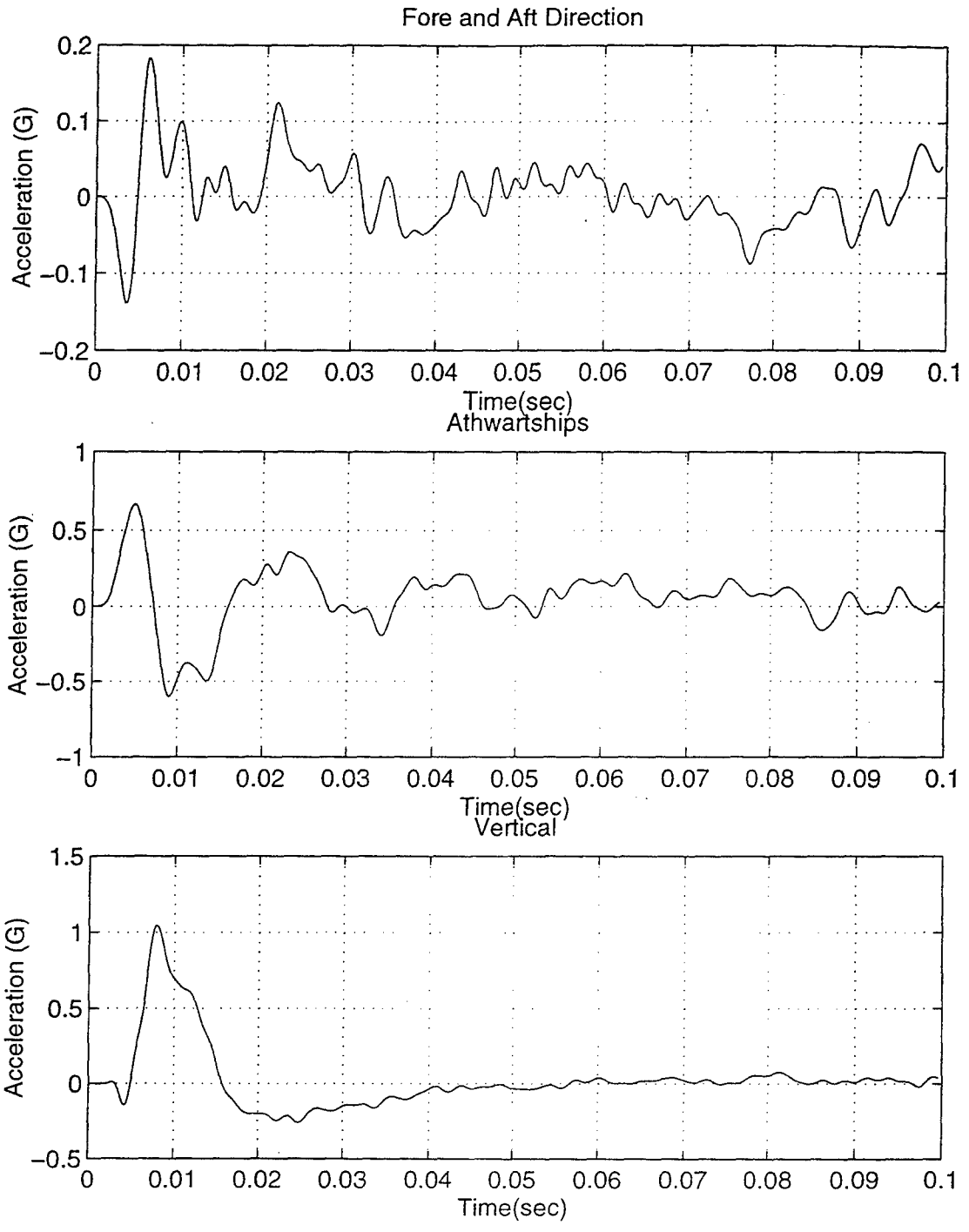

Figure 57. MER 1 Accelerations (Node 4448)

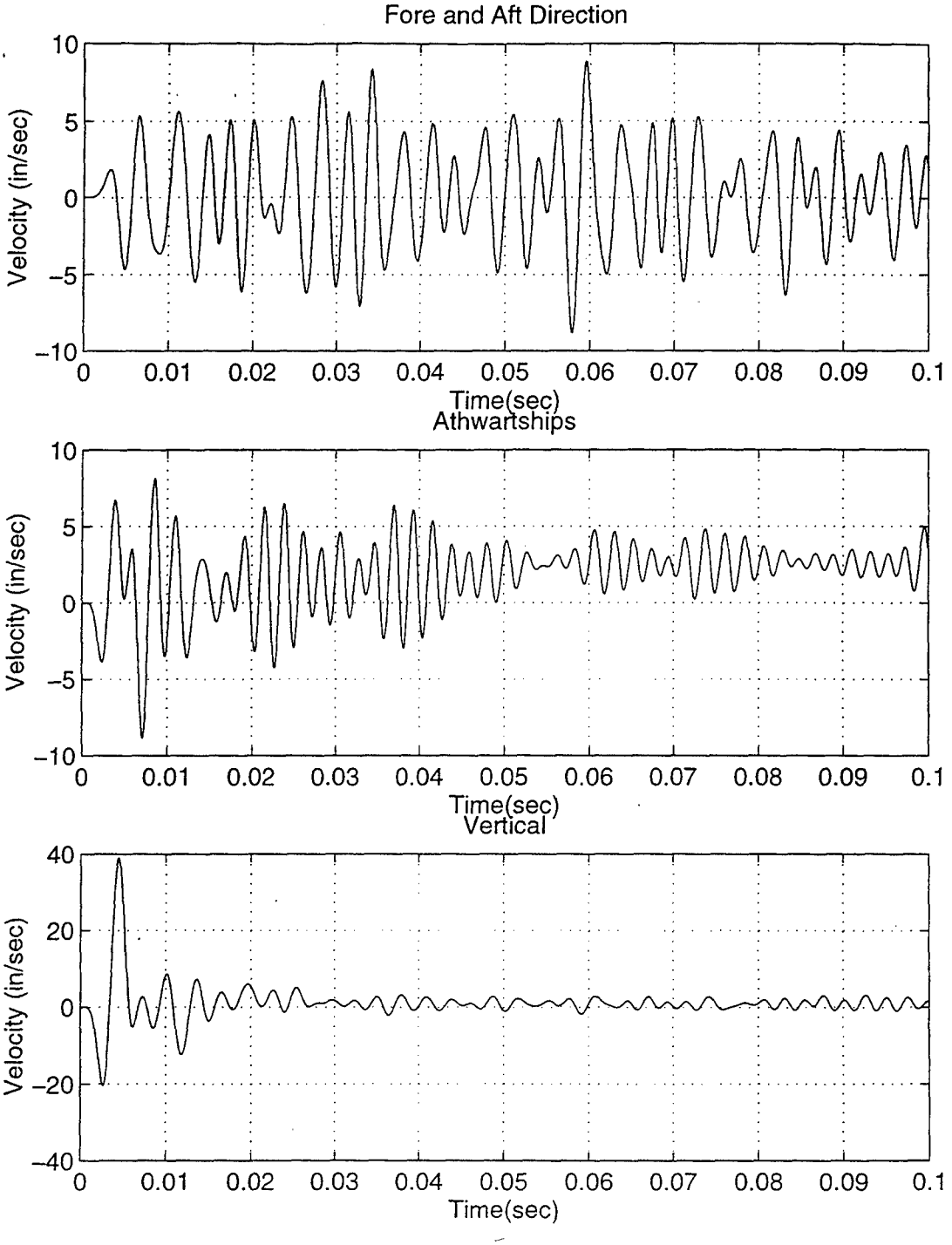

Figure 58. MER 2 Velocities (Node 4543)

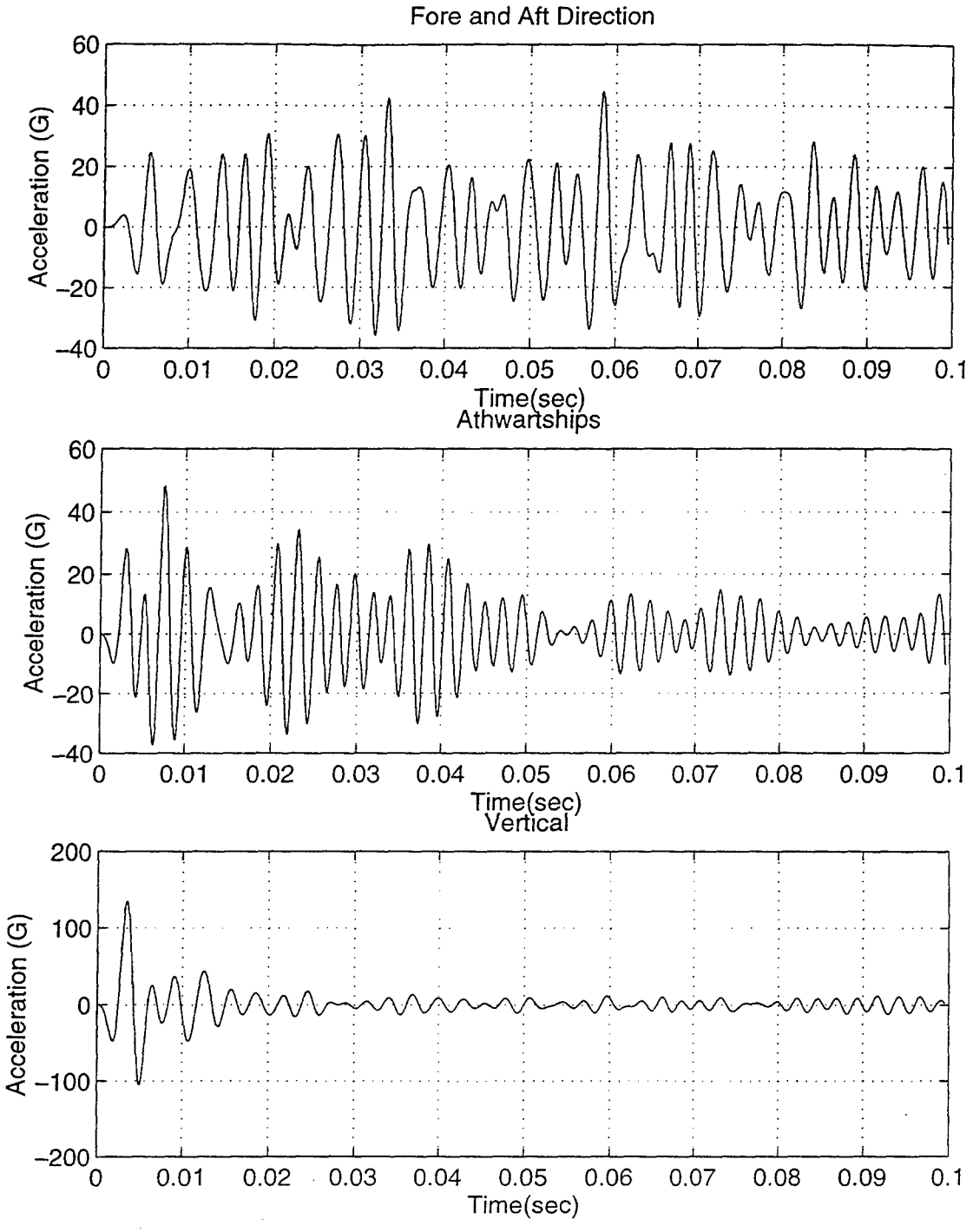

Figure 59. MER 2 Accelerations (Node 4543)

VII. CONCLUSIONS AND RECOMMENDATIONS

The introduction of a fluid volume model with a structure and utilizing the USA /CFA interface provides a means to capture the effects of cavitation upon a surface vessel in the early time frames of an underwater explosion. The effects of cavitation closure as seen in the two dimensional model can be quite significant and inflict another impulsive force upon the ship as reported in the DDG 53 shock trial reports [Ref. 22] in addition to the incident wave, bubble pulsations, bottom reflection, or bottom refraction. This increases the complicated task of predicting surface ship behavior when exposed to an underwater explosion. CFA OFF modeling may provide a conservative approach in predicting ship response to an underwater explosion in early time. Finite element modeling, time integration calculations, and tactical placement of an explosive device must be carefully done to accurately model surface ship behavior. Plane wave modeling with a surface ship model and a fluid mesh may provide more accurate overall ship and internal equipment responses.

With improving systems and capacity, the testing of new ship models with specific interior designs from the ship designer with the underwater shock analyst utilizing the USA/CFA code can prove to be a formidable method in predicting forcing functions on internal equipment of a surface vessel. In view of the changes of the DDG Flight IIA designed compared to the present DDG Flight II, this particular method may provide some cost benefits in future ship shock trials.

Recommend continuing studies in the following areas:

1. Improve on the two and three dimensional model with internal masses or fluids.
2. Obtain actual DDG-51 Flight IIA DDG designs from NAVSEA which can be imported into an FEM program such as IDEAS or MSC/PATRAN which can be tested with the USA code for both linear and non-linear responses.
3. Introduce other surface ship model types such as the slice hull.
4. Model the underwater tactical scenario with significant shallow water bottoms in order to study "littoral" responses of a surface ship close to the shore.

APPENDIX A. BULK CAVITATION PROGRAM

The following program calculates the bulk cavitation zone for various weights and depths of TNT. The program can be easily modified for other explosive material.

```
%The following program will compute the bulk cavitation zone of an underwater
%explosion of TNT explosive with depth and weight of charge as inputs.
%
%TNT characteristics
A1=1.18;A2=-.185;K1=22505;K2=.058;

%D=input('Enter depth of your charge ')
%W=input('Enter the weight of TNT explosive ')
Co=4967;                                          %speed of sound in water (ft/sec)
Pa=14.7;                                          %atmospheric pressure

x=[0:5:1200]';
n=length(x);
yu=diag(zeros(n));
yl=diag(zeros(n));
for j=1:n
     y(1)=0;
        for i=1:500
           r1=sqrt(((D-y(i))^2)+(x(j)^2));        %real charge distance
           r2=sqrt(((D+y(i))^2)+(x(j)^2));        %image charge distance
           theta=K2*W^(1/3)*((W^(1/3)/r1)^A2);    %decay constant (msec)
           dr=(r2-r1)/(Co*theta/1000);            %decay rate
           Pmax=K1*((W^(1/3)/r1)^A1);             %Incident shock wave
                 P1=Pmax*exp(-dr);                          %Inc shock wave @ raref arriv
           P1=Pmax*exp(-dr);                      %Inc shock wave @raref arr
           P2=K1*((W^(1/3)/r2)^A1);               %rarefrac at arrival time
           Ph=64*y(i)/144;                        %hydrostatic pressure

           F=P1+Pa+Ph-P2;                         %F(x,y) equation for upper boundary
                    if (F<=0)
                 break
                    else
                       y(i+1)=y(i)+.1;
              end
        end
     yu(j)=y(i);
     y(1)=0;
        for s=1:500
              r1=sqrt(((D-y(s))^2)+(x(j)^2));%real charge distance
           r2=sqrt(((D+y(s))^2)+(x(j)^2));        %image charge distance
           theta=K2*W^(1/3)*((W^(1/3)/r1)^A2);    %decay constant (msec)
           Pmax=K1*((W^(1/3)/r1)^A1);             %Incident shock wave
           P1=Pmax*exp(-dr);                      %Inc shock wave @ raref arriv
           P2=K1*((W^(1/3)/r2)^A1);               %rarefrac at arrival time
           Ph=64*y(s)/144;                        %hydrostatic pressure
           dr=(r2-r1)/(Co*theta/1000);            %decay rate
           g1=(D+y(s))/r2;
           g2=r2-(2*D*g1);
           g3=(g2/r1)*(((A2*r2)/r1)-A2-1);
           g4=P1/(Co*theta/1000);
           g5=(A1*P1)/(r1^2);
           g6=P1+Pa+Ph;
           G=-(g4*(1+g3))-(g5*g2)+(64*g1/144)+(A1*g6/r2); %Combined G(x,y) lowcav bound
                 if (G>=0)
                    break
                 else
                    y(s+1)=y(s)+.1;
                 end
        end
     yl(j)=y(s);
         if (yl(j)<=yu(j))
             z=j;
             break
         else
             z=n;
         end

end
yu=(-1)*yu(1:z);
yl=(-1)*yl(1:z);
xf=x(1:z);
```

APPENDIX B. CROSS-SECTIONAL HULL INPUTS

The following are sample inputs for the two-dimensional model only.

```
assign output2='OT1',unit=11,delete $
assign output2='IDEAS1.op2',unit=12,unknown
ID USA,CROSS HULL3
SOL 109  $ MSC
DIAG 8,13  $
TIME 99
$
$ START SDRC'S I-DEAS OPTION
compile phase0 souin=mscsou nolist noref $
$ add CALL to get output2 geometry datablocks early in solution.
alter 297 $ before call seprep2
type parm,,i,y,ounit2=12 $
if (post < 0) then   $
  OUNIT1=OUNIT2
  CALL OUT2GEOM  CSTM,GPL,GPDT,EPT,MPT,GEOM2,GEOM3,GEOM4,
                 GEOM1,DIT,DYNAMICS,EQEXIN,BGPDT,CASECC//
                 OUNIT1/0 $
endif $
$ END SDRC'S I-DEAS OPTION
$
compile subdmap=selg,souin=mscsou,noref,nolist $
ALTER    14 $ AFTER SSG1
type parm,,i,n,storit = 0
call dbstore pjx,,,,//seid/0/'DBALL'/s,storit $
OUTPUT2  BGPDTs,EQEXINs,,,///11//25000 $
$
compile subdmap=sekr,souin=mscsou,noref,nolist $
ALTER    49 $ AFTER gpsp
type parm,,i,n,foundit = 0 $
call dbfetch /pjx,,,,/seid/0/0/0/s,foundit $
OUTPUT2  uset,pjx,cstms,,///11//25000 $
$
compile subdmap=DTRANRS,souin=mscsou,noref,nolist $
alter 1
type db ECTS
ALTER    6 $ before TRD1
OUTPUT2  ECTs,BDD,KDD,MDD,///11//25000 $
$add EOF marker
OUTPUT2  //-9/12/ $
$
EXIT     $

CEND
TITLE=CROSS HULL
LOADSET=10
TSTEP=25
SPC    =     1
DISP(plot)=ALL
velocity(plot)=all
stress(plot)=all


BEGIN BULK
PARAM   AUTOSPC      YES
PARAM   POST          -2


$ TSTEP,SID,N1,DT1,NO1
TSTEP,25,40,0.025,1
$
$ LSEQ,SID,DAREA,LID
LSEQ,10,10,1
GRID           1       0  -336.0   240.0    12.0       0
GRID           2       0  -336.0   240.0     0.0       0
```

```
CROSS SECTIONAL HULL3B PROBLEM
1,0,0,1,1,0,0



 USAF
 GAL
 F F F F
 F F F
```

```
AUGMAT INPUT FOR CROSS HULL3 PROBLEM
GAL HULL3.FLU HULL3.GEO HULL3.PRE     $ STRNAM FLUNAM GEONAM PRENAM
F F F F                               $ FRWTGE FRWTST FRWTFL LUMPFM
F F F T                               $ FLUSKY DAAFRM SYMCON DOFTAB
T T F F                               $ PRTGMT PRTTRN PRTSTF PRTAUG
F F F F                               $ MODTRN STRLCL INTWAT CFADYN
NASTRAN-MSC                           $ MAINKY
0                                     $ NTYPDA
452 1356 6 3                          $ NSTR   NSFR   NFRE   NFTR
1                                     $ NSETLC
0 1 80 1                              $ NDICOS JSTART JSTOP  JINC
```

```
FLUID MASS RUN FOR CROSS SECTION HULL3B
HULL3.FLU   HULL3.GEO  GAL HULL3.DAA     $ FLUNAM GEONAM GRDNAM DAANAM
T T T T                              $ PRTGMT PRTTRN PRTAMF CALCAM
T T F F                               $ EIGMAF TWODIM HAFMOD QUAMOD
F F T T                               $ PCHCDS NASTAM STOMAS STOINV
F F F F                               $ FRWTFL FRWTGE FRWTGR FRESUR
F T F F                               $ RENUMB STOGMT ROTGEO ROTQUA
F F F F                               $ PRTCOE STRMAS SPHERE ROTSYM
F T F F                               $ OCTMOD CAVFLU FRWTFV INTCAV
F F                                   $ BOTREF MASREF
FLUID.VOL FLUID.VOL                   $ CAVNAM FACNAM
NASTRAN-MSC                           $ MAINKY
0 452 0 80                           $ NSTRC  NSTRF  NGEN   NGENF
0 0 40                                $ NBRA   NCYL   NCAV
0 3034                                $ NFVNC  NFVNF
9.3455-5 57120.                       $ RHO    CEE
10                                    $ NVEC
240. 0. 1. 0.                        $ DEPTH  CXFS   CYFS   CZFS
14.7 386.4                            $ PATM   GRAVAC
0                                     $ NUMCON
0                                     $ NSRADI
0                                     $ NSORDR
```

```
USA-NASTRAN CFA TIMINT RUN FOR CROSS HULL3 PROBLEM
HULL3.PRE HULL3.POS    $ PRENAM POSNAM
HULL3.RES              $ RESNAM WRTNAM
F F F                  $ REFSEC FLUMEM STRVEL
1 0                    $ NTINT  NCHGAL
0. 3.E-5               $ STRTIM DELTIM
3.E-2  0. 0.           $ FINTM  ADAMP  BDAMP
T F F F                $ EXPWAV SPLINE VARLIN PACKET
F T F F                $ HYPERB EXPLOS DOUBDC VELINP
F F F                  $ BUBPUL SHKBUB BOTREF
1                      $ NCHARG
0. 14.7                $ HYDPRE PATM
0. -1.44E3 0.          $ XC     YC     ZC
0. -351.8   0.          $ SX     SY     SZ
201                    $ JPHIST
1. 0.                  $ PNORM  DETIM
3.E-5                  $ DTHIST
2                      $ CHGTYP
100. 100.  120.          $ WEIGHT SLANT CHGDEP
1 150  0               $ NSAVER NRESET NSODFL
0 0 0 0                $ LOCBEG LOCRES LOCWRT NSTART
T F F                  $ FORWRT STBDA2 ASCWRT
T F F                  $ NOAMBI PRTVOL PRTINI
.5 0.                  $ FVBETO FVBET1
1 1 1                  $ ICAVSW IORDF  IORDV
124 1440 3034          $ NFVWAV NFVELM NFVNOD
T                      $ DISPLA
0 0                    $ NPREVT NPREVF
T T                    $ LISTRE PRTPLT
2 0 0                  $ NWETHS NDRYHS NUMSET
42 2                   $ NODOUT NFROUT
3209 2                 $ NODOUT NFROUT
2 0 0                  $ NWETHS NDRYHS NUMSET
42 2                   $ NODOUT NFROUT
3209 2                   $ NODOUT NFROUT
4 0                    $ NPREHS NUMSET
42 0                   $ NEQHPR IPRS
1600 1                 $ NEQHPR IPRS
2994 0                 $ NEQHPR IPRS
3021 0                 $ NEQHPR IPRS
F                      $ SCALEF
```

```
hull3B MODEL
HULL3.POS
1001,40,0,0,1
```

```
assign inputt2='UT1',unit=11 $
assign master='hull3B.MASTER' $
assign output2='IDEAS2.op2',unit=12,unknown
RESTART version=1, keep $
ID USA, HULL3B
SOL 109  $ MSC
DIAG 8,13  $
TIME 120
$
compile subdmap=DTRANRS,souin=mscsou,noref $
ALTER    7,7 $ eliminate TRD1
delete   /PNLD,,,,/ $
INPUTT2  /UHV,,,,//11 $
EQUIVX UHV/UDVT/-1 $
CEND
TITLE= THESIS HULL3B MODEL

LOADSET=10
TSTEP=46
DISP(plot)=ALL
STRESS(plot)=ALL
VELOCITY(plot)=ALL
ACCELERATION(plot)=All
BEGIN BULK
TSTEP,46,1001,3.0e-5,1
ENDDATA
```

APPENDIX C. COMBAT SYSTEMS AREA RESPONSES-1962 ELEMENT MODEL

The following plots represent the responses for CSER 1,2, 3 and the SPY radar room for the 1962 element model.

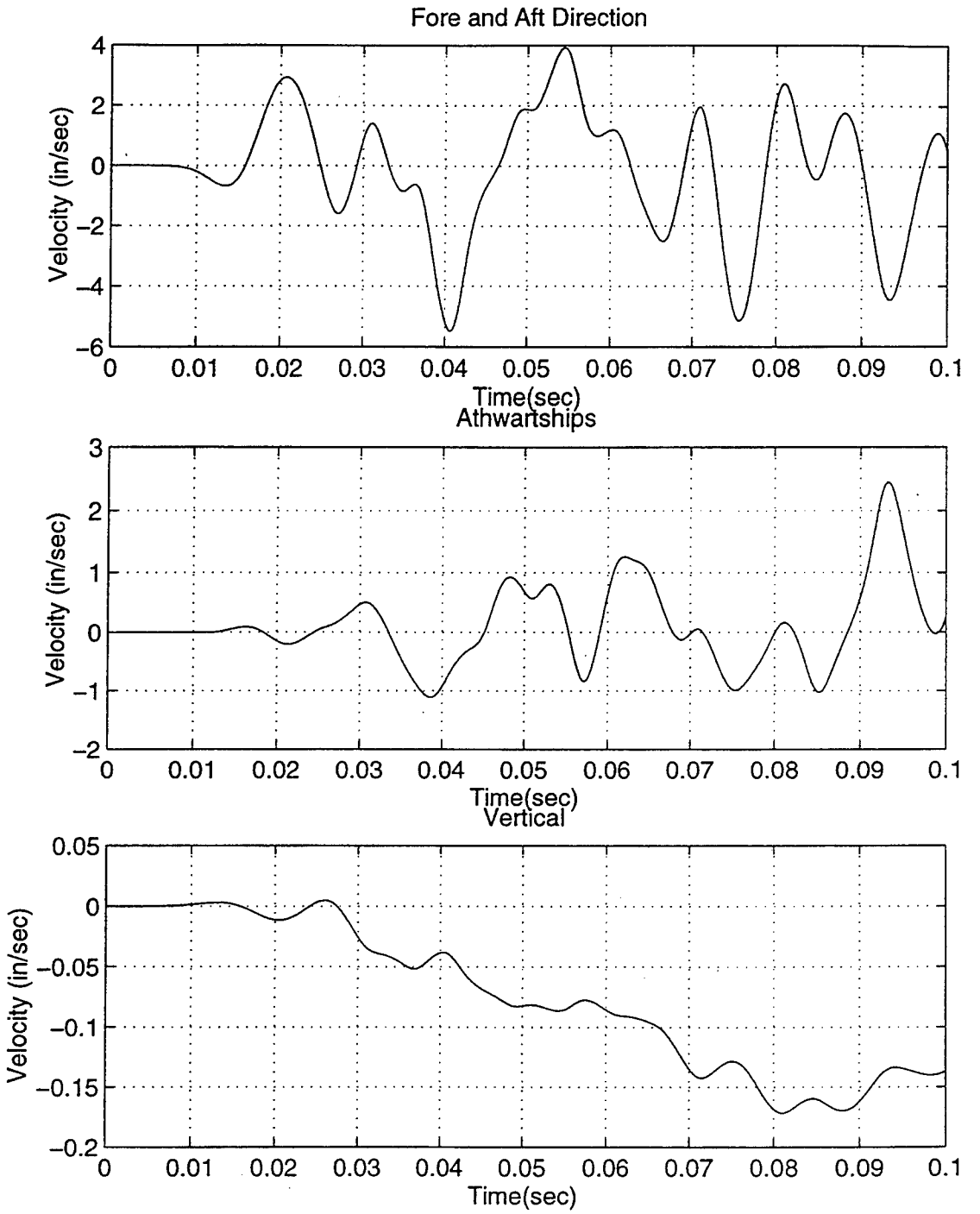

Figure 60. CSER 1 Velocities (Node 1649)

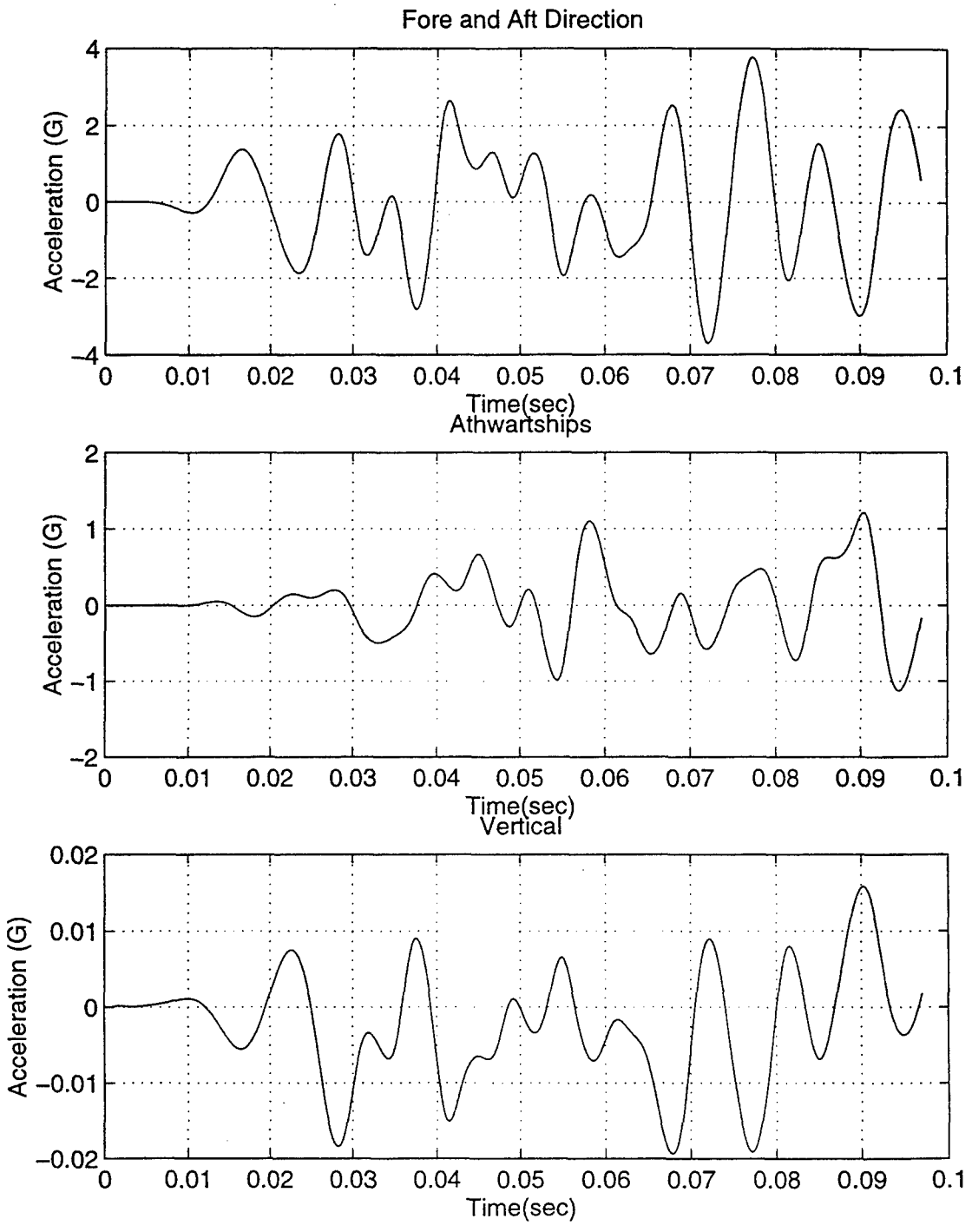

Figure 61. CSER 1 Accelerations (Node 1649)

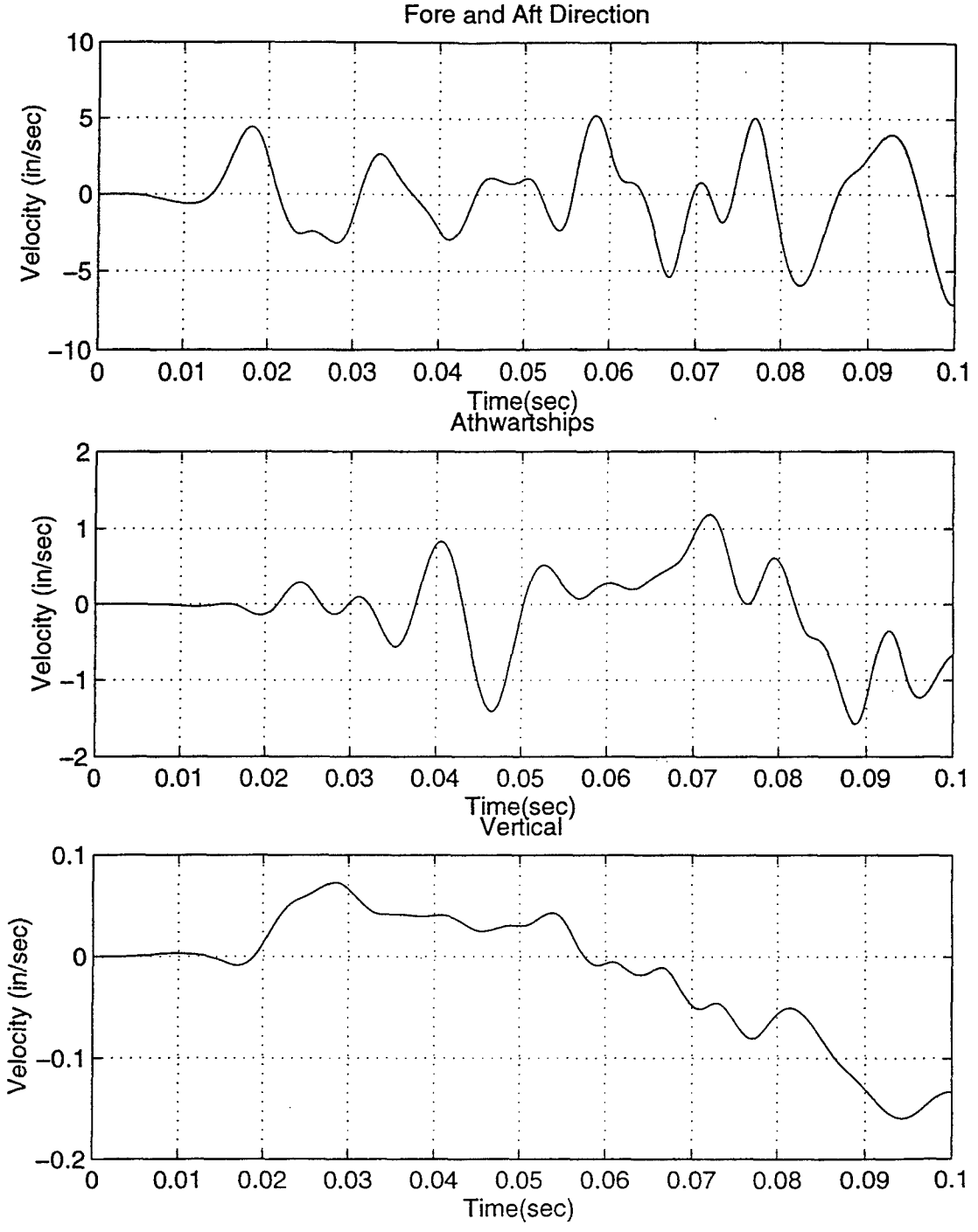

Figure 62. CSER 2 Velocities (Node 1748)

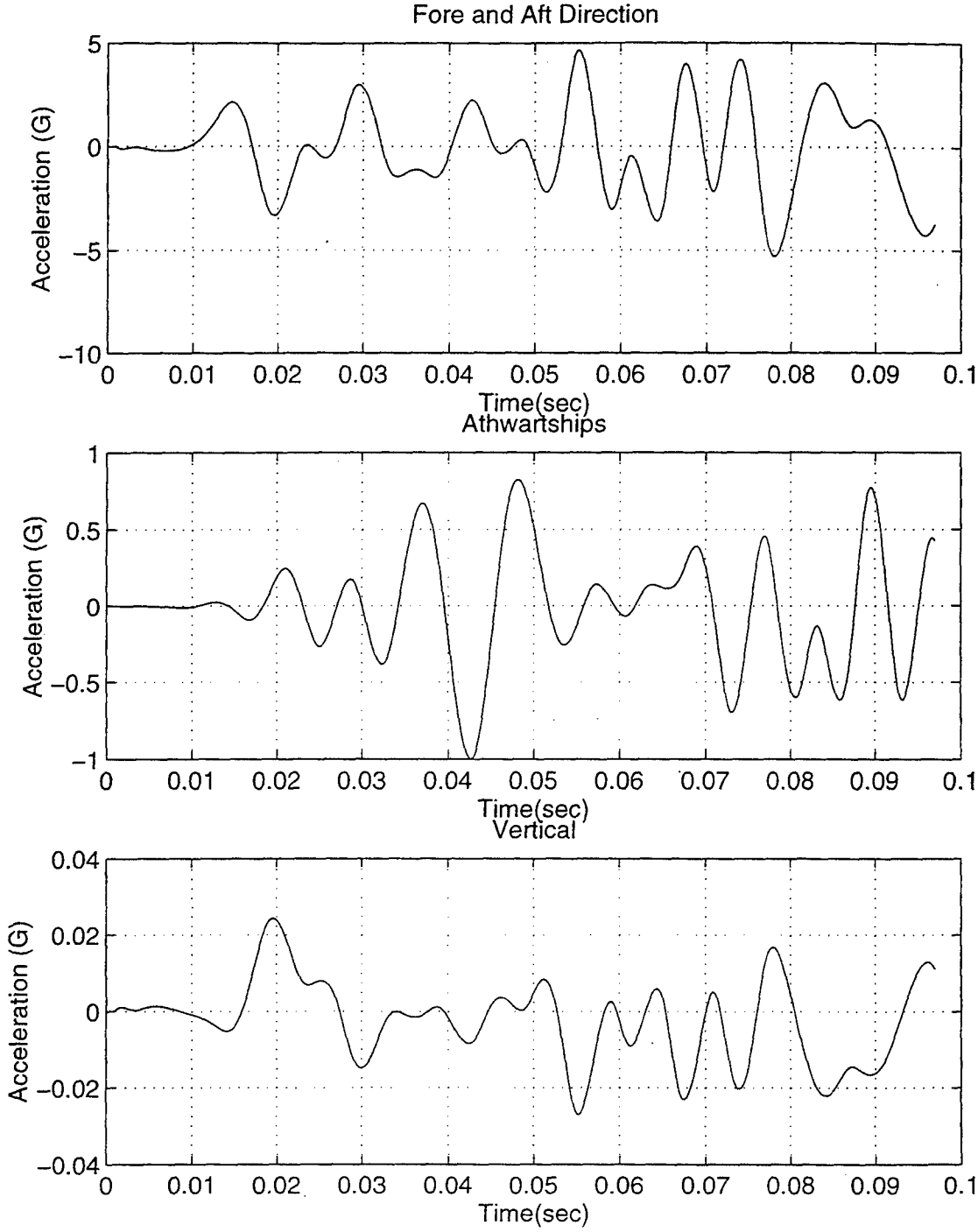

Figure 63. CSER 2 Accelerations (Node 1748)

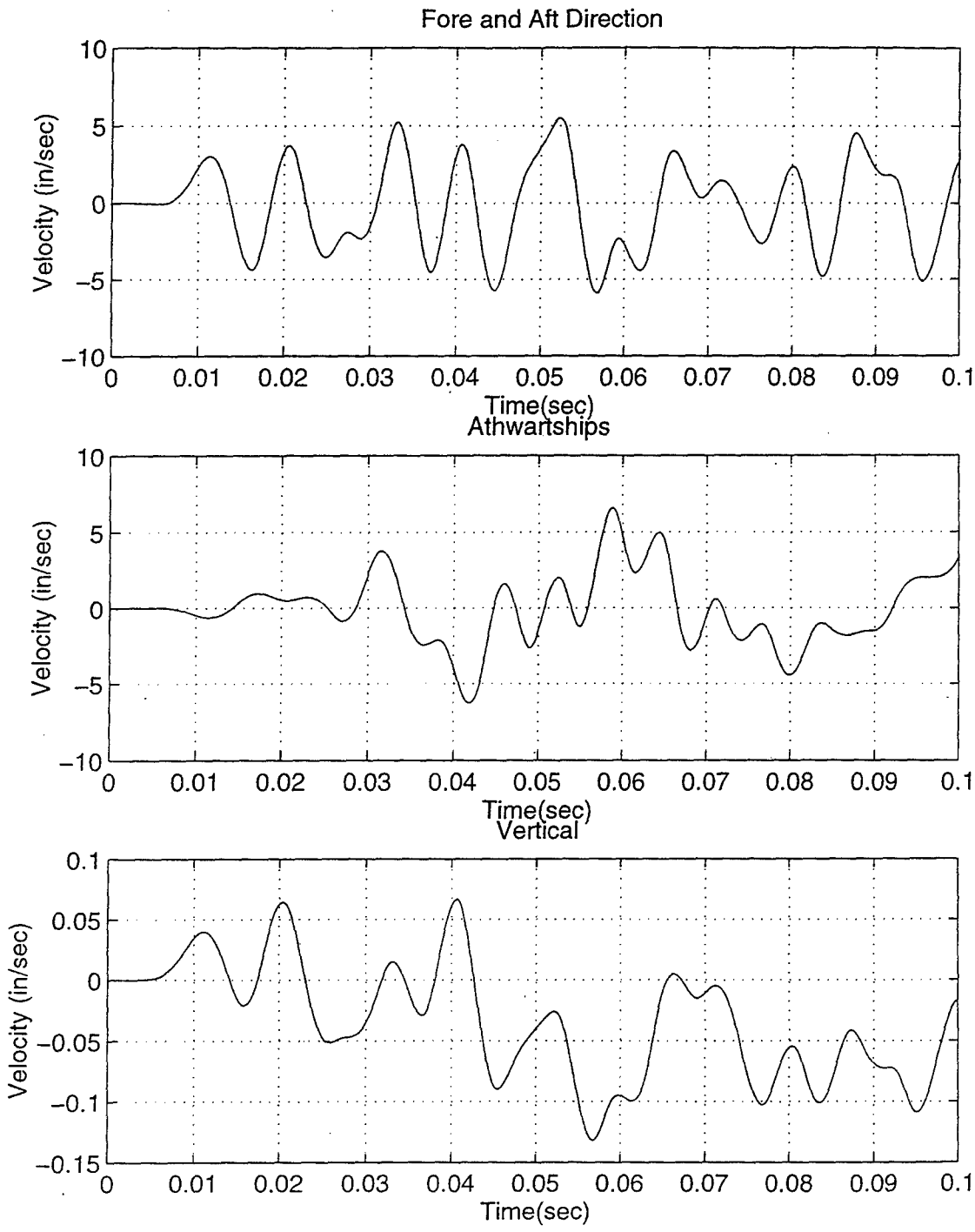

Figure 64. CSER 3 Velocities (Node 1990)

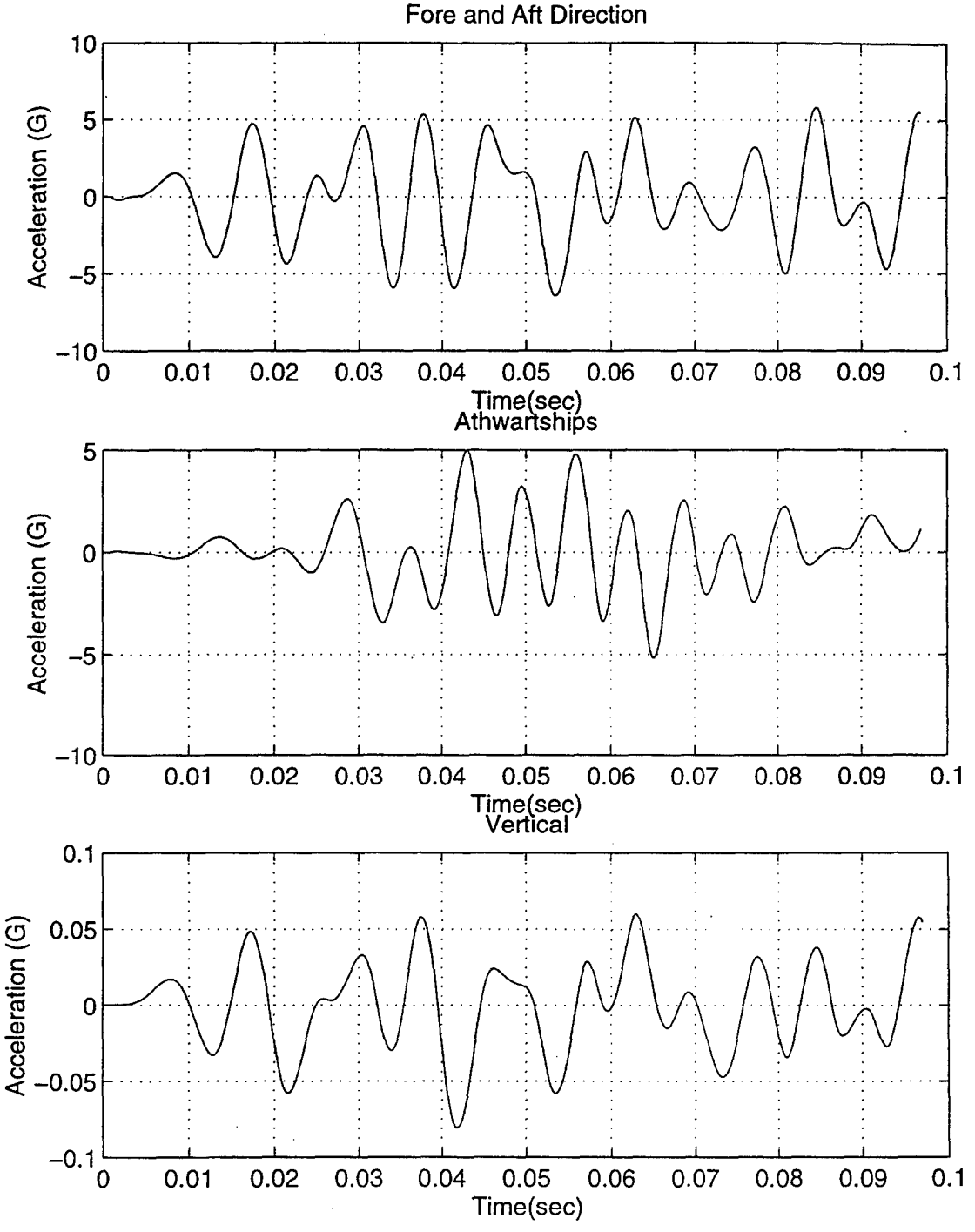

Figure 65. CSER 3 Accelerations (Node 1990)

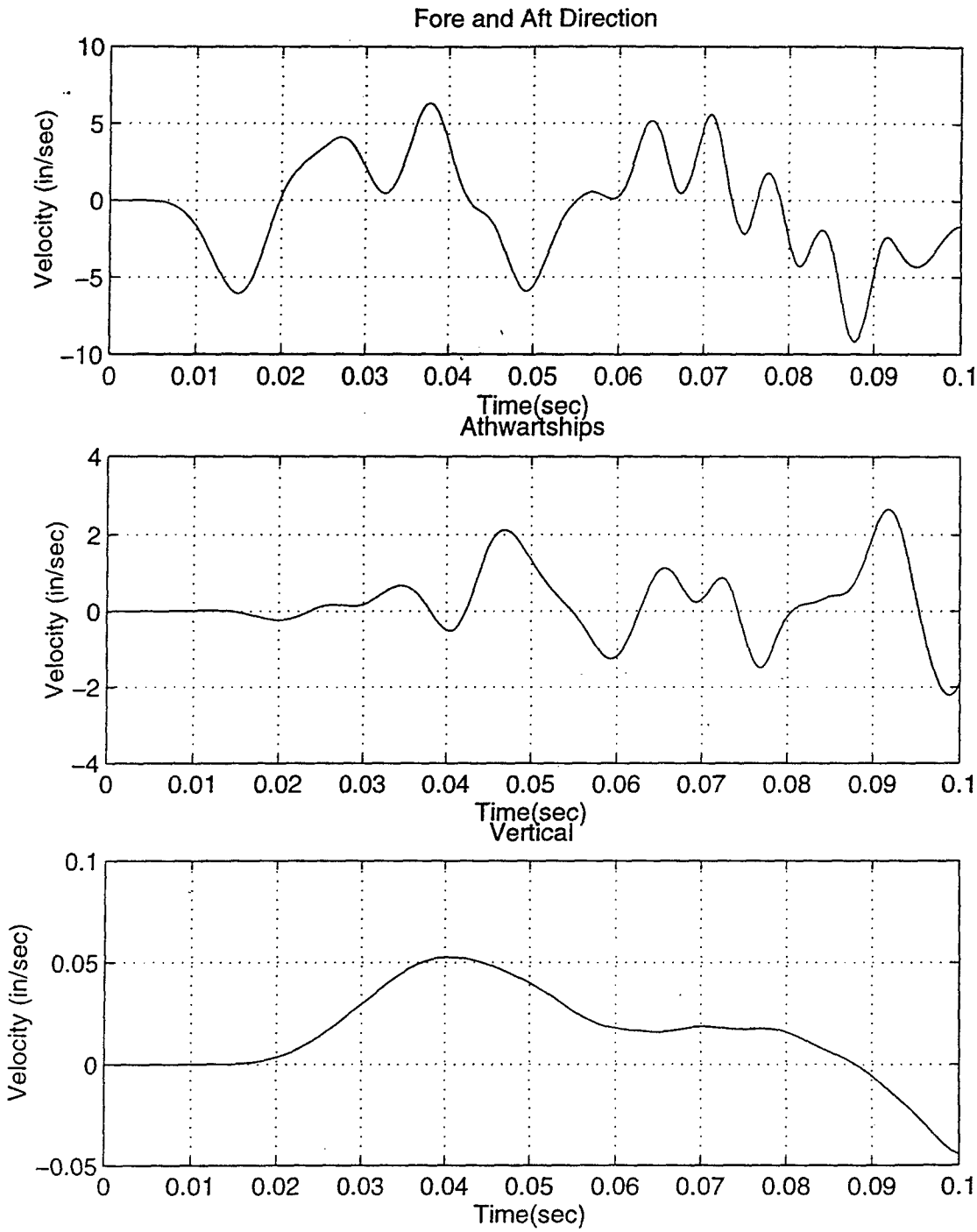

Figure 66. SPY Radar Room Velocities (Node 2534)

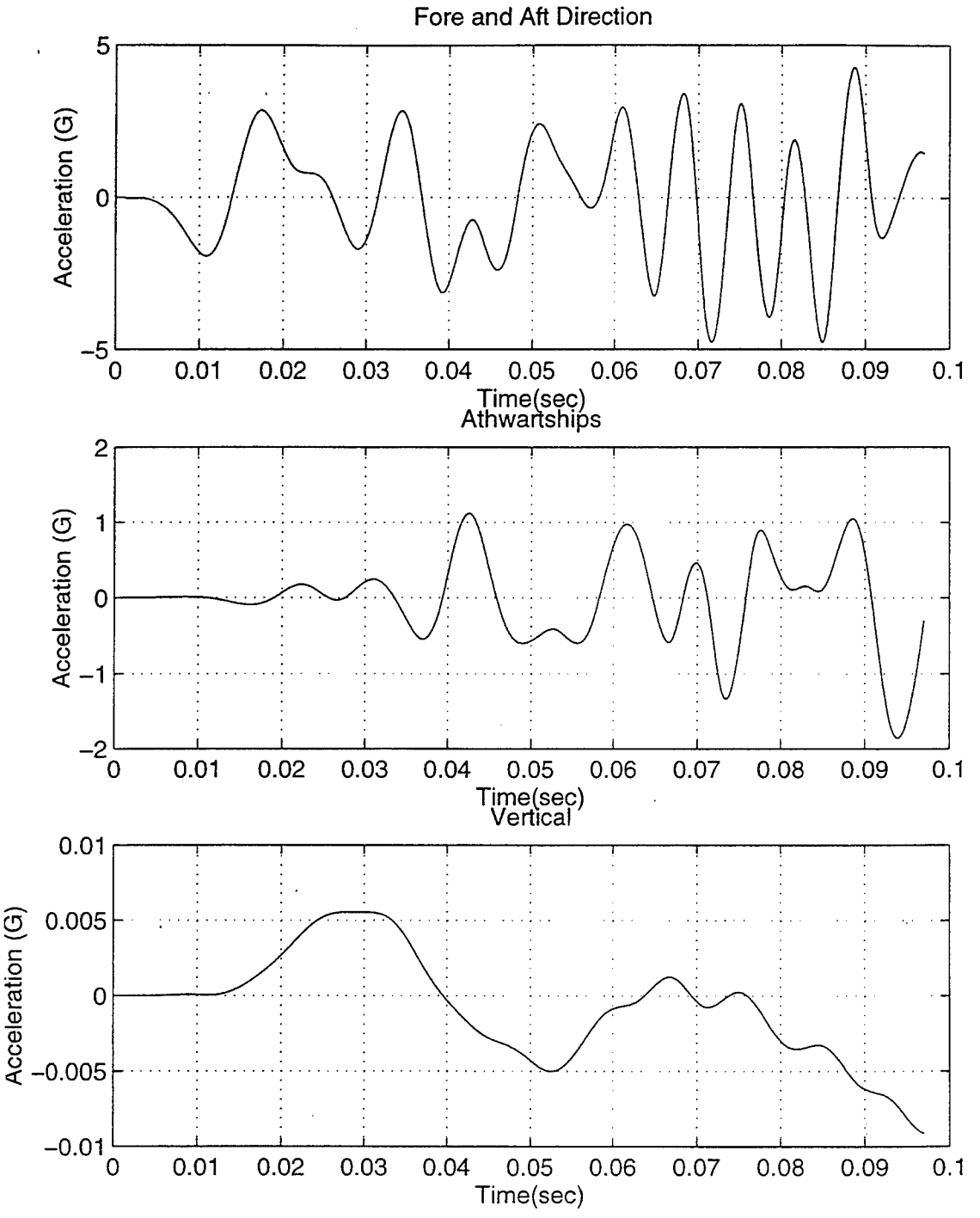

Figure 67. SPY Radar Room Accelerations (Node 2534)

APPENDIX D. SMEAR PLATE DATA

The following illustrates the smeared plate area method and ratios that were extracted from [Ref. 23].

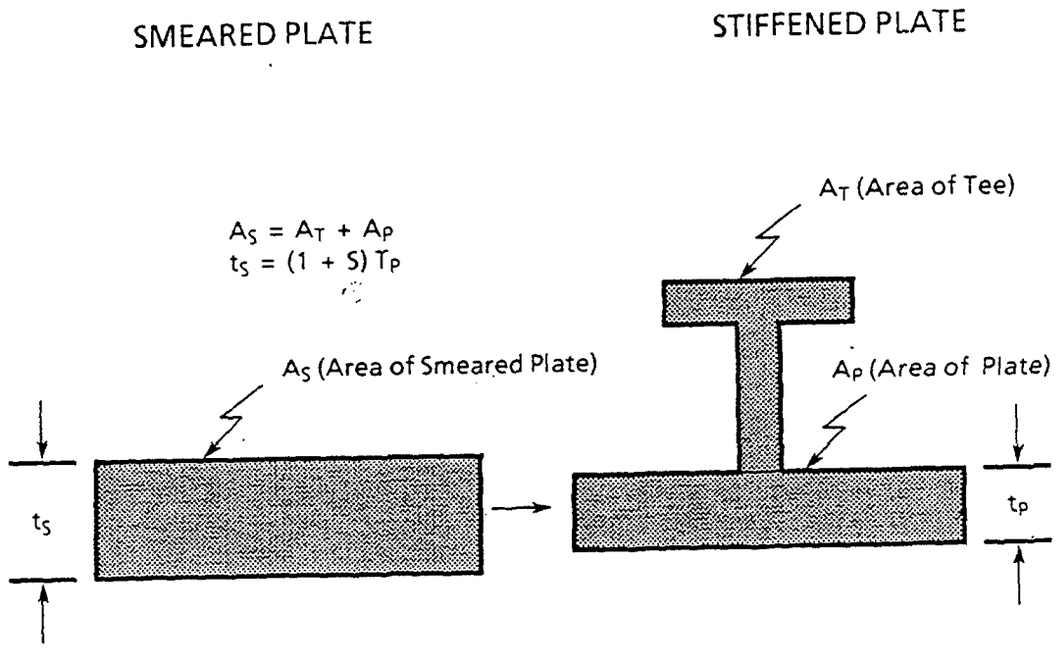

Figure 68. Smeared Plate Area Method [Ref. 14]

SEGMENT PROPERTIES

	PROPERTIES OF STIFFENED PLATES						
	AREA		N.A. TO	SEC MOD			SMEAR
SEG	TOTAL IN2	SHEAR IN2	PLATE IN	PLATE IN3	FLANGE IN3	WT/FT LBF/FT	RATIO
1	11.00	.66	.51	28.56	2.96	37.37	.10
2	8.13	.72	.69	19.71	3.86	27.61	.22
3	8.01	.71	.68	19.78	3.84	27.22	.22
4	10.01	1.06	.95	36.86	6.64	33.99	.22

APPENDIX E. COMBAT SYSTEM EQUIPMENT WEIGHTS

The following table comprises the general combat system equipment utilized in the distribution of lump massing in the 5698 element model whose weights derived from [Ref. 25] and placed in locations utilizing [Ref. 24].

Space	Location	Weight (lb)
Communication Center	2-126-1-C	1200
Radio Trans. Room	2-158-1-C	5884
Array Room No. 1	03-128-2-Q	14692
Array Room No. 2	03-128-2-Q	14692
Array Room No. 3	03-155-1-C	14692
Array Room No. 4	03-155-2-C	14692
Radar Room No. 1	03-128-0-C	27720
Radar Room No. 2	03-142-0-C	27720
Radar Room No. 3	01-274-1-C	12035
Power Supp/Conv Room	3-126-0-Q	11850
Power Conversion Room	3-319-0-Q	11850
Sonar Equip. Room No. 1	1-18-0-Q	11545
Sonar Equip. Room No. 2	2-18-0-Q	11545
Sonar Equip. Room No. 3	3-18-0-Q	11545
Sonar Dome	External to bow	117246
Combat Sys. Equp. Rm 1	2-53-1-C	4000
Combat Sys. Equp. Rm 2	2-126-2-C	23285
Combat Sys. Equp. Rm 3	1-300-0-C	4000
Combat Inform. Center	1-126-0-C	12120
Tomahawk Equp. Room	2-153-2-C	1421
5"54 Loader Drum Room	1-46-0-C	41658
VLS No. 1	01-78-0-M	138453
VLS No. 2	01-338-0-M	258853
Starboard Torpedo Tube	01-342-1-M	2430
Port Torpedo Tube	01-342-2-M	2430
Gun Mount 21	03-115-0-M	13600
Gun Mount 22	02-310-0-M	13600

APPENDIX F. COMBAT SYSTEMS AREA RESPONSES-5698 ELEMENT MODEL

The following plots represent the responses for CSER 1,2, 3 and the SPY radar room for the 5698 element model.

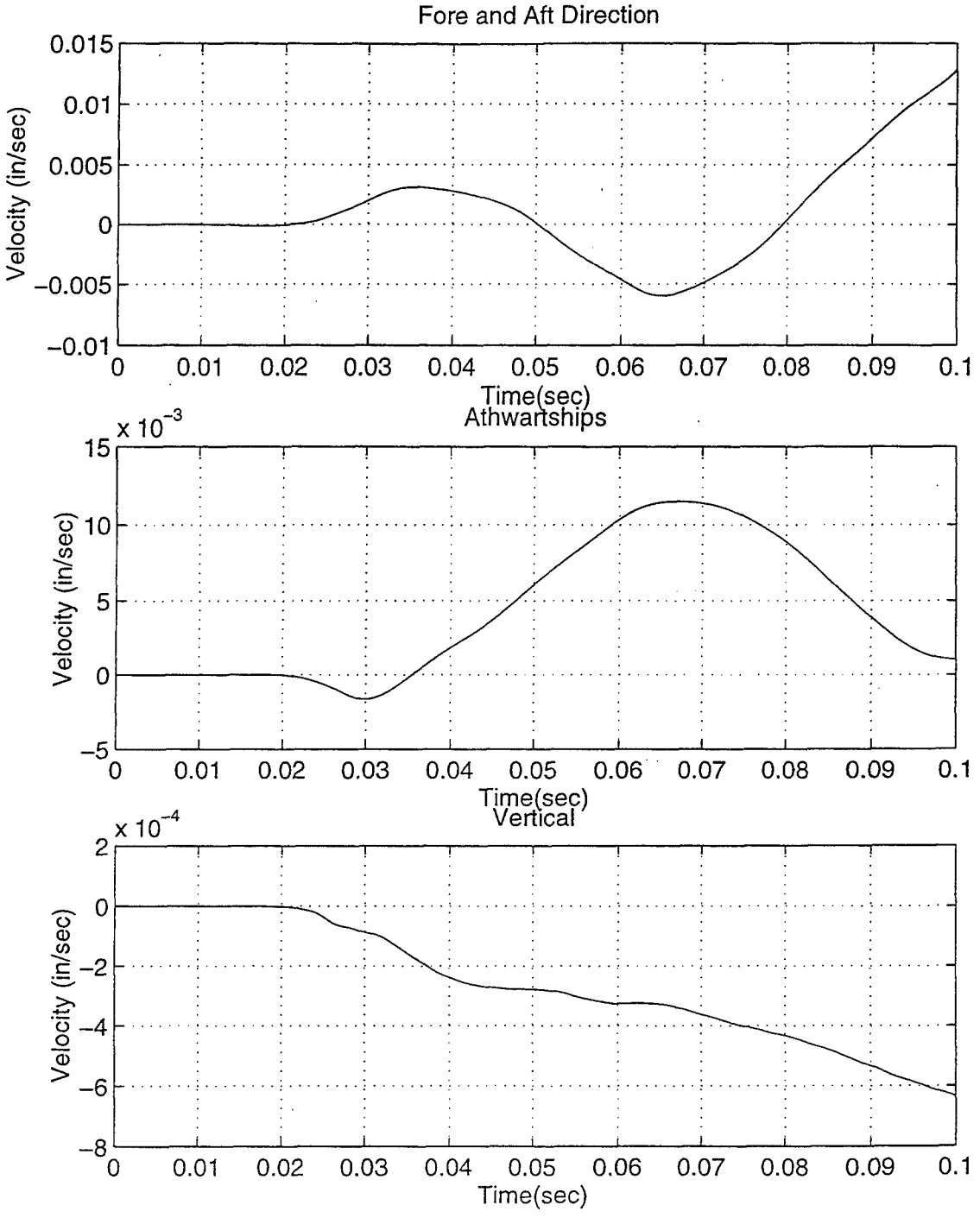

Figure 69. CSER 1 Velocities (Node 3567)

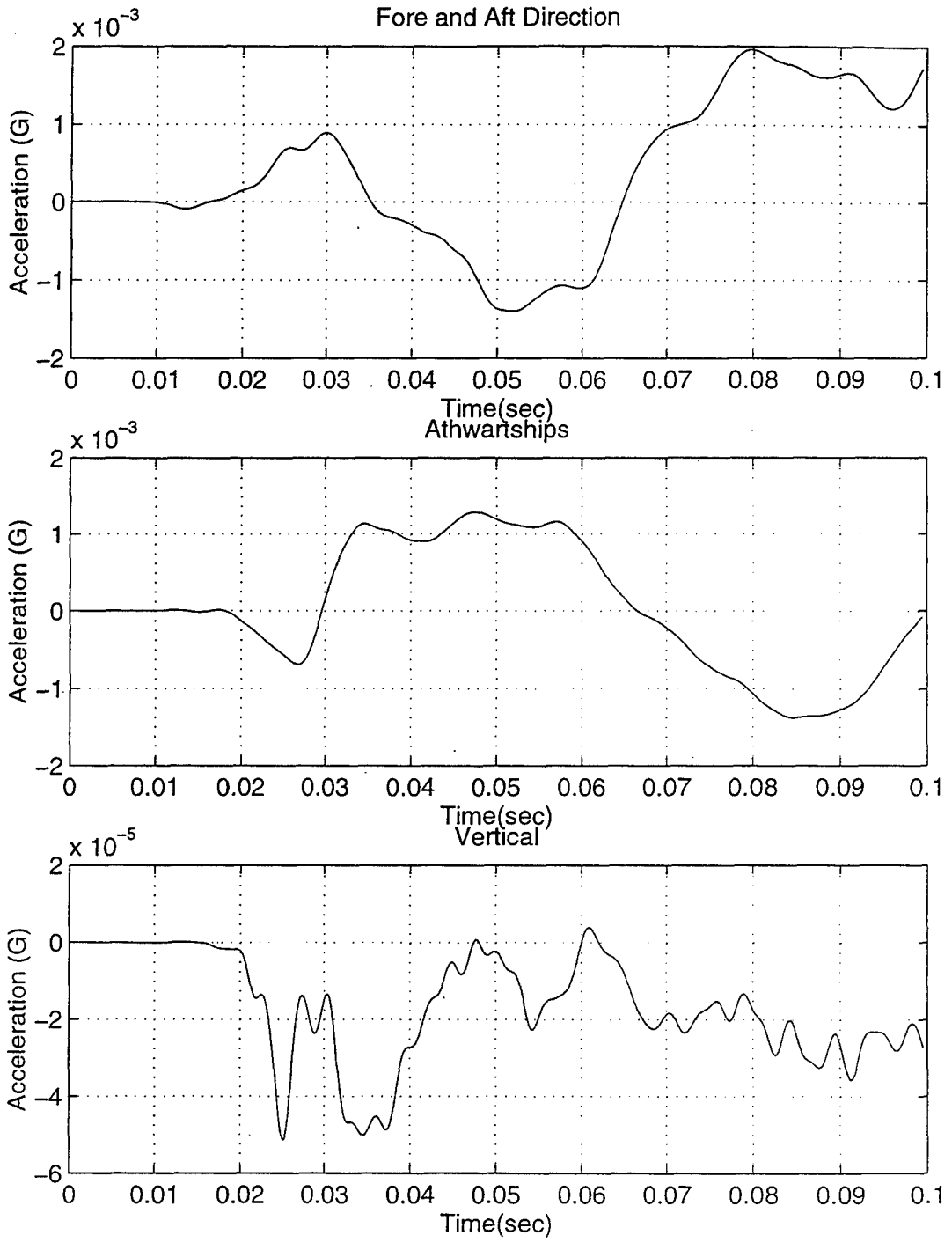

Figure 70. CSER 1 Accelerations (Node 3567)

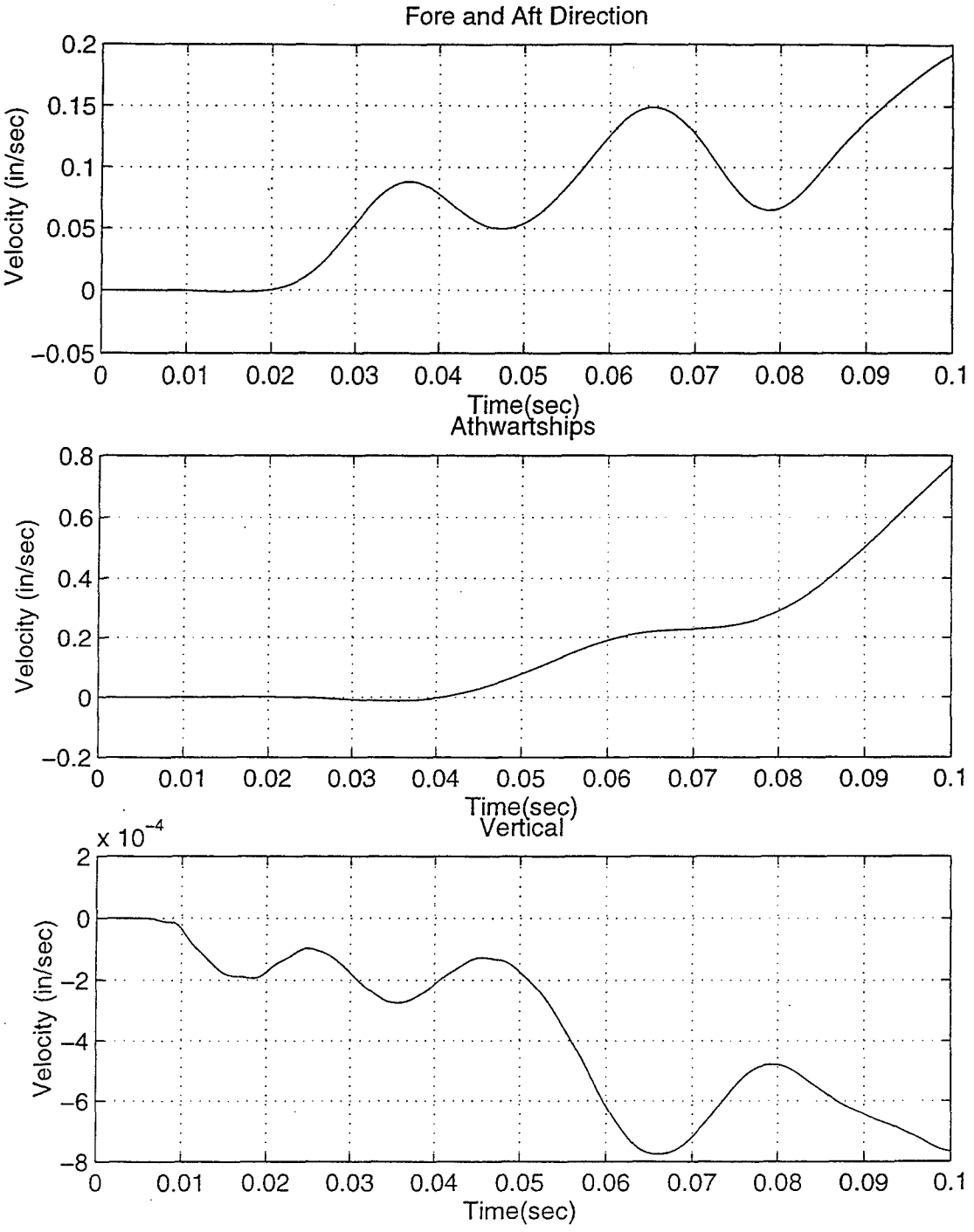

Figure 71. CSER 2 Velocities (Node 3669)

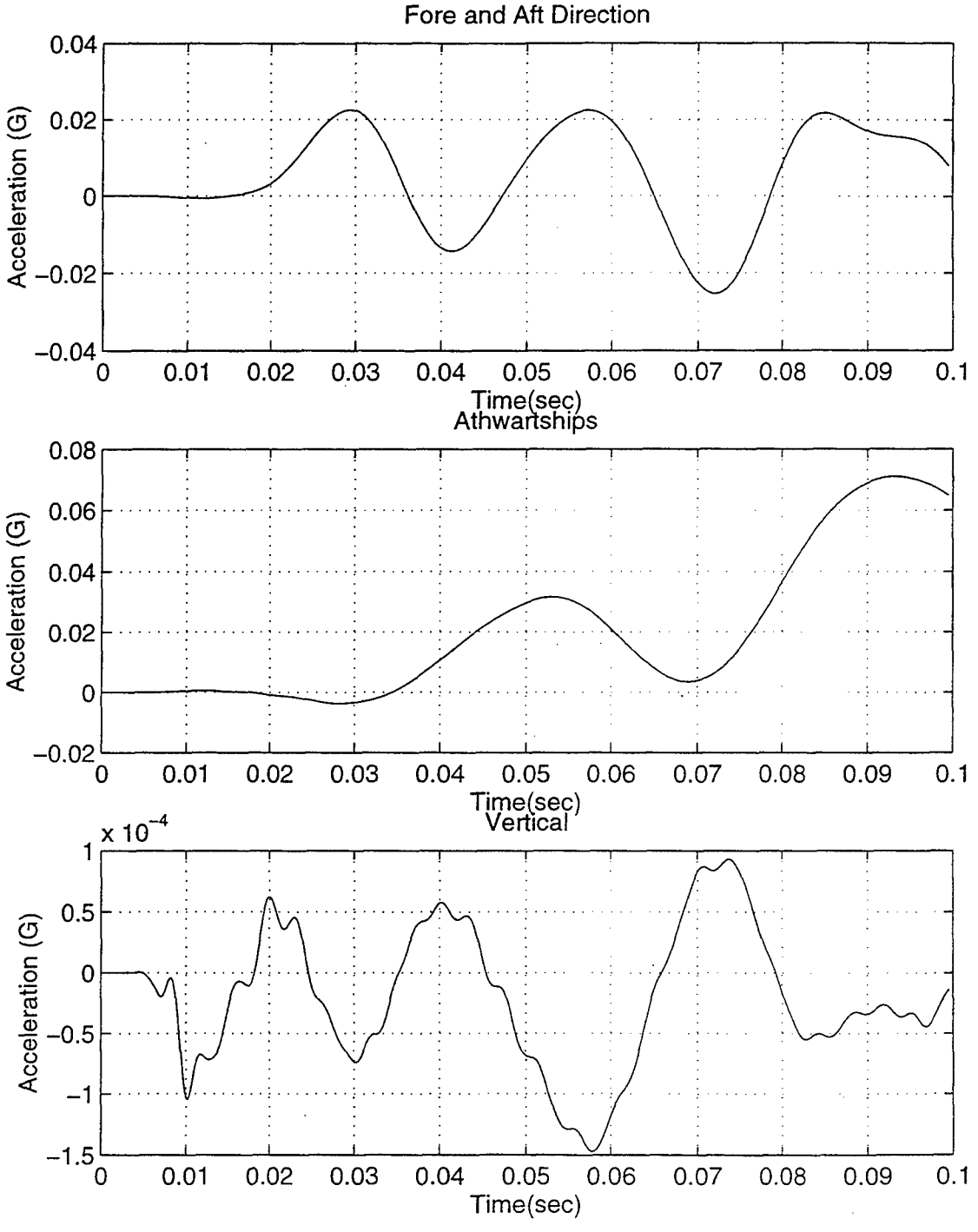

Figure 72. CSER 2 Accelerations (Node 3669)

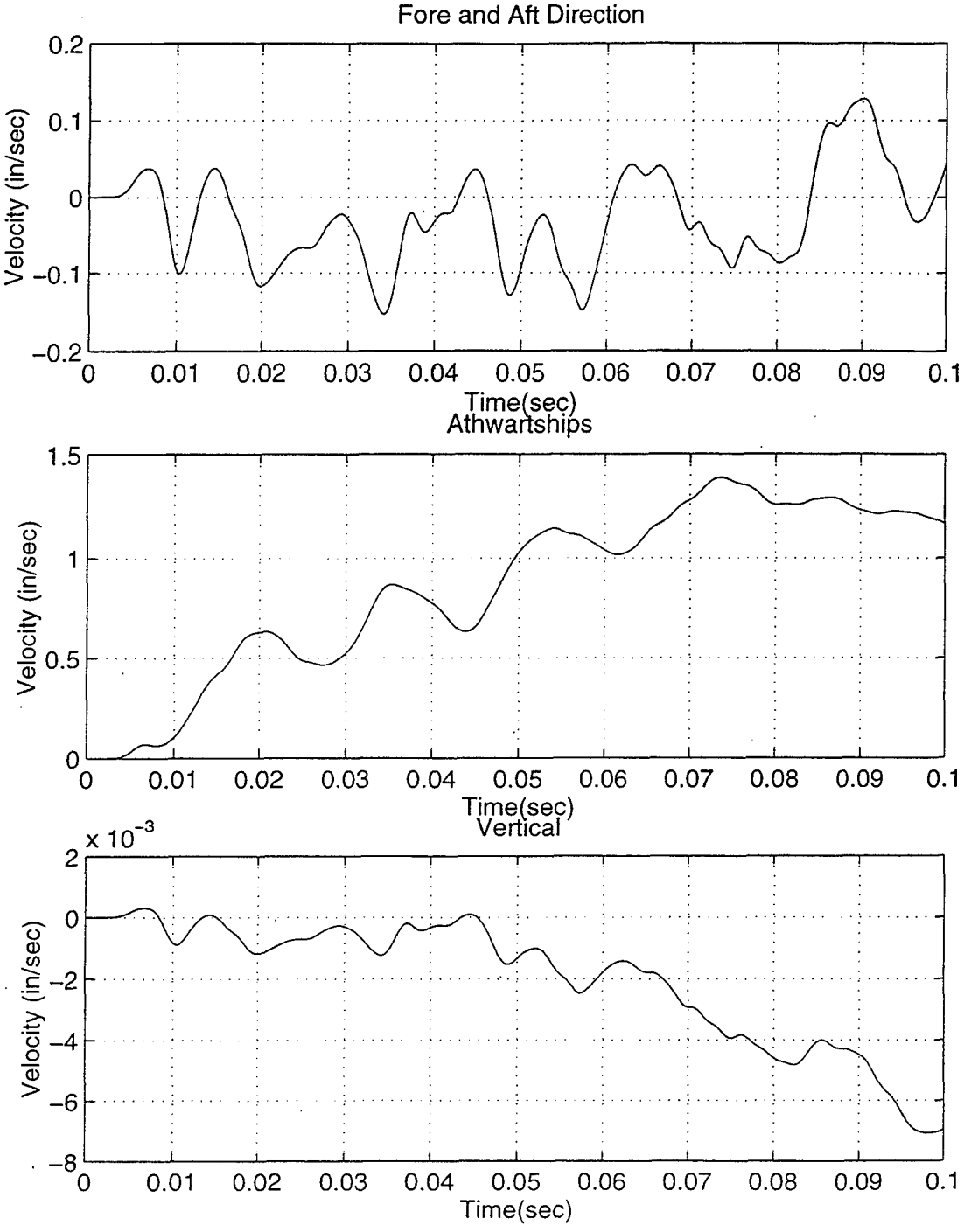

Figure 73. CSER 3 Velocities (Node 3541)

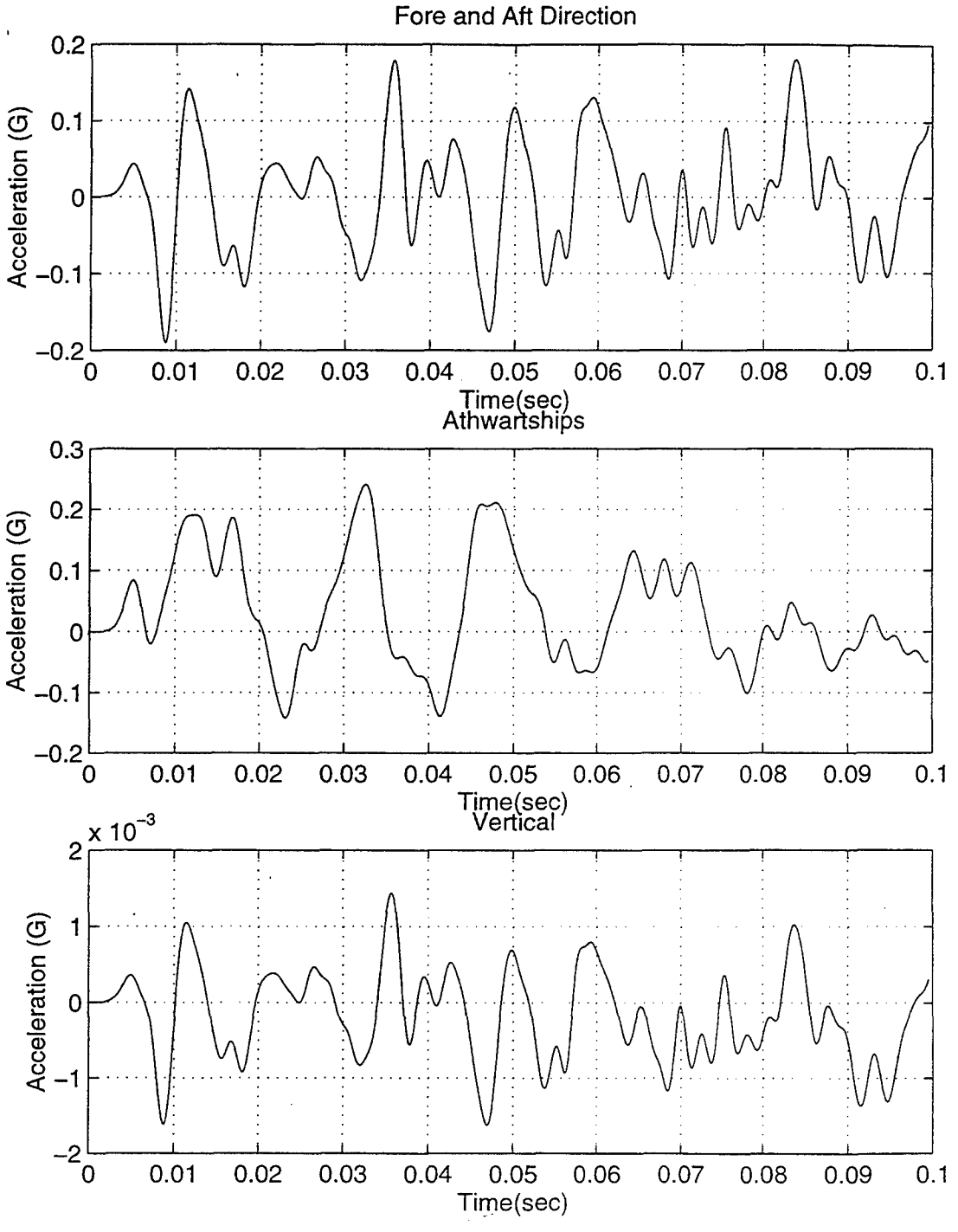

Figure 74. CSER 3 Accelerations (Node 3541)

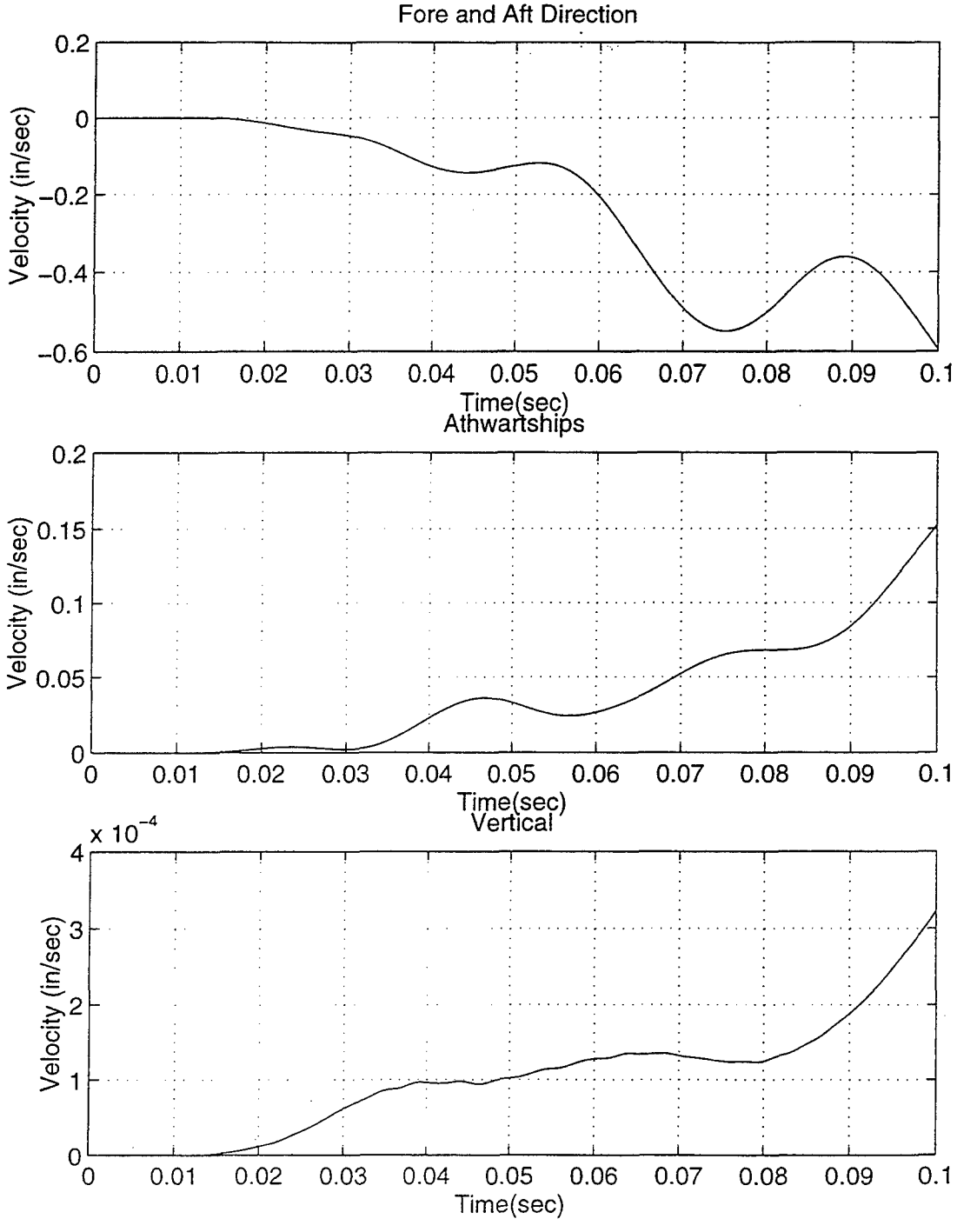

Figure 75. SPY Radar Room Velocities (Node 6955)

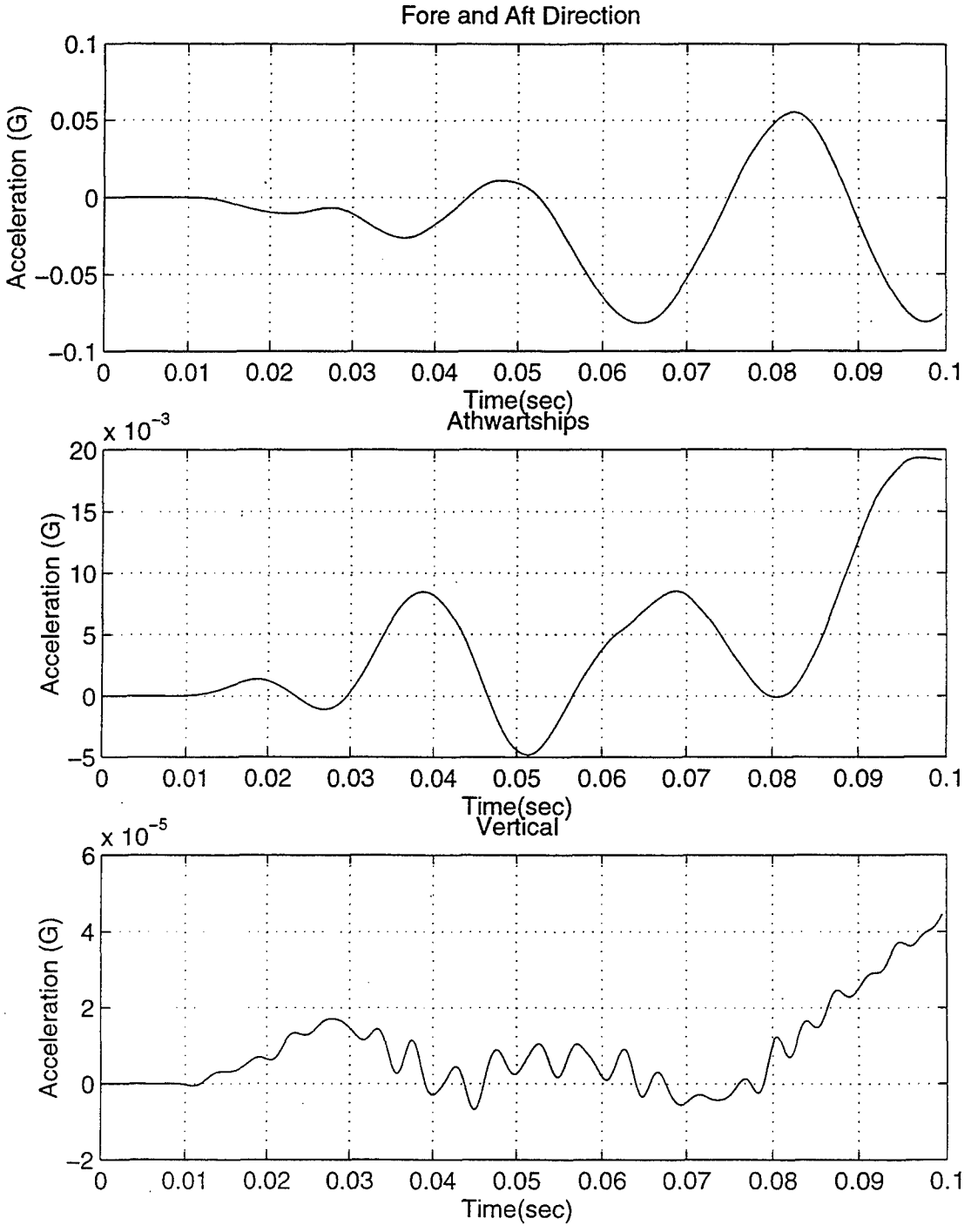

Figure 76. SPY Radar Room Accelerations (Node 6955)

LIST OF REFERENCES

1. Kelso, F.B. et. al., "From the Sea, Preparing the Naval Service for the 21st Century". September 1992.

2. Military Specification , MIL-S-901D, *Shock Tests, High Impact Shipboard Machinery, Equipment and Systems, Requirements for*, March 1989.

3. Hicks, A.N., "Explosion Induced Hull Whipping", Advances in Marine Structures, Elsevier Applied Science, 1986, pp. 390-406.

4. DeRuntz, J.A. Jr., "The Underwater Shock Analysis Code and Its Applications," Paper Presented at the 60th Shock and Vibration Symposium, Vol I, pp. 89-107, November 1989.

5. Lawry, M.H., *I-DEAS Masters Series 2.0 Student Guide,* Structural Dynamics Research Corportation, 1994.

6. Macneal-Schwendler Corp. *MSC/NASTRAN V67.5, Users Manual*, The Macneal-Schwendler Corporation, 1993.

7. Bleich, H.G. and Sandler, I.S., "Interaction Between Structures and Bilinear Fluids", International Journal of Solids and Structures, pp 617-638, 1970.

8. Ewing, D. L., et. al. , "A Surface Combatant for the 21st Century: DDG 51 Flight IIA", Naval Engineers Journal, Volume 107, Number 3, p 224, May, 1995.

9. Cole, R. H. *Underwater Explosions*, pp 3-13, Princeton University Press, 1948.

10. Geers, T.L. "Residual Potential and Approximate Methods for Three Dimensional Fluid-Structure Interaction Problem", Journal of the Acoustic Society of America, Vol.49, pp. 1505-1510, 1971.

11. Shin, Y.S.,"Naval Ship Shock Design and Analysis", Course Notes for Underwater Shock Analysis, Naval Postgraduate School, Monterey, CA, 1996.

12. Costanzo, F.A. and Gordon, J.D., "An Analysis of Bulk Cavitation in Deep Water," DTNSRDC, UERD Report, May 1980.

13. The Mathworks, Inc., *The Student Edition Of Matlab, User Guide*, Prentice Hall, 1992.

14. ASSET/MONOSC (ADVANCED SURFACE SHIP EVALUATION TOOL MONOHULL SURFACE COMBATANT) PROGRAM, User Manual, Boeing Computer Services, 1990.

15. DeRuntz, J.A., Jr., Underwater Shock Analysis Short Course Workshop, Unique Software Applications, Monument, Colorodo, 1996.

16. DeRuntz, J. A., Jr., *The Underwater Shock Analysis Code, Reference Manual,* DNA 5615F, Lockheed Missiles and Space Co., 1980.

17. DeRuntz, J.A. Jr., FLUMAS Manual, Unique Software Applications, Monument, Colorodo, May 1996.

18. DeRuntz, J.A. Jr., AUGMAT Manual, Unique Software Applications, Monument, Colorodo, May 1996.

19. DeRuntz, J.A. Jr., TIMINT Manual, Unique Software Applications, Monument, Colorodo, May 1996.

20. Newton, R. E., "Effects of Cavitation on Underwater Shock Loading-Part I", Naval Postgraduate School, Monterey, CA, 1978.

21. Newton, R. E., "Effects of Cavtitation on Underwater Shock Loading-Plane Problem, Final Report", Naval Postgraduate School, Monterey, Ca, 1981.

22. USS John Paul Jones (DDG-53) Shock Trial Final Report, AEGIS Program Manager (PMS-400), November 1994.

23. DDG-51 ASSET Design Summary, Naval Postgraduate School, 1996.

24. DDG-51 Flight IIA Study, Drawings, Naval Sea Systems Command, 1993.

25. Fassnacht, F. B.,DDG-51 Combat Systems Enclave, Naval Postgraduate School, 1994.

26. Cunningham, R.E. "Simplified Finite Element Modeling of Stiffened Cylinders Subjected to an Underwater Explosion", Master's Thesis, Naval Postgradueate School, Monterey, Ca, 1996.

INITIAL DISTRIBUTION LIST

		No. of Copies
1.	Defense Technical Information Center 8725 John J. Kingman Road, Ste 0944 Ft. Belvoir, VA 22060-6218	2
2.	Dudley Knox Library Naval Postgraduate School 411 Dyer Rd. Monterey, California 93943-5101	2
3.	Professor Young S. Shin, Code ME/Sg Department of Mechanical Engineering Naval Postgraduate School Monterey, California 93943	3
4.	Defense Nuclear Agency Attn: M. Giltrud 6801 Telegraph Road Alexandria, Virginia 22310-3398	1
5.	Carderock Division, Naval Surface Warfare Center Indian Head Division, White Oak Detachment Attn: Hans Mair Code 460 (Explosion Damage Division, Code 460) Silver Spring, MD 20903-5640	1
6.	Carderock Division, Naval Surface Warfare Center Attn: Harry P. Gray Code 673 9500 MacArthur Blvd. Bethesda, Maryland 20084-5000	1
7.	Naval Sea Systems Command Attn: Mark Mclean Code 06K213 2531 Jefferson Davis Highway Arlington, VA 22242-51	1
8.	Sandia National Laboratories Attn: L. Weingarten P. O. Box 969 Livermore, California 94551-0969	1

9.	John DeRuntz, Jr. USA 19875 Indian Summer Lane Monument, Colorado 80132	1
10.	Peter Mendoza The MacNeal-Schwendler Corporation 815 Colorado Blvd Los Angeles, CA 90041-1777	1
11.	Prof. Khin Yong Lam The University of Singapore 10 Kent Ridge Crescent Singapore 119260	1
12.	LT Leonard D. Santiago, USN 59 Santa Teresa Way Salinas, CA 93906	3
13.	Naval/Mechanical Engineering Curricular Office, Code 34 Naval Postgraduate School 700 Dyer Rd, Room 115 Monterey, CA 93943-5107	1
14.	Department Chairman, Code ME/Mc Department of Mechanical Engineering Naval Postgraduate School Monterey, CA 93943-5107	1